Administrative unit: **University of Padova**

Department: **Land, Environment, Agriculture and Forestry (LEAF)**

PhD Program: **Land, Environment, Resources and Health (LERH)**

Batch: 31st

GEOMATICS AS SUPPORT TO REMOTE SENSING DATA ANALYSIS FROM UAV TECHNOLOGY USING GIS OPEN SOURCE PLATFORMS

PhD Program Coordinator: Prof. Davide Matteo Pettenella
Supervisor: Prof. Antonio Vettore

PhD candidate: Marco Piragnolo

Sede Amministrativa: **Università degli Studi di Padova**

Dipartimento; **Territorio e Sistemi Agro-Forestali (TESAF)**

_____

CORSO DI DOTTORATO DI RICERCA: **Land, Environment, Resources, Health (LERH)**
Ciclo: 31°

LA GEOMATICA COME SUPPORTO ALL'ANALISI DEI DATI TELERILEVATI TRAMITE TECNOLOGIA UAV USANDO PIATTAFORME GIS OPEN SOURCE

Coordinatore: Prof. Davide Matteo Pettenella
Supervisore: Prof. Antonio Vettore

Dottorando: Marco Piragnolo

Table of contents

Abstract

The recent years saw a growing usage of remote sensing platforms, such as satellites and unmanned aircraft vehicles (UAVs). The Copernicus observation programme is an example of a new satellite constellation improving and promoting easy free access dataset, timely updated. The high popularity of UAVs is related to the obtaining high-resolution data, quickly at a relatively low cost. As result, sensors with high spatial and temporal resolution produce a great number of data, and these data increase exponentially.

Consequently, the software for image processing play a key role in the diffusion of this technology. The satellites take advantage of dedicated software for imagery analysis. The UAVs use structure from motion techniques for photogrammetric processing. However, the data analysis for both sensors is based on the classic pixel-based and object-based remote sensing techniques. Moreover, there is a growing demand for innovative tools to analyse huge dataset and to integrate the information for environmental analyses, monitor geomorphological aspects and land use studies, in particular in rural areas.

This thesis aims to study how GIS software using open source libraries can integrate information extracted from the satellite and the UAVs imagery, using a machine learning approach in a multi-level remote sensing framework. The main research questions are: (1) Can the classic techniques of remote sensing be used to extract suitable land use/land cover (LULC) maps – suitable in terms of classification accuracy – for the very high-resolution imagery of UAVs? (2) Can information from images of UAVs be merged with data from satellite images in the same area to achieve better results? (3) Which methods are optimal to analyse imagery of UAVs, and which benefits can be achieved through the use of more sophisticated techniques, such as the integration of multisource spatial information?

To answer the research questions, a multi-level framework has been developed to integrate the information derived from remote sensing techniques. The framework has been implemented using R cran libraries, and it includes a machine learning benchmark as an alternative to pixel-based and object-based approach. The benchmark allows for testing several algorithms, in terms of accuracy and processing time for classifying LULC maps.

The thesis presents the result of five papers, and the main findings relating to the major research questions can be summarized as follows: (1) The classic remote sensing techniques can be applied to UAVs high-resolution imagery to obtain a fast image classification. The maximum likelihood algorithm has a better result than the minimum distance algorithm in terms of accuracy.

(2) It is possible to integrate the satellite and UAVs temporal series. The scale affects the size of the training areas. Thus, to integrate the satellite and UAV information, the size of the regions of interest (ROIs) shall be larger than the ground sample distance (GSD) of the satellite. The use of large ROIs can avoid the noise from nearby areas. In addition, to limit the noise due to high-resolution images, the value of the digital number (DN) inside the ROIs should be homogenous. (3) The machine learning can be applied to both satellite and UAVs imagery and integrate spatial information. The dataset derived from high-resolution imagery can be considered as big data paradigm, in terms of data size and the processing time. Using a subset greater than the 8% of the total is possible to have a good results (kappa score ranges between 80% and 90%) and fast processing time. In addition, sensitivity analysis can help to define the contribution of each layer of the multi-level framework.

Riassunto

Negli ultimi anni vi è stato un crescente utilizzo di piattaforme di telerilevamento, come i satelliti e i velivoli senza pilota (UAVs). Il programma di osservazione Copernicus è un esempio di come una nuova costellazione di satelliti fornisca un dataset aggiornato e di facile accesso, mentre l'elevata popolarità degli UAVs è legata alla possibilità di ottenere rapidamente dati ad alta risoluzione a basso costo. I sensori con un'elevata risoluzione spaziale e temporale generano un gran numero di dati che aumentano esponenzialmente, di conseguenza il software per l'elaborazione delle immagini gioca un ruolo fondamentale nella diffusione della tecnologia; alcuni esempi sono l'utilizzo della structure for motion per l'elaborazione fotogrammetrica applicato alle immagini ottenute da UAVs e lo sviluppo di software basati sulle metodologie pixel-based e object-based specifici per il telerilevamento. Infine, considerando l'elevato volume di dati prodotti, vi è una crescente domanda di strumenti innovativi per analizzare, integrare ed estrarre informazioni da grandi dataset al fine di eseguire monitoraggi ambientali, analisi geomorfologiche e studi sull'uso del suolo, in particolare nelle zone rurali.

Questa tesi ha l'obbiettivo di studiare come i software GIS che utilizzano le librerie open source, possano integrare le informazioni derivate da immagini satellitari e da UAVs applicando le tecniche del machine learning in un framework di telerilevamento multi-livello. Le principali domande di ricerca sono: (1) Le classiche tecniche di telerilevamento potrebbero essere utilizzate per estrarre mappe di copertura del suolo / uso del suolo (LULC) adeguate - adatte in termini di precisione di classificazione - per le immagini ad altissima risoluzione degli UAVs? (2) Le informazioni provenienti dalle immagini degli UAVs potrebbero essere unite alle informazioni provenienti dalle immagini satellitari nella stessa area per ottenere risultati migliori? (3) Quali metodi sono ottimali per analizzare le immagini degli UAVs e quali benefici potrebbero essere ottenuti attraverso l'uso di tecniche più sofisticate, come l'integrazione di informazioni spaziali multi-source?

Per rispondere alle domande di ricerca è stata sviluppato un framework multi-livello per integrare le informazioni derivate dal telerilevamento. Il framework è stato implementato usando le librerie R cran e sviluppando un benchmark di machine learning come alternativa alle tecniche pixel-based e object-based. Il benchmark consente di testare diversi algoritmi in termini di precisione e tempo di elaborazione e di produrre mappe di LULC.

I risultati che rispondono alle domande di ricerca precedentemente formulate sono presentati nei cinque paper che compongono la tesi e possono essere così riassunti: (1) Le tecniche di telerilevamento classiche possono essere applicate alle immagini ad alta risoluzione degli UAVs per

ottenere una classificazione rapida delle immagini. L'algoritmo maximum likelihood ha ottenuto un risultato migliore rispetto al minimum distance in termini di precisione. (2) La scala influisce sulle dimensioni delle aree di training. Di conseguenza, per integrare le informazioni satellitari e da UAVs, le dimensioni delle regioni di interesse (ROIs) devono essere maggiori della risoluzione spaziale (GSD) dell'immagine satellitare. L'uso di ampie ROIs permette di ridurre il rumore prodotto dalle zone vicine. Inoltre, per limitare il rumore prodotto dalle immagini ad alta risoluzione, i valori dei digital number (DN) all'interno delle ROIs devono essere omogenei. (3) Il machine learning può essere applicato alle immagini satellitari, alle immagini prodotte con l'utilizzo di UAVs e può trarre beneficio dall'integrazione delle informazioni spaziali. Il dataset derivato da immagini ad alta risoluzione può essere considerato, in termini di dimensioni e tempo di elaborazione, un big data. Utilizzando un sottoinsieme superiore all'8% del totale, è possibile ottenere una buona precisione (kappa tra 80% e 90%) e buoni tempi di elaborazione. Inoltre, l'analisi della sensibilità può aiutare a definire il contributo di ogni layer in una struttura a più livelli.

1. Research synopsis

1.1. Research background and justification

The past years saw a wide use of remote sensing platforms, such as satellites, airborne and unmanned aircraft vehicles (UAVs), and a growing demand for innovative tools for remote sensing analysis. The Copernicus observation programme, directed by the European Space Agency, is an example of a new satellite constellation improving and promoting an easy free access dataset, timely updated. The satellites orbit around the Earth from hundreds to thousands of kilometres in height, so the temporal resolution is fixed. Consequently, the monitoring plan cannot continue and be personalized. The satellites carry on board many kinds of sensors with various characteristics in terms of spatial and radiometric resolution. The spatial resolution ranges from the metre to decimetre scales, and it depends on sensors. The sensors register the electromagnetic energy reflected from objects as a digital number (DN). Consequently, the DN is affected by the atmospheric path and cloud coverage. In addition to the satellite platforms, the airborne acquisition, which is done at a lower altitude than that of satellites, can overstep these problems. The airborne imagery has better resolution than those from satellites, but the imagery suffers from great geometric and radiometric distortion. These errors are due to instability and turbulence during the flight. Nevertheless, the advantage of the airborne campaign is to set the area of interest and the temporal and spatial resolution, which are related to the altitude of flight. In contrast, a flight campaign is more expensive than satellite acquisition, limited by meteorological conditions, and it requires good planning. Finally, in recent years, the UAVs have seen great attention from the scientific community. Technically, the reasons are the continuous and rapid technology improvement in hardware Global Position System and Global Navigation Satellite System (GPS-GNSS), power pack, sensors and in the software. These reasons follow the typical development of technology: the prices and weight of the components have decreased, and the precision has increased. Therefore, new technologies have been developed to limit manual operation, reduce risk, and simplify flight operations, prospecting to obtain high-resolution data "on demand" quickly at a relatively low cost. The remote control from a ground station is a key point to improve the quality of a survey with high flexibility of usage. On one hand, the campaign of UAVs for imagery acquisition is low cost, and it grants high temporal and spatial resolution (centimetre or decimetre). On the other hand, the disadvantages are due to the limited power supply that influences the size of the covered area and the carry load. Furthermore, the ground control points (GCPs) are necessary to have a good precision survey to achieve a spatial accuracy of 10–15 cm (Turner et al., 2012). Otherwise, directly georeferenced mosaics with 1

cm/pixel of spatial resolution have a spatial absolute accuracy of 65–120 cm. Hence, the high flexibility of usage, the low cost, the high spatial and temporal resolution, compared to satellite or airborne platforms, are making UAVs a widespread remote sensing platform, accessible to an increasing number of users. UAVs have been used in numerous applications such as homeland security, dangerous operations, and research. Research fields include cultural heritage, archaeology, 3D surveys, environmental studies, forestry, land use and risk management, and precision agriculture (Berni et al., 2009b; Herwitz et al., 2004; Hunt et al., 2010; Jensen et al., 2009; Lelong et al., 2008; R.B Haarbrink, 2006; Remondino et al., 2011)

Software for image processing plays a key role in the spread of remote sensing technology. Sentinel satellites take advantage of dedicated software for imagery analysis, i.e., Sentinel Application Platform. UAVs use structure from motion techniques to compensate for the low accuracy of the positioning systems. These techniques, coupled with algorithms of computer vision, have led to the development of various software for photogrammetric processing available with commercial licenses and open source licenses (Remondino, Del Pizzo, 2012).

The technology of UAVs has been reviewed from (Grenzdörffer et al., 2008; Sona et al., 2014), highlighting the following points regarding photogrammetric, radiometric and data size aspects and the analysis framework.

The photogrammetric problems concern the limited dimension of the camera, such as lack of knowledge of the internal orientation angle, distortion of frames, overlapping frames, low precision of GPS-GNSS, and a high number of GCPs.

The radiometric problems are related to image interpretation, correct use of radiometric information, new techniques for the processing of multispectral data and calculation of the derived (Honkavaara et al., 2012; Torres-Sánchez et al., 2014). The sensors with high spatial and temporal resolution produce a great number of data, and these data increase exponentially (Zaslavsky et al., 2013).

The data analysis is based on classic remote sensing techniques, pixel-based and object-based, but the size and processing time can be related to the Big Data paradigm: Big Data is not only a physical storage but also a number of files, tables, records and processing time (Singh and Singh, 2012). To solve problems of size and scalability of the dataset, many authors have proposed new frameworks, the GIS environment, and objects algorithms (Lin et al., 2013; Peña et al., 2013; Zhao et al., 2009).

Hence, there is a growing demand for innovative information extraction and analysis tools to monitor geomorphological aspects for environmental analyses, land use, fragmentation of habitats and risk assessment (Van Asselen and Verburg, 2013). In the literature, many authors have proposed new frameworks, the GIS environment, and objects algorithms to solve problems of size and scalability of the dataset (Baumann et al., 1997; Zhao et al., 2009), new approaches for data fusion (Weih and Riggan, 2010), and imagery analysis, i.e., machine learning (D Anthony et al., 2015; Guo et al., 2014; Papageorgiou et al., 2011).

1.2. State of knowledge on the research topic

In recent years, remote sensing analysis has been popular in numerous civilian and research applications such as cultural heritage, ecology, forestry and land use mapping with a wide availability of remote sensing data, which are collected using different kinds of sensors, platforms, and spatial and temporal resolution. Nonetheless, the erogeneity of the platforms and the sensor have a common remote sensing background, but it requires different approaches and software for extracting information. In this paragraph, we recount some basic remote sensing concepts and summarize the commonly used satellites and UAVs application. The band ratio and the vegetation indices (VI) used in this work are described in Annex I, and the machine learning algorithms are described in Annex II.

The remote sensing analysis consists of the pre-processing, the image enhancement, the image transformation, the image analysis, and the classification. The pre-processing techniques correct geometric and radiometric errors of imagery, whereas the geometric correction eliminates distortion due to surface curvature and atmospheric interaction. Airborne imagery and UAV imagery have high geometric distortion due to not having the nadiral direction of the camera, the rotation around three axes, and the low precision of GPS-GNSS. Thus, images can be georeferenced and registered after geometric correction. The different sun elevations, sun azimuth, aerosol particles, atmospheric conditions, and sensor calibrations produce radiometric errors. These errors affect the object observations, and a radiometric correction eliminates radiometric errors. The quantity of electromagnetic energy collected by the sensor is described using DN. The DN is related to spectral resolution, but it has not a physical meaning. Indeed, the DN can be converted in physical units as radiance or reflectance. Irradiance is the electromagnetic energy that comes from the sun and illuminates a specific area. Radiance is the quantity of energy observed by the sensor from the top of the atmosphere. Reflectance is the quantity of energy reflected by an area, and it is a specific characteristic of materials. Therefore, radiance and reflectance are obtained from DN using specific formulas and sensor parameters (1) (Using the USGS Landsat 8 Product 01-08-206http://landsat.usgs.gov/Landsat8_Using_Product.php).

$$L\lambda = MlQcal + Al \qquad (1)$$

where:

$L\lambda$ = TOA spectral radiance (Watts/ (m2 * srad * μm))

Ml = Band-specific multiplicative rescaling factor from the metadata

Al = Band-specific additive rescaling factor from the metadata

$Qcal$ = Quantized and calibrated standard product pixel values (DN)

To calculate reflectance the formula is (2):

$$\rho\lambda' = M\rho Qcal + A\rho \qquad (2)$$

where:

$\rho\lambda'$ = TOA planetary reflectance, without correction for solar angle

$M\rho$ = Band-specific multiplicative rescaling factor from the metadata

$A\rho$ = Band-specific additive rescaling factor from the metadata

$Qcal$ = Quantized and calibrated standard product pixel values (DN)

TOA planetary reflectance with a correction for the sun angle is (3):

$$\rho\lambda = \frac{\rho\lambda'}{cos\,(\theta sz)} = \frac{\rho\lambda'}{cos\,(\theta se)} \qquad (3)$$

where:

$\rho\lambda$ = TOA planetary reflectance

θse = Local sun elevation angle

θsz = Local solar zenith angle. θsz = 90° - θse

Then, TOA planetary reflectance is (4):

$$\rho\lambda = \frac{M\rho Qcal + A\rho}{cos\,(\theta sz)} \qquad (4)$$

The radiometric correction is done using different approaches such as empirical line correlation (Johnson et al., 2003; Smith and Milton, 1999), MODTRAN atmospheric (Zarco-Tejada et al., 2013a, 2012, 2009), SMARTS atmospheric correction (Zarco-Tejada et al., 2013b) and the band ratio. Moreover, radiometric calibration methods developed for satellite imagery improved significantly

the quality of the imagery (Haghighattalab et al., 2016). The visual interpretation can be enhanced through the application of filters, manipulating DN to adjust brightness, contrast, and edge and using the band ratio and VI. The band ratio and the VI are image transformations based on a mathematical operation such as sum, difference, spectral rationing, principal component analysis, and index calculation, which creates new images. The band ratio and VI helps the classification process and reduces error in orthomosaics due to different illumination of individual frames, and they allow correcting the flaws in brightness caused by the zenith angle of the sun in the individual frames (Herwitz et al., 2004). The advantage of image transformations is to highlight information not clearly visible in multispectral images. Consequently, the indices calculation is widely used in agricultural and forestry applications, where data fusion can involve different sources, e.g., satellite and airborne platforms and merge contextual information (Weih and Riggan, 2010). In the literature, these techniques are applied in numerous precision agriculture, ecology, forestry, land use and risk management studies using classification techniques. The image classification is a process of assigning labelled classes to pixels. The main classification methods are unsupervised pixel-based, supervised pixel-based and object-based methods.

The precision agriculture (PA) allows adapting the techniques of fertilization, irrigation, and weeds treatment on the specific needs of the field, reducing crops risk and damage. To reach this goal, updated data on health crops status are necessary. An example is a study of the aerobiological quality of potato and tomato crops (Techy et al., 2008) that used two UAVs for extracting time data. The red, green, blue camera (RGB), multispectral camera, and thermal camera have been used for effectiveness monitoring on a wide range of crops, e.g., vines, olives, peach, mandarin, oranges, sugar cane, corn, sunflower and to produce vigour maps (Berni et al., 2009a). The research has highlighted significant errors in temperature estimation with a thermal camera due to flight elevation and to atmosphere interaction. The water stress and the vigour map of vineyards can be studied using the normalised difference vegetation index (NDVI) and the crop water stress index (CWSI) to show the water stress (Baluja et al., 2012). Similar studies have found a correlation between the water stress and the pathogenic agents in sugar beet plantation (Bendig et al., 2012) and the water stress and the fluorescence in olive, peach, and orange orchard using multispectral cameras (Zarco-Tejada et al., 2009). The water stress using the photochemical reflectance index (PRI) has been studied in orange and mandarin trees in a commercial orchard. Indeed, a PRI object-based classification has identified a correlation to leaf-level (Zarco-Tejada et al., 2012). In olives crops, (Calderón Madrid et al., 2014) have studied the relation between PRI and infection caused by

Verticillium. In coffee plantations, anomalies caused by water stress, invasive species, and errors in fertilization were identified using a red, green, near infrared (NIR) camera (Herwitz et al., 2004). It is well-known that a UAV flight requires normally some GCPs for the correct positioning of the multicopter, and the fieldwork is expensive and time-consuming. In addition, the information cannot be used in real-time. Therefore, the real-time kinematic GPS correction (RTK), without GCP, can solve the issue, and it has been applied for the fertilization and the nitrogen studies, measuring distortions from 0.18 to 0.29 cm. On one hand, this type of survey is only suitable for areas with few variations in height (Sugiura et al., 2005). On the other hand, the ability to process maps of fertilization in real time allows minimizing the consumption of fertilizers. The fertilizers can be applied at the right time and in optimum quantity, but this type of survey is power consuming. Hence, good flight efficiency requires the development of software solutions to optimize the routes of the drone (Tokekar et al., 2013).

The vegetation monitoring is an important indicator of local climate change. In Antarctica, the moss bed habitats were studied using the UAVs (Lucieer et al., 2010). The comparison of UAVs imagery and the moisture indices allows identifying the moss habitat. The indices were calculated from a digital elevation model (DEM).

Ecological studies have been conducted using the visual interpretation and the classification software. The stereoscopic vision and three-dimensional images were used to map small habitats, to identify trees, to estimate biomass and to manage natural environments (Gademer et al., 2010). In addition, biomass, dead wood, and riparian vegetation have been studied trough the object-based classification and the pixel-based classification (Dunford et al., 2009). The object-based technique produces good results when it is applied to single high-resolution images, but it is more time consuming than the pixel-based approach. Moreover, the object-based technique applied to an orthomosaic is less useful than an object-based technique applied to the single image. Indeed, the process is more difficult because illumination of each frame is not homogeneous. Likewise, a statistical approach based on a linear regression model was used to identify the biomass with RGB images without radiometric correction but considering contextual information such as the height of trees. Indeed, the plant height and VI can be used for biomass modelling. The indices, such as the GnyLi (from the name of the creators), which uses the absorbance in the near infrared and short range infrared reflectance, the modified green red vegetation Index (MGRVI), and the red green blue Vegetation Index (RGBVI), have shown a positive performance in the early growth stages,

compared to the late growth stages. In contrast to expectations, the combination of vegetation indices and plant height did not significantly improve the model performance (Bendig et al., 2015).

Related to vegetation studies, the canopy identification is an important topic that has a great interest in forestry applications. However, the high number of variables makes the canopy identification difficult task, so the pixel and object-based algorithms do not always work efficiently, and sometimes they cannot identify correctly the canopy features. Therefore, a machine learning approach and the object-based approach were compared (Hung et al., 2012). The support vector machine (SVM) classification method works recursively and learns from the data for building a decision hyperplane. Likewise, as a supervised classification method, given training data, the SVM divides the dataset groups or classes. The classification results, using only the SVM algorithm or only an object-based algorithm produces some lacunae. The combination of the two algorithms improves the result. To overcome the issue, another strategy is to use LIDAR sensors for the canopy monitoring (Korhonen et al., 2011; Solberg et al., 2009; Wallace, 2013).

Studies about land use/land cover (LULC) use a LIDAR sensor, pixel-based and object-based algorithms and machine learning for data fusion and multi-temporal analysis. Thus, the comparison of the algorithms is needed for identifying the correct approach based on the dataset. Indeed, the LIDAR dataset composed of a 1 metre resolution acquisition merged with 0.5 - 2 metre satellite images was classified with the supervised maximum likelihood algorithm and the object-based algorithm. The results highlighted that the object-based classification was less precise than the supervised maximum likelihood classification because it is not able to evaluate variability inside classes (Walter, 2004). A second discussion point is the integration of the multi-temporal analysis. This research has been conducted with the unsupervised, the supervised and object-based (Weih and Riggan, 2010) approaches and to compare the algorithms using different imagery resolutions of the mean resolution of 10 metres and high resolution of 1 metre. On one hand, the results show the unsupervised method had an advantage using the multi-temporal data, but no quality improvement has been found using the high-resolution dataset. On the other hand, the supervised method had an improvement using the high resolution data, but no quality improvement has been found using multi-temporal dataset. In addition, the object-based method had an improvement from the merger of high-resolution data and the normal resolution images. Finally, the multi-temporal data provide no improvement to the classification. In particular, using a mean resolution dataset, object-based, unsupervised and supervised methods had similar performances.

Recently, LULC has been studied using the machine learning method. This new approach has been applied in the studies about the cotton crop (Papageorgiou et al., 2011), variable-rate fertilization (Zheng et al., 2013), classification of invasive weed species (Hung et al., 2014) an ecological study on habitat (Gonçalves et al., 2016) and for the automatic detection of the UAVs' landing site (D Anthony et al., 2015; Guo et al., 2014).

The previous sensors and technologies have also been applied to geomorphology and landscape fields. For example, LIDAR and high resolution UAVs imagery can be used to identify the ephemeral gullies. Indeed, a 5 centimetres high resolution DEM has been used for analysing of the gullies that range from 10 to 30 cm deep and 30 to 100 cm wide (Frankenberger et al., 2008). A similar scale of problems were found on rangeland and vegetation studies, quantification of plant cover (Rango et al., 2009), and terracing identification (Diaz-Varela et al., 2014). Applying a decision tree and a fuzzy algorithm on dry rangeland imagery, the result showed more separable classes on coarse scale segmentation than on fine scale (Laliberte and Rango, 2009). Similar results were found in a sub-decimetre classification of rangelands, where the classification at group level was more efficient than a classification at the species level (Laliberte and Rango, 2011). Then, the classification is affected by the features of the object, such as size, but the identification of the correct scale of analysis is a difficult task. When a small scale is set, wide objects are produced. Indeed, this approach can reduce the errors until a threshold is reached, but exceeding the threshold produces overestimation errors (Torres-Sánchez et al., 2015). Thus, the relation between training areas dimension and segmentation dimension suggested a correlation with real world objects (Ma et al., 2015). Accordingly, the spatial information is important for landscape application and for PA, e.g., for studying crop plants in their first stages or for weed plant identification (Pérez-Ortiz et al., 2015). Finally, scale depends on the altitude of flight. Hence, flights executed at different altitudes have been analysed with the purposes to identify the best parameter to identify the weeds in maize and sunflower crops using the unsupervised algorithm (k-means and repeated k-means or Rk-means), and semi-supervised (KNN, linear SVM version or LinSVM and kernel SVM) methods. The SVM achieved the best performance and was easy to automate with less interaction of the user (Pérez-Ortiz et al., 2016).

The UAVs are also employed in the management plan, traffic control (Lei et al., 2014; Meuel et al., 2013), prevention of risk, specialised operations such mine operations (Lee and Choi, 2016) and wildfire monitoring. For example, the wildfire management is a dangerous operation, and it needs real-time information about the dimension and the wildfire characteristic. Consequently, a specific

framework and a decision support system have been developed for monitoring and predicting the wildfire propagation (Ambrosia et al., 2011; Merino et al., 2012).

Table 1 and Figure 1 report the information based on the literature review about the topic, the classification technique, the algorithm applied, the software, dataset resolution and the index applied. At first, it is necessary to distinguish between the photogrammetric software, the GIS software, and the remote sensing software. Second, it is necessary to distinguish between the commercial software and open-the source software. Regarding commercial photogrammetric software, Agisoft Photoscan® has been used in four works, and it is the most popular software. Two works used Leica Photogrammetric Suite® and one work used Pix4UAV®. Concerning the open-source photogrammetric software, Bundler has been used only in two works. Thus, for photogrammetric purposes, the commercial licence software is mostly used. Analysing the GIS platforms, three studies used ArcGIS® commercial software, and three studies used unspecified GIS software. Only one study used the open-source Grass GIS. Some open libraries such as R software statistical computing and graphics, computer vision library OpenCv, and Gaussian process regression and classification toolbox (GpmlTolobox) have been used in three works. Thus, when the focus is on GIS analysis, the commercial licence seems the best ranked. In contrast, it is not possible to identify the number of open source GIS installation. Considering remote sensing software, eCognition® is the common object-based platform. It has been used in five works, but if we count the two works with Definiens® (eCognition renamed), there are seven works that used this object-based software. Other commercial software is Erdas Image 9.3®, Envi 4.4®, and PARGE®. Finally, one work combined the Kodak DCS Camera Manager®, Kodak Photodesk® software, and Adobe Photoshop®. In conclusion, the commercial software is preferred to the open-source solutions for photogrammetric application and analysis applications. This preference is an important point because it leaves interesting opportunities to develop new tool and open-source solutions.

Table 1 Summary table of literature review

Author	Topic	Technique	Algorithm	Software	Dataset	Resolution	Index
Ambrosia *et al.* 2011	Fire monitoring	short-wave-, mid- and thermal-infrared (VIS-IR-TIR)	Multi-band temperature threshold algorithm	-	UAV	-	NBR
Baluja *et al.* 2012	Precision agriculture, water stress, grapevine	Thermal multispectral	watershed	Grass GIS	UAV	10 - 30 cm	NDVI TCARI/OSAVI
Bendig *et al.* 2012	Precision agriculture, water stress, infectious agent sugar beet	RGB+NIR images	Histogram analysis	ArcGIS®	UAV	1.4 - 17 cm	NDVI
Bendig *et al.* 2015	Precision agriculture, biomass estimation	RGB imagery	Regression model	Agisoft PhotoScan Professional Esri ArcGIS® 10.2.1	UAV	1 cm	NDVI GnyLi near infrared GRVI MGRV RGBVI
Berni *et al.* 2009a	Precision agriculture, crop status, corn olive peach	Thermal and multispectral	-	Leica Photogrammetric Suite®	UAV	20 - 40 cm	PRI LAI NDVI TCARI/OSAVI
Berni *et al.* 2009b	Precision agriculture, crop status olive orchard	Thermal	-	-	UAV	40	CSWI
Calderón Madrid *et al.* 2014	Precision agriculture, infection monitoring olive orchard	Hyperspectral and Thermal Camera	-	-	UAV	20 - 40 cm	PRI CWSI TCARI TCARI/OSAVI
Diaz-Varela *et al.* 2014	Precision agriculture, agricultural terraces	Object-based	Multiresolution segmentation	eCognition® 8	UAV	11 cm	NDVI DifMin TopIndex Terrain Shape Index
Dunford *et al.* 2009	Forestry, vegetation and dead wood	Pixel-based Object-based	Decision tree Segmentation	-	UAV	6.8 - 21.8 cm	-
Frankenberger *et al.* 2008	Landscape erosion, gullies channel	Lidar	-	OpenCV image processing library	UAV	10 cm	-
Gademer *et al.* 2010	Ecology, natural habitat	Stereoscopic view	-	-	UAV	5 - 11 cm	

Gonçalves *et al.* 2016	Ecology, natural habitat	Machine learning Pixel-based	Random Forest	Agisoft PhotoScan Professional® Gis software R software package	UAV	6 cm	Band ratio
Herwitz *et al.* 2004	Precision agriculture, coffee production	RGB	Masking routine	Kodak DCS Camera Manager® Kodak Photodesk software® Adobe Photoshop®	UAV	50 cm - 1m	NDVI G/R brightness correction index
Hung *et al.* 2012	Forestry, canopy structure	SVM Object-based	Mean shift clustering	-	UAV	20 cm	-
Jensen *et al.* 2009	Process analysis	-	-	-	UAV	5 cm	-
Johnson *et al.* 2003	Precision agriculture, grapevine	RGB	-	GIS	UAV	20 cm	-
Laliberte & Rango 2009	Landscape, rangeland vegetation	Object-based	Decision tree Fuzzy	Leica Photogrammetric Suite® 9.0 Definiens Professional® 5	UAV	5 cm	-
Laliberte & Rango 2011	Landscape, rangeland vegetation	Object-based	Decision tree	eCognition® 8	UAV	5 cm	-
Laliberte & Rango 2011	Process analysis	Object-based	Decision tree	eCognition® 8	UAV	5 cm	-
Lei et al. 2014	Process analysis	Feature extraction	Harris SIFT SURF	-	UAV	-	-
Lucieer *et al.* 2010	Ecology, moss beds	-	-	ArcGIS®	UAV	1.5 cm	WI
Ma *et al.* 2015	Process analysis	Object-based	Random Forest Correlation based Feature Selection (CFS)	eCognition® 8.7	UAV	20 cm	-
Merino *et al.* 2012	Fire monitoring	RGB and non-thermal OEM infrared micro-camera	training-based thresholding method pixel similarity	-	UAV	-	-
Meuel *et al.* 2013	Process analysis	Super-Pixel-based	Super Pixel segmentation	-	UAV	-	-
Pérez-Ortiz *et al.* 2015	Precision agriculture, weed mapping in sunflower	RGB+NIR Machine learning	Unsupervised, semi-supervised, supervised	Agisoft Photoscan Professional Edition®	UAV	-	NDVI ExG
Pérez-Ortiz *et al.* 2016)	Precision agriculture,	Object-based	k-mean clustering	Agisoft Photoscan Professional Edition®	UAV	1.4 cm	ExG

			SVM				
	Maize, sunflower						
Rango *et al.* 2009	Landscape, rangeland vegetation	Object-based	-	Definiens Professional®	UAV	5 - 6 cm	-
Sugiura *et al.* 2005	Precision agriculture, crop status nitrogen	R-G-NIR	-	GIS	UAV	1 - 7 cm	LAI NDVI
Techy et al. 2008	Precision agriculture, aerobiol. sampling crops	-	Path planning	-	UAV	-	-
Tokekar *et al.* 2013	Precision agriculture nitrogen	RGB NIR	TSPN algorithm implementation	GPML Toolbox	UAV	1 m	NDVI
Torres-Sánchez et al. 2015	Precision agriculture, weed mapping maize, sunflower, wheat	Object-based	Multiresolution segmentation	ENVI® 4.4., eCognition®	UAV	1.14 - 1.62 cm	ExG NDVI
Turner *et al.* 2010	grapevine	Thermal multispectral	Orthoectification	Bundler software PMVS2	-	1 cm	PRI
Turner *et al.* 2012	Geometric correction	Structure for motion Computer vision	-	Bundler software	UAV	1 cm	
Wallace 2013	Forestry, Canopy structure	Lidar	-	-	UAV	-	FCI LCI GCI ACI
Walter 2004	Land Use/Land Cover	Object-based	Supervised Maximum likelihood	GIS	Airborne Optical LIDAR	50 cm 2 m 1 m	NDVI
Weih & Riggan 2010	Land Use/Land Cover	Unsupervised Supervised Object-based	-	Feature Analyst Erdas Image® 9.3	SPOT-5 Aerial imagery	5 m 30 cm - 1m	-
Zarco-Tejada *et al.* 2009	Precision agriculture, water stress olive, peach, and orange	Thermal and multispectral	FluorMOd model MODTRAN atmospheric correction	-	UAV	15-40 cm	Cab
Zarco-Tejada *et al.* 2012	Precision agriculture, water stress, orange mandarin	Hyperspectral image	FluorMOd model MODTRAN atmospheric correction	-	UAV	40 cm	PRI

| Zarco-Tejada et al. 2013b	Precision agriculture, water stress grapevine	Thermal and multispectral Micro hyperspectral	MODTRAN atmospheric correction	PARGE (ReSe Applications)®	-	2.5-15-40	R515/R570 TCARI/OSSAVI
Zarco-Tejada et al. 2013a	water stress grapevine	Narrow band multispectral	SMARTS atmospheric correction MODTRAN atmospheric correction Object-based	-	-	10-20	PRI
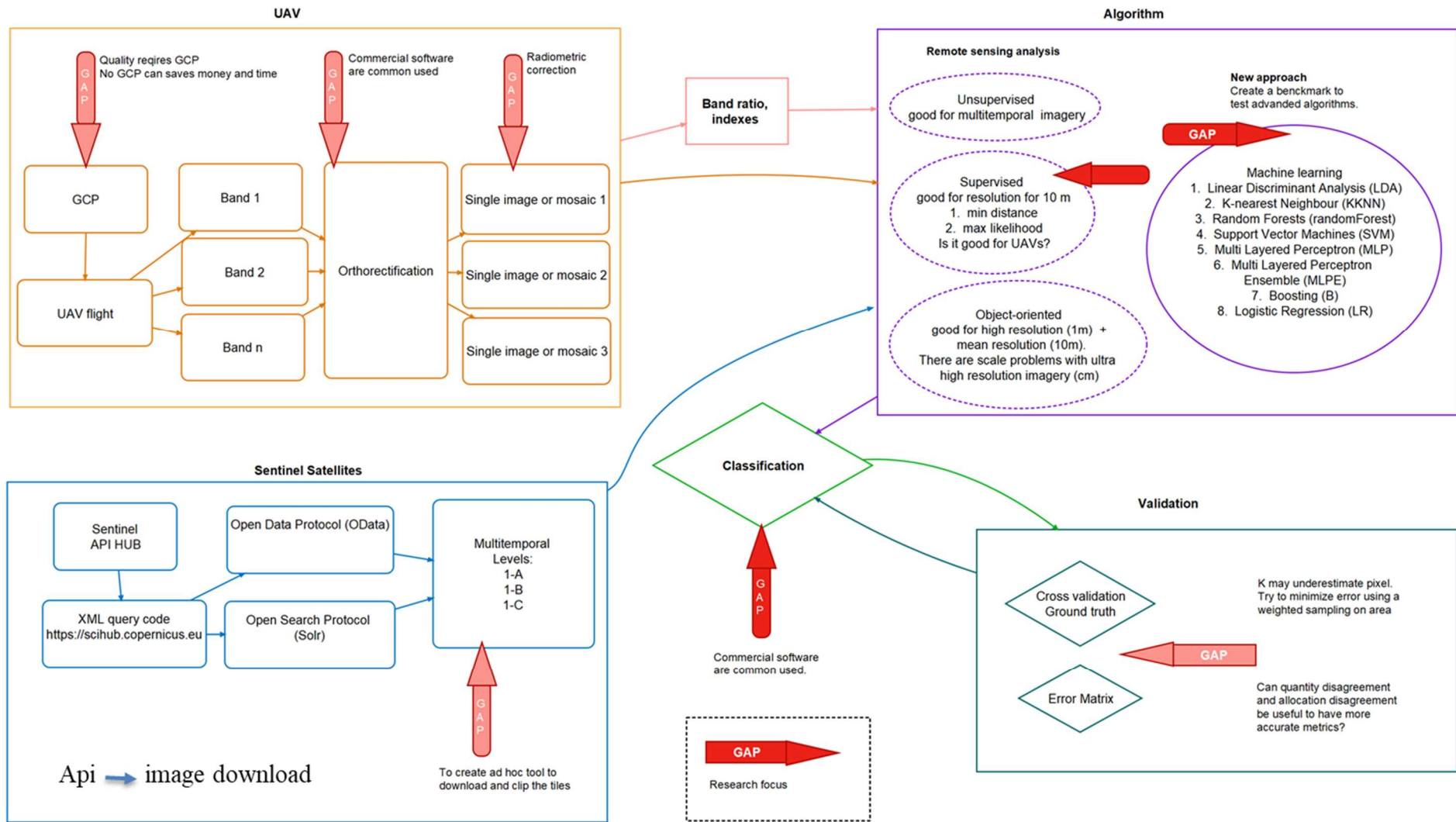
Figure 1 The figure summarizes the main gaps identified from the literature review and the research focus of the thesis

1.3. Research questions and objectives

Chapter 1 introduces the scientific motivation of this work, defines the study object and provides the research topic of this PhD and considering the state of knowledge on the topic, GIS software can integrate information obtained through UAV imagery, satellite imagery, radiometric analysis, and spatial information in order to create LULC maps. The goal is the answer to the following questions:

1. can the classic techniques of remote sensing be used to extract suitable land use/land cover maps – suitable in terms of classification accuracy – from the very high-resolution imagery of UAVs?

2. can information from images of UAVs be merged with data from satellite images in the same area to achieve better results?

3. which methods are optimal to analyse imagery of UAVs, and which benefits can be achieved through the use of more sophisticated techniques, such as the integration of multisource spatial information?

Seen from the above research questions, the specific objectives of this project are:

1. to test standard classification methods of remote sensing.

2. to test advanced classifiers to UAVs only and to UAVs and satellite data integrated together.

3. to integrate spatial and morphological information of objects to the machine learning methods applied for classification.

Paper I presents the conceptual multilevel remote sensing framework to integrate information obtained through UAVs imagery, satellite imagery, radiometric analysis, and spatial information. Moreover, the paper provides a preliminary classification of land use map using open source GIS software.

Piragnolo, M. and Pirotti, F. (2016) 'UAV Technology Integration for Remote Sensing Image Analysis', in Doctoral Consortium, pp. 12–19. Available at: http://www.scitepress.org/DigitalLibrary/PublicationsDetail.aspx?ID=Za27VqkeJrw%3D&t=1.

Paper II focuses on the integration of temporal series collected from Sentinel II and UAVs imagery for monitoring the permanent pastures. The analysis is conducted using VI. The overall objective is to define for each index a set of thresholds to define if a pasture can be classified as permanent pastures and to detect mowed permanent pastures.

Piragnolo, M., Lusiani, G. and Pirotti, F. (2018) 'Comparison of vegetation indices from RPAS and Sentinel-2 imagery for detecting permanent pastures', in International Archives of the Photogrammetry, Remote Sensing and Spatial Information Sciences - ISPRS Archives, pp. 1381–1387. doi: 10.5194/isprs-archives-XLII-3-1381-2018.

Paper III presents a benchmarking of 9 different machine learning algorithms for land-cover mapping using Sentinel-2 imagery. The supervised classification based on regions of interest has been executed on 4% and 50% of dataset pixels. The validation is carried out using a control dataset which consists of an independent classification in 11 land-cover classes, obtained by manual visual interpretation of high resolution images (20 cm ground sampling distance) by experts. The results highlight the performance should be evaluated in terms of accuracy metrics and in terms of computational speed, where using a high number of the pixels can require longer processing times for both classification and training.

Pirotti, F., Sunar, F. and Piragnolo, M. (2016) 'Benchmark of machine learning methods for classification of a Sentinel-2 image', *ISPRS - International Archives of the Photogrammetry, Remote Sensing and Spatial Information Sciences*, XLI-B7, pp. 335–340. doi: 10.5194/isprsarchives-XLI-B7-335-2016.

Paper IV presents a benchmarking for studying the behaviour of two popular machine learning algorithms Random Forest (RF) and Support Vector Machine (SVM) for LULC classification using UAV imagery. The training sets have been randomly obtained as a subset of 2 to 20% of the total number of raster cells, with stratified sampling according to the land-use classes. The results identify the best result for training size larger than 7–8% of the total.

Piragnolo, M., Masiero, A. and Pirotti, F. (2017) 'Open source R for applying machine learning to RPAS remote sensing images', *Open Geospatial Data, Software and Standards*. Open Geospatial Data, Software and Standards, 2(16), p. 7. doi: 10.1186/s40965-017-0033-4.

Paper V presents the optimization of the machine learning benchmark of 9 different machines learning the integration of spatial and morphological information. The spatial and morphological information are: the DTM, the canopy height model (CHM), the slope, the aspect, the roughness, the distance from an arbitrary point from the roads, and the elevation differences from an arbitrary point to the nearest road. The goal is to identify the suitable areas for two classes of forestry machines, which are the skyline and the forwarder. The results highlight the three best performance algorithms in terms of metrics and timing. Finally, a sensitivity analysis identifies the importance of the layers in the classification process.

(In preparation)

2. Paper I: UAV Technology Integration for Remote Sensing Image Analysis

UAV Technology Integration for Remote Sensing Image Analysis

Marco Piragnolo and Francesco Pirotti

CIRGEO, Interdepartmental Research Center of Geomatics, University of Padua, Viale dell'Università, 16
35020 Legnaro, Italy

1. RESEARCH PROBLEM

In this paper, we focus on a multilevel remote sensing framework to integrate information obtained through UAV images, satellite images from Sentinel I and II, radiometric analysis, and spatial information in order to derive informative maps to be used for educated decision support. The goal is the answer to the following questions:

1. Could the classic techniques of remote sensing be used to extract suitable land use maps – suitable in terms of classification accuracy – also for the very high resolution UAV images?

2. Which methods are optimal to analyze UAV images and which benefits could be achieved through the use of more sophisticated techniques, such as the integration of multisource spatial data to add to the feature vector?

3. Could information from UAV images be merged with data from satellite images in the same area, in order to achieve better results?

2. OUTLINE OF OBJECTIVES

Based on the above research questions, the specific objectives of this project are:

1. To test standard classification methods of remote sensing to UAV multispectral images.

2. To integrate spatial and morphological information of objects to the machine learning methods applied for classification

3. To test advanced classifiers to UAV only and to UAV and satellite data integrated together.

3. STATE OF THE ART

In the last years there was a growing demand for innovative tools to monitor geomorphological aspects for environmental analyses, land use, fragmentation of habitats and risk assessment (Piragnolo et al., 2014a; Piragnolo et al., 2014b; Van Asselen et al., 2013) in particular in rural areas which, in many cases, have proved to be of strategic importance to national and regional economy (Marsden, 2010; van Eupen et al., 2012).

Recently, unmanned aircraft vehicles (UAVs) have seen great attention from the scientific community. There are many aspects regarding this attention, the main one is the prospect to get highresolution data "on demand" quickly at a relatively low cost. The technology in terms of cost and availability follows the typical development curve: the prices and weight of the components have decreased, data accuracy has increased, and all with a lower power demand, or a constant power and greater durability of the apparatus as a whole. The market has come at a point where the cost for the apparatus, with RGB or multispectral sensors, becomes accessible to amateur users and to a large audience. Research fields are cultural heritage, archaeology, 3D survey, environmental, forestry and precision agriculture (Berni, 2009; Haarbrink and Koers, 2006; Herwitz, 2004; Hunt, 2010; Lelong, 2008; Remondino et al., 2011). Software for image processing is playing a key role in the diffusion of UAV technology. Since the accuracy of the positioning systems and orientation is not comparable to the classical systems of aerial photogrammetry, the software would compensate this limit with a massive

use of

image matching and structurefrom motion (SfM) techniques. These techniques, coupled with computer vision algorithms, have led to the development of various software for photogrammetric processing available with commercial licenses and Open Source licenses (Remondino et al. 2012). Several authors (Grenzdörffer et al., 2008; Sona et al., 2014) have reviewed this new technology and they have reported some problems in photogrammetric, radiometric aspects and data size:

1. Photogrammetric problems concern the limited size and quality of the sensor in the camera mounted on the UAV; i.e. missing information regarding the internal orientation, distortion of frames, overlapping of frames, low precision of GPS-INS, a high number of the ground control point (GCP) required.

2. Radiometric problems are related to image interpretation, correct use of radiometric information, new techniques for the processing of Multispectral Data and calculation of derived index (Honkavaara et al., 2012, Torres-Sanchez et al., 2014).

3. Sensors with high spatial and temporal resolution produce massive data size which increases exponentially (Zaslavsky, 2013). Data size and processing time can be related to the Big Data paradigm: Big Data not only relates to physical storage, but also to the velocity of acquisition and variability of a number of files, tables, records and processing time (Singh, 2012).

Photogrammetric techniques will be used to obtain the basic data. The evaluation and improvement of the accuracy of the photogrammetric survey will be studied marginally as it has to be taken into account to provide the spatial error budget. In literature, many authors have proposed new frameworks, GIS environments and

objects algorithms in order to solve problems of size and scalability of the dataset (Baumann, 2014; Lin et al., 2013; Peña et al., 2013; Zhao and He, 2009). Radiometric analyses for segmentation and classification for GIS environment are the issues that will be considered in this study.

4. METHODOLOGY

The issues that will be considered are related to analysis in GIS environment thus with full spatial support like image interpretation, spectral information, the calculation of derived indices and the integration of other spatial data (data fusion). UAV data will be collected in test areas where ground information is acquired from experts assigning agricultural classes depending on crop type and yield. These data will be analysed in order to understand whether the classic techniques of remote sensing could be applied - i.e. minimum distance, maximum likelihood algorithms (Richards, 2006) and spectral angle mapping SAM (Kruse, 1993) – to correctly return the class of the area. Whether new techniques are necessary and which benefits could be achieved through the use of more advanced techniques, such as the integration of spatial data to increase the number of features describing significantly the phenomena, which we want to model. The integration of information obtained through photogrammetric methods and remote sensing, such as Sentinel-2 data, might improve the quality of derived products such as land use maps. The accuracies of the classification methods will be evaluated by weighing both the feature information from the reflectance from the spectral bands (optical information), and the information on the spatial proximity between classes or morphological information of the objects; spatial and morphological information is the third dimension obtained by photogrammetric technique (Dalponte et al., 2008). The first example of the feature vector with elements that will be tested is [b1, b2, b3, b4, b5, H, P] where bx are the bands of wavelength increasing from

blue to near infrared, H refers to height from the ground, and P refers to the slope. Standard classifiers and sophisticated classifiers such as support vector machines (SVM) (Melgani and Bruzzone, 2004) and Random Forest (Brieman 2001) will be tested.

Considering the continuous use of multiband UAV digital images, it is necessary to structure data and to apply a harmonious management. It is important to manage the "raw" data, and information obtained from the various stages of the processing, to define the standard products; these data must be kept for further analysis.

5. EXPECTED OUTCOME

5.1. Multilevel Remote Sensing Framework

The expected outcome is to set a procedure for classification and relative algorithms for integrating satellite and UAV data with other spatial information. The best algorithms in term of performance could be integrated into a multilevel remote sensing framework. The framework could integrate the information obtained through photogrammetric methods and remote sensing techniques (Figure 1). The first classification at a smaller scale will be executed on satellite images. Classification results and accuracies will be evaluated using a control dataset, which consists of an independent classification. In case of errors, a deeper analysis at a larger scale will be necessary, e.g. using aerial or drones orthopotos. In Figure 2 we present an initial classification of a test area. It is located at the south-east of the city of Padova, in Italian Veneto Region. The classification is based on Sentinel II images using random Random Forest algorithm. Figure 3 shows the UAV image of the test area flown with a drone. The overlap shows a disagreement between the urban class of classification (red pixels) and crops that can be recognized in UAV orthomosaic. The final classification will be cross validated using a ground-

truth dataset acquired by a team of professionals working in the field of land-use maps.
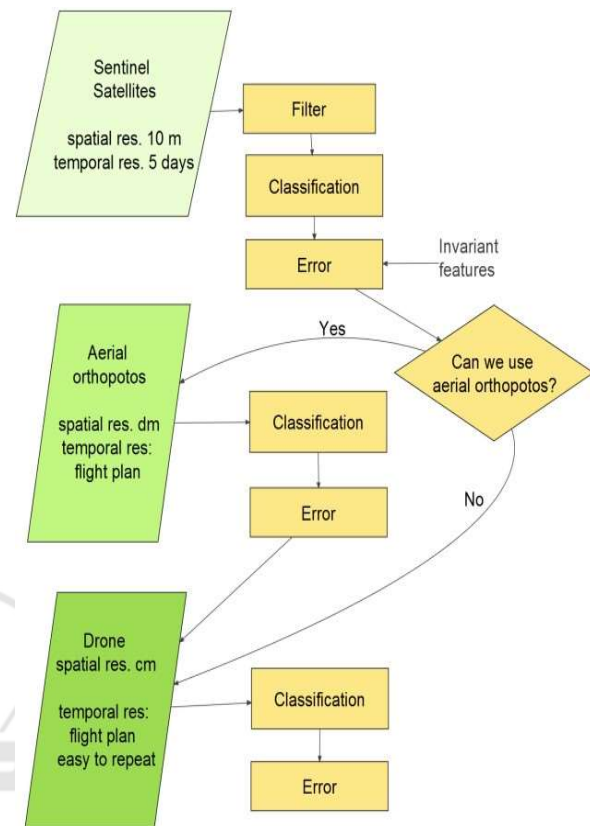

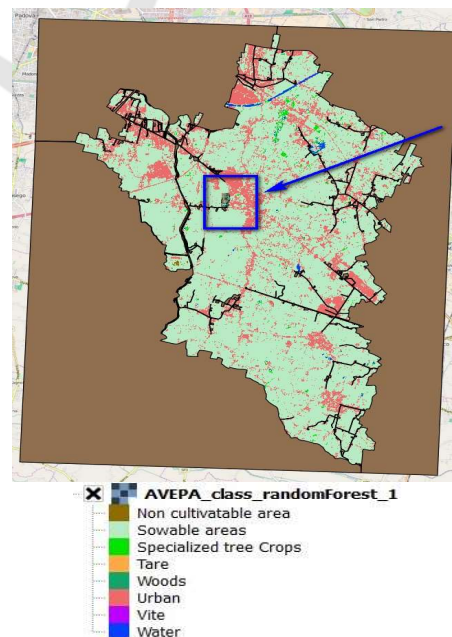Figure 1: The multilevel framework.

Figure 2: Classification map of land use produced by the random forest algorithm.

The expected outcome is a robust procedure to integrate UAV and satellite data to support decision procedures mainly, but not limited to, the field of agricultural crop administration.

Figure 3: The testing area was flown by drone.

5.2. UAV Fly Test

Testing area is located in Legnaro inside Campus of Agripolis of the University of Padova, at south-east of the city of Padova, in Italian Veneto Region. It measures 242 meters width, 508 meters height extension, and the area is twelve hectares. It was chosen because it contains heterogeneous crops, not flat geomorphology, and ground truth is well known. In November 2015 eighteen ground control points (GCP) were put in the area, and the coordinates were collected with GPS in

Real Time Kinematic. The root mean square error of measures is between 0.008 and 0.011 centimetres. Then the area was flown by Agency of Veneto Region for payment in Agriculture (AVEPA), with eBee UAV, Figure 4.

Figure 4: Position of the GCP in the testing area.

Ebee UAV was equipped with three Sensefly cameras, Red Green Blue (RGB), Near Infrared (NIR) and multispectral. RGB camera model was WX. NIR camera model was S110 NIR with three bands, green with central wavelength at 550 nm, red with central wavelength at 625 nm, near infrared with central wavelength at 850 nm. Multispectral camera model was multiSPEC 4C with four bands, green with central wavelength at 550 nm, red with central wavelength at 660 nm, Red edge with central wavelength at 735 nm, near infrared with central wavelength at 790 nm. RGB and NIR camera images had a pixel size of 4.5 centimetres. Multispectral camera images had a pixel

size of 18 centimetres. All images were processed with photogrammetric software Agisoft Photoscan and then orthorectified. The root mean square error for X, Y coordinates for a GCP averaged over all images is reported in Table 1. The error averaged by Photoscan over all the GCP locations is 0.396 pixel. Single band orthomosaic were exported as GeoTIFF file.

Table 1: GCP errors calculated with Photoscan. The error (m) is the root mean square error for X, Y and Z for a GCP point. The proj. is the number of projections for a GCP over all the images.

GCP	XY error (m)	Z error (m)	Error (m)	Proj.	Error (pix)
1	0.0198	0.0002	0.0198	86	0.3340
2	0.0291	-0.0089	0.0304	83	0.3630
3	0.0286	0.0074	0.0295	75	0.3180
4	0.0260	-0.0109	0.0281	92	0.4170
5	0.0156	0.0233	0.0280	106	0.3440
6	0.0331	-0.0307	0.0452	102	0.3180
7	0.0498	-0.0051	0.0500	91	0.4220
8	0.0237	-0.0394	0.0460	109	0.3430
9	0.0193	-0.0069	0.0205	91	0.5160
10	0.0324	0.0783	0.0848	81	0.3980
11	0.0115	-0.0082	0.0141	85	0.4350
12	0.0316	0.0116	0.0336	88	0.3780
13	0.0111	-0.0116	0.0160	116	0.4260
14	0.0480	0.0392	0.0620	84	0.3470
15	0.0267	-0.0550	0.0611	100	0.4100
16	0.0562	0.0613	0.0832	89	0.4590
17	0.0467	-0.0005	0.0467	78	0.3540
18	0.0300	-0.0135	0.0329	45	0.5410
Tot	0.0198	0.0002	0.0456		0.3960

Band	Camera	Wavelength nm
Blue	RGB	450
Green	multiSPEC 4C	550
Red	NIR	625
Red	multiSPEC 4C	660
Red Edge	multiSPEC 4C	735
Nir	multiSPEC 4C	790
Nir	NIR	850

We used Semi-Automatic Classification Plugin Version 4.9. To test two algorithms, Minimum distance and Maximum likelihood, we chose four classes that are, 1 - urban, 2 - ploughed land, 3- crops and 4- vegetation, and we identified regions of interest (ROI) using the specific tool. Minimum distance classification is shown in Figure 5.

5.3. Classification

In the previous step, we have orthorectified nine bands. Then we have selected seven bands in order to have continuous spectrum coverage without overlaps (Table 2), and we uploaded the images in QGis.

Table 2: Bands selected for the classification test.

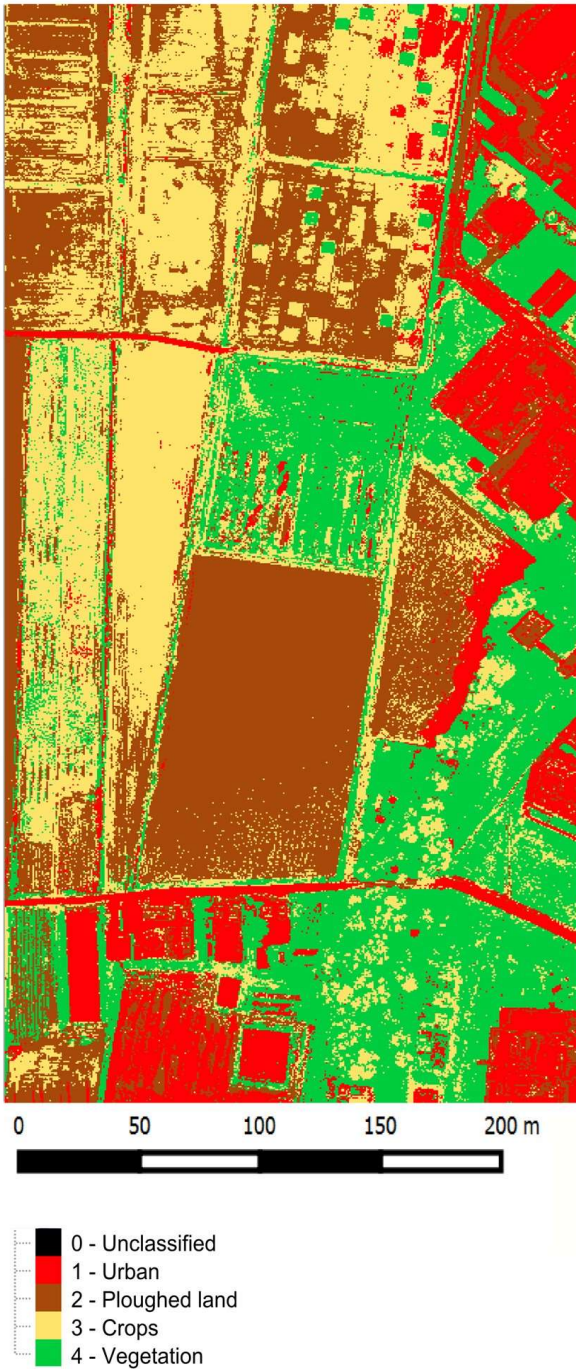Table 4 shows the error matrix. Kappa index for Maximum likelihood is 0.92.

Figure 5: Classification with Minimum Distance algorithm.

In order to assess the classification accuracy a comparison ROI was created and it was used to calculate error matrix (Table 3) and Kappa index. Kappa index for Minimum distance classification is 0.64. Then we applied the same procedure for Maximum likelihood algorithm. Figure 6 shows the classification map, and

Figure 6: Classification with Maximum likelihood algorithm.

Table 3: Error matrix for Minimum distance classification.

Class	Reference				
	1	2	3	4	Tot.
1	32718	4313	0	479	37510
2	10779	389257	2276	0	402312
3	877	53722	32506	29239	116344
4	0	0	6793	50438	57231
Tot.	44374	447292	41575	80156	613397

Table 4: Error matrix for Maximum likelihood classification.

Class	Reference				
	1	2	3	4	Tot.
1	42746	306	0	0	43052
2	1438	442206	6342	0	449986
3	0	4610	27994	842	33446
4	190	170	7239	79314	86913
Tot.	44374	447292	41575	80156	613397

5.4. Conclusion

This work is a preliminary analysis to explore the potentiality of Satellite images coupled with UAV images. We have defined a procedure for integrating satellite and UAV data, and we have tested two classic remote sensing algorithms, Minimum distance and Maximum likelihood with UAV data. Images were collected with eBee drone, using different sensors. Then they were orthorectified and classified in four classes, urban, ploughed land, crops and vegetation. The accuracy of classification was estimated with the K index. Maximum likelihood got 0.91, while Minimum distance got 0.64. In literature, Maximum likelihood algorithm is one of the most popular classifiers used in remote sensing from the satellite. In this preliminary test with images from a drone, Maximum likelihood algorithm gives a better result than Minimum distance classifier. In Figure 7 we can see two comparisons between the algorithms and ground truth. On left

images, Minimum distance algorithm classifies trees as buildings, while Maximum likelihood assigns trees to vegetation class. On right images, Minimum distance Algorithm produces confused classification. Maximum likelihood is more precise, but it mixes crops and vegetation.

6. STAGE OF THE RESEARCH

At the moment the research is at the initial phase as the project started a few months ago. In this contribution, we want to present the research question and the methods, which will be tested in the project.
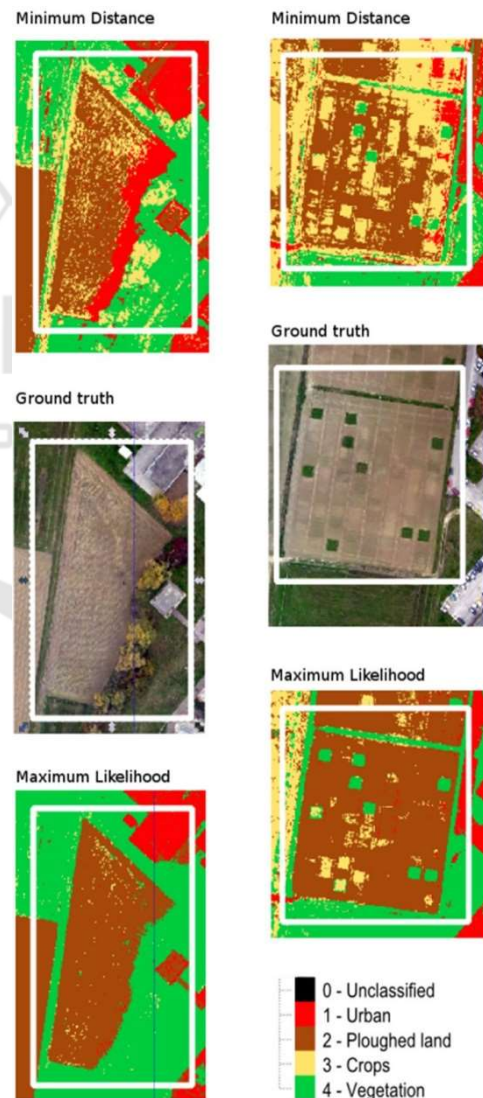

Figure 7: Comparison between classifications obtained two Minimum distance and Maximum likelihood algorithms.

REFERENCES

Baumann, P., 2014. Spatio-Temporal Big Data the rasdaman approach, p.32. Available at: http://2014.ogrs-community.org/2014_workshops/Ras daman/BigDataRasdamanWorkshop.pdf.

Berni, J., Zarco-Tejada, P. J., Suarez, L., Fereres, E., 2009. Thermal and narrowband multispectral remote sensing for vegetation monitoring from an unmanned aerial vehicle. IEEE Transactions on Geoscience and Remote Sensing, 47, pp.722–738.

Breiman, L., 2001. Random forests. Machine Learning, 45, 5–32. doi:10.1023/A:1010933404324.

Coppa, U., Guarnieri, A., Pirotti, F., and Vettore, A., 2009. Accuracy enhancement of unmanned helicopter positioning with low-cost system. Applied Geomatics, 1(3), pp.85–95.

Dalponte, M., Bruzzone, L., Gianelle, D., Member, S., 2008. Fusion of Hyperspectral and LIDAR Remote Sensing Data for Classification of Complex Forest Areas. IEEE Transactions on Geoscience and Remote Sensing, 46(5), pp.1416–1427.

Grenzdörffer, G., Engel, A., Teichert, B., 2008. The photogrammetric potential of low-cost UAVs in forestry and agriculture. International Archives of Photogrammetry Remote Sensing and Spatial

Information Sciences, 1, pp.1207–1213. Available at: http://www.isprs.org/proceedings/XXXVII/congress/1_pdf/206.pdf.

Haarbrink, R., Eisenbeiss, H., 2008. Accurate DSM production from unmanned helicopter systems. International Archives of Photogrammetry Remote Sensing and Spatial Information Sciences, Vol. XXXVI, pp.1259–1264. Available at: http://www.isprs.org/proceedings/XXXVII/congress/1_pdf/214.pdf.

Herwitz, S.R., Johnson, L.F., Dunagan, S.E., Higgins, R.G., Sullivan, D. V., Zheng, J., Lobitz, B.M., Leung, J.G., Gallmeyer, B. a., Aoyagi, M., Slye, R.E., Brass, J. a., 2004. Imaging from an unmanned aerial vehicle: Agricultural surveillance and decision support. Computers and Electronics in Agriculture, 44(1), pp.49–61.

Honkavaara, E., Kaivosoja, J., Mäkynen, J., Pellikka, I., Pesonen, L., Saari, H., Salo, H., Hakala, T., Marklelin, L., Rosnell, T., 2012. Hyperspectral Reflectance Signatures and Point Clouds for Precision Agriculture By Light Weight UAV Imaging System. ISPRS Annals of Photogrammetry, Remote Sensing and Spatial Information Sciences, I-7(September), pp.353–358.

Hunt, E.R., Dean Hively, W., Fujikawa, S.J., Linden, D.S., Daughtry, C.S.T., McCarty, G.W., 2010. Acquisition of NIR-green-blue digital photographs from unmanned aircraft for crop monitoring. Remote Sensing, 2(1), pp.290–305.

Kruse, F. A., Lefkoff, A.B., Boardman, K.B. Shapiro, A.T., Barloon, P.J., Goetz, A.F.H., 1993. The Spectral Image Processing System (SIPS) - Interactive Visualization and Analysis of Imaging Spectrometer Data. Remote Sensing of Environment, 44, pp.145–163. doi:10.1016/0034-4257(93)90013-N.

Lelong, C.C.D., Burger, P., Jubelin, G., Roux, B., Labbé, S., Baret, F., 2008. Assessment of unmanned aerial vehicles imagery for quantitative monitoring of wheat crop in small plots. Sensors, 8(5), pp.3557–3585.

Lin, F.-C., Chung, L.-K., Ku, W.-Y., Chu, L.-R., Chou, T.-Y., 2013. The Framework of Cloud Computing Platform for Massive Remote Sensing Images. Advanced Information Networking and Applications (AINA), 2013 IEEE 27th International Conference on, pp.621–628. Available at: http://ieeexplore.ieee.org/xpls/icp.jsp?arnumber=6531812.

Marsden, T., 2010. Mobilizing the regional eco-economy: evolving webs of agri-food and rural development in the UK. Cambridge Journal of Regions, Economy and Society, 3 (2), pp.225–244. Available at: http://cjres.oxfordjournals.org/content/3/2/225.abstract.

Melgani, F. and Bruzzone, L., 2004. Classification of hyperspectral remote sensing images with support vector machines. Geoscience and Remote Sensing, IEEE Transactions on, 42(8), pp.1778–1790.

Peña, J.M., Torres-Sánchez, J., de Castro, A.I., Kelly, M., López-Granados, F., 2013. Weed Mapping in EarlySeason Maize Fields Using Object-Based Analysis of Unmanned Aerial Vehicle (UAV) Images. PLoS ONE, 8(10), pp.1–11.

Piragnolo, M., Pirotti, F., Vettore, A., Salogni, G., 2014a. ANTHROPIC RISK ASSESSMENT ON BIODIVERSITY. ISPRS - International Archives of the Photogrammetry, Remote Sensing and Spatial Information Sciences, XL-5/W3, pp.21–26. doi:10.5194/isprsarchives-XL-5-W3-21-2013.

Piragnolo, M., Pirotti, F., Guarnieri, A., Vettore, A., Salogni, G., 2014b. Geo-Spatial Support for Assessment of Anthropic Impact on Biodiversity. ISPRS International Journal of Geo-Information, 3, pp.599–618. doi:10.3390/ijgi3020599.

Remondino, F., Barazzetti, L., Nex, F., Scaioni, M., Sarazzi, D., 2011. UAV photgrammetry for mapping and 3D modeling current status and future perspectives. International Archives of the Photogrammetry, Remote Sensing and Spatial

Information Sciences, XXXVIII (September), pp.14–16.

Remondino, F., Del Pizzo, S. 2012. Low-cost and opensource solutions for automated image orientation–a critical overview. Progress in Cultural Heritage Preservation, pp.40–54. Available at: http://link.springer.com/chapter/10.1007/978-3-642-34234-9_5.

Richards, J. A., Jia, X., 2006. Remote Sensing Digital Image Analysis: An Introduction. Berlin, Germany: Springer.

Singh, S., Singh, N., 2012. Big Data analytics. 2012 International Conference on Communication, Information and Computing Technology (ICCICT), pp.1–4. Available at: http://ieeexplore.ieee.org/lpdocs/epic03/wrapper.htm?arnumber=6398180.

Sona, G., Pinto, L., Pagliari, D., Passoni, D., Gini, R., 2014. Experimental analysis of different software packages for orientation and digital surface modelling from UAV images. Earth Science Informatics, 7(2), pp.97–107.

Torres-Sánchez, J., Peña, J.M., de Castro, a. I., LópezGranados, F., 2014. Multi-temporal mapping of the vegetation fraction in early-season wheat fields using images from UAV. Computers and Electronics in Agriculture, 103, pp.104–113.

Van Asselen, Sanneke, and Peter H. Verburg. 2013. Land Cover Change or Land-Use Intensification: Simulating Land System Change with a Global-Scale Land Change Model. Global Change Biology, 19, pp.3648–3667. doi:10.1111/gcb.12331.

Van Eupen, M., Metzger, M.J., Pérez-Soba, M., Verburg, P.H., van Doorn, a., Bunce, R.G.H., 2012. A rural typology for strategic European policies. Land Use Policy, 29(3), pp.473–482. Available at: http://dx.doi.org/10.1016/j.landusepol.2011.07.007.

Zaslavsky, A., Perera, C., Georgakopoulos, D., 2013. Sensing as a Service and Big Data, in: arXiv Preprint arXiv:1301.0159. Bangalore.

Zhao, W., Ma, H. and He, Q., 2009. Parallel K-Means Clustering Based on Map Reduce. Cloud Computing, 5931, pp.674–679. Available at: http://link.springer.com/chapter/10.1007/978-3-642-10665-1_71

3. **Paper II: Comparison of vegetation indices from RPAS and Sentinel-2 imagery for detecting permanent pastures**

COMPARISON OF VEGETATION INDICES FROM RPAS AND SENTINEL-2 IMAGERY FOR DETECTING PERMANENT PASTURES

M. Piragnolo [a,b] , G. Lusiani [c] , F. Pirotti [a,b]

[a] CIRGEO, Interdepartmental Research Center of Geomatics, University of Padua, Viale dell'Università 16, 35020 Legnaro, Italy
[b] TESAF Department, University of Padua, Viale dell'Università 16, 35020 Legnaro, Italy - francesco.pirotti@unipd.it
[c] AVEPA, Agenzia Veneta per i Pagamenti in Agricoltura, via Niccolò Tommaseo 67/C 35131, Padova, Italy - giovanni.lusiani@avepa.it

Commission III, WG III/10

KEY WORDS: remotely piloted aircraft systems, RPAS, UAV, Sentinel-2, Copernicus, NDVI, vegetation indices, agricultural monitoring

ABSTRACT:

Permanent pastures (PP) are defined as grasslands, which are not subjected to any tillage, but only to natural growth. They are important for local economies in the production of fodder and pastures (Ali et al. 2016). Under these definitions, a pasture is permanent when it is not under any crop-rotation, and its production is related to only irrigation, fertilization and mowing. Subsidy payments to landowners require monitoring activities to determine which sites can be considered PP. These activities are mainly done with visual field surveys by experienced personnel or lately also using remote sensing techniques. The regional agency for SPS subsidies, the Agenzia Veneta per i Pagamenti in Agricoltura (AVEPA) takes care of monitoring and control on behalf of the Veneto Region using remote sensing techniques. The investigation integrates temporal series of Sentinel-2 imagery with RPAS. Indeed, the testing area is a specific region were the agricultural land is intensively cultivated for the production of hay harvesting four times every year between May and October. The study goal of this study is to monitor vegetation presence and amount using the Normalized Difference Vegetation Index (NDVI), the Soil-adjusted Vegetation Index (SAVI), the Normalized Difference Water Index (NDWI), and the Normalized Difference Built Index (NDBI). The overall objective is to define for each index a set of thresholds to define if a pasture can be classified as PP or not and recognize the mowing.

INTRODUCTION

Permanent pastures (PP) are defined as grasslands, which are not subjected to any tillage, but only to natural growth, (self-seeded). There is more precisely defined by European Union's fundamental reform of the Common Agricultural Policy (CAP), which introduced the new Single Payment Scheme (or Single Farm Payment, SPS) for direct subsidy payments to landowners. The SPS definition of permanent pastures is as follows: "land used to grow grasses or other herbaceous forage naturally (self-seeded) or through cultivation (sown) and that is not included in the crop rotation of the holding for five years or longer". PP are a major source of nutrients for livestock and are of major importance from an ecological point of view and as carbon sinks in the carbon cycle. They are also important for local economies in the production of fodder and pastures (Ali et al. 2016). Under these definitions, a pasture is permanent when it is not under any crop-rotation, and its production is related to only irrigation, fertilization and mowing. The production capacity is therefore mostly associated with environmental factors and a certain type of human activity (Xu et al. 2008). Managing PP requires some activities of monitoring and control. In literature, investigations over PP have been carried out to determine the amount of vegetation cover under a certain type of actions (Schmidt et al., 2010), to evaluate the effects of grazing from livestock (Bastin et al. 2012, Blanco et al. 2009, Li et al. 2016), the impact of climate change over PP and ecological aspects thereof (Saornil et al., 2008, Förster et al., 2012).

Subsidy payments to landowners require monitoring activities to determine which sites can be considered PP. These activities are mainly done with visual field surveys by experienced personnel or lately also using remote sensing techniques. To monitor large areas with remote sensing, high-density temporal series are necessary, at least one image every ten days (Morel et al. 2014, O'Connor et al. 2012). In Italy, the Parmigiano-Reggiano area was subjected to investigation, using a persistency index of the Normalized Difference Vegetation Index (NDVI) from Landsat scenes over 10 years; PP has a persistency index value of >0.04, whereas pastures that are not permanent cycle through a range between -0.02 e -0.04 (Bocci et al., 2011). High-density temporal images are often not always available: for example because of cloud-cover, which is common in some areas. In addition, a delay between the tillage of a site and a cloudless image from a satellite might cause an incorrect false negative due to young vegetation growth happening between the tillage and the satellite visit.

Lately, remotely piloted aircraft systems (RPAS) have gained a strong momentum in terms of usage. This is due mainly to lower costs, lighter apparatus and longer lasting batteries, which allow longer flights and lower costs. In addition, improvements in software development have contributed to a growth in popularity of close-range remote sensing with RPAS (Rutzinger et al., 2016). Multispectral cameras mounted on RPAS allow custom deployment for multi-band imagery over areas of interest. RPAS is, therefore, a suitable candidate to fill the gaps in the timeline where satellite imagery is not available (Pirotti et al., 2015), be it

for long revisit times, for cloud cover or for a combination of both (Pirotti et al., 2017).

In the following note a specific region is considered were the agricultural land is intensively cultivated for the production of hay harvesting four times every year between May and October. The regional agency for SPS subsidies, the Agenzia Veneta per i Pagamenti in Agricoltura (AVEPA) takes care of monitoring and control on behalf of the Veneto Region. Usually, the controls are made manually with trained personnel moving physically to the area that must be assessed. Latest developments in remote sensing technologies have pushed AVEPA to investigate over using such technologies for decision support. The objectives of the presented investigation are to integrate temporal series of Sentinel-2 imagery with RPAS imagery for monitoring candidates to PP. The analysis uses existing vegetation indices to relate reflectivity of different amounts of grass cover, which indicates how the pasture is managed and if it can be considered PP. The indices that will be used are the following: NDVI, to monitor vegetation presence and amount, the Soil-adjusted Vegetation Index (SAVI) to take into consideration the effect of soil, the Normalized Difference Water Index (NDWI) to test if information on wetness improves results, and the Normalized Difference Built Index (NDBI) to see if such information also provides significant information to define a pasture.

The overall objective is to define for each index a set of thresholds to define if a pasture can be classified as PP or not and to detect mowed PP.

MATERIALS AND METHOD

2.1 Study area and dataset

The study area is located in the north of Italy, in the Veneto Region; five sites in the area were investigated (Figure 1)
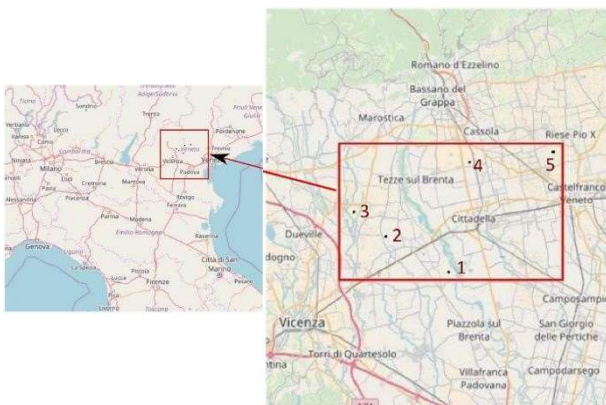

Figure 1. Study area with five sites: 1 Piciacio, 2 Albereria, 3 Palmirona, 4 Rossano, 5 Dussin

The five sites are distributed in different municipalities, where land use and the cultural calendar is known; cultural calendar means that the type of crop present at a time of the year is known. The areas are defined as Piciacio, Albereria, Palmirona, Rossano and Dussin (see Figure 2).

The five test areas were surveyed with a remotely piloted aircraft system, the "eBee Sensfly" equipped with a multispectral

multiSPEC 4C camera. Flights were carried out between April and October 2016 for five flights over each site. The sensor records incoming radiation in four bands, respectively Green (G) - 550 nm, Red (R) - 660 nm, Red Edge (RE) - 735 nm and Near Infrared NIR - 790 nm). A number of targets were used as Ground Control Points (GCPs) whose coordinates were measured with a GNSS receiver in RTK mode. The images were processed with Pix4D© creating an orthomosaic with ground sampling distance of 0.2 m.
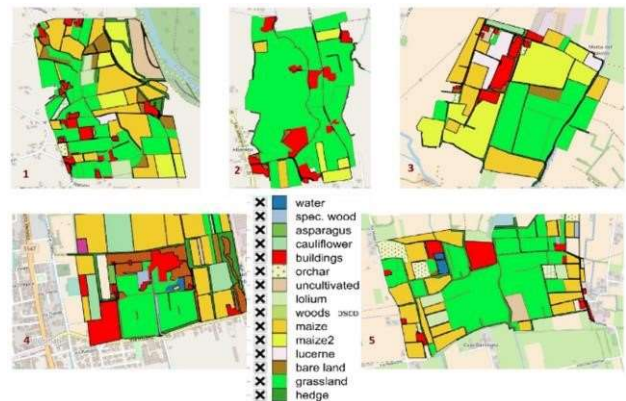

Figure 2. Land-use maps of the five sites: 1 Piciacio, 2 Albereria, 3 Palmirona, 4 Rossano, 5 Dussin

Satellite imagery of the area was downloaded for dates as close as possible to the dates of the RPAS flights (Figure 3. Sentinel-2 images, freely available from the European Space Agency (ESA), where used. The following vegetation indices were extracted: NDVI, SAVI, NDWI, and NDBI. For each of these indices, local statistics, i.e. average and standard deviation, have been extracted for three different groups: urban, PP and mowing on PP. The urban class is related to rooftops, which should have more stable values of these indices, and can, therefore, be used to monitor small differences which can be caused by factors other than the surface composition – e.g. atmospheric effects.
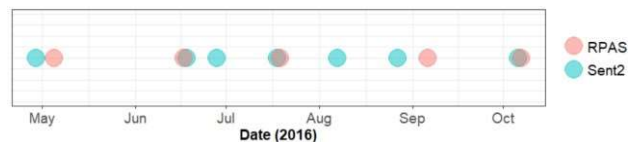

Figure 3. Timeline of data acquisition

2.2 Tested vegetation indices

2.2.1 NDVI: is the well-known normalized ratio between red (R) and near infrared (NIR) (Rouse et al. 1973) and it is one of the most used vegetation indices (Baluja et al. 2012, Bendig et al. 2015, Diaz-Varela et al. 2014, Herwitz et al, 2004, Pérez-Ortiz et al. 2015, Sugiura et al. 2005, Tokekar et al. 2013, Torres-Sánchez et al. 2015, Tucker 1979, Turner et al. 2010). The formula is the following:

$$NDVI = \frac{NIR-R}{NIR+R} \qquad (1)$$

The anatomy and physiology of the leaf absorbs radiation from wavelengths around the red area of the spectrum and reflects the

near infrared. The index varies between -1 and 1. Higher values are related to healthy photosynthetic vegetation, lower values are related to stressed vegetation or no vegetation (bare soil). In literature, NDVI is used to study monitor vegetation health, hydrologic stress and the amount of biomass. In this study, NDVI has been extracted from RPAS and satellite imagery. In RPAS imagery, the NIR band that is available from the MultiSPEC 4C sensor is related to a wavelength of 790 nm. Therefore, NDVI was calculated using this wavelength as NIR band. Sentinel-2 has different bands in the NIR area of the spectrum. Usually, band number 8 is used for NDVI extracting, having information from radiation in the 842 nm and 10 m ground sampling distance (GSD). In our case, we used also band 7, which has a GSD of 20 m, but represents reflectance from radiation at 783 nm, very close to the recorded wavelength of the MultiSPEC 4C NIR band.

2.2.2 SAVI originates from the NDVI index (Huete *et al.* 1988) and uses a constant factor, L, for correcting for luminance. L varies depending on terrain conditions and vegetation cover. An L value of 0 indicates areas with dense vegetation cover, whereas 1 indicates areas without or with very little vegetation.
The formula is the following:

$$SAVI = \frac{NIR - R}{NIR + R} \qquad (2)$$

In this investigation, we empirically applied an L value equal to 0.5. The hypothesis is that upon mowing, the pasture there will be a significant radiometric contribution by bare soil. Therefore, SAVI can give an improved description of the situation of the pasture cover.

2.2.3 NDWI is a normalized ratio between a NIR band and a Short-Wave Infrared (SWIR) band, respectively around 860 nm and 1240 nm wavelengths. It is an index is correlated with the water content of vegetation. It is widely used in precision agriculture, forest health monitoring and other applications were the status of vegetation is sensible to its modification in terms of water content. It varies between -1 e 1, where green healthy vegetation has values between 0.02 and 0.6 (Sentinel-Hub, 2018, Quadratic 2018). In literature, NDWI is calculated using SWIR at 1240 nm because in this region there is high reflectance by water and low absorbance by cellulose. Other areas in the wavelength spectrum, which have a strong reflectivity by water, are in the interval between 1500-2500 nm. In case of dense vegetation, these are less efficient. Nevertheless, Sentinel 2 does not have a band a wavelength of 1240 nm. The bands 11 and 12 have a wavelength of 1610 and 2190 nm can be used for this purpose. Using the band 11, the dry vegetation reflectivity is 0.3 and the green vegetation reflectivity is 0.6. Using the band 12 the dry vegetation reflectivity is 0.15 and the green vegetation reflectivity is 0.4 (Gao, 1996). Band 11 has been used to calculate the NDBI index. To avoid overlapping with band 11, and considering the sparse vegetation cover of mowing and the summer hydric stress, NDWI index has been calculated to using the band 12.

$$NWI = \frac{NIR\ 0.842 - NIR\ 2.190}{NIR\ 0.842 + N\ \ 2.190} \qquad (3)$$

2.2.4 NDBI is a normalized ratio between a SWIR and NIR bands, and it varies between -1 e 1. It is useful to recognize urban areas from vegetated areas, o water bodies. The vegetated areas and agricultural lands have negative or zero values, whereas barren lands or buildings have positive values (Zha et al. 2003). In this

study, the NDBI ratio has been calculated using the band number 8 and 11 of Sentinel 2 around 842 nm and 1610 nm wavelengths. The aim is to recognize bare soil and the not vegetated areas due to harvesting in agricultural land.

$$NBI = \frac{NIR\ 1.610 - NIR\ 0.842}{NIR\ 1.610 + NIR\ 0.842} \qquad (4)$$

RESULTS AND DISCUSSION

Results report on average and standard deviation of values of indices mentioned in the previous section, for three classes, PP, mowed PP and urban elements (i.e. rooftops). Discussion of these values refers to Figure 5, which is available in the next page.

NDVI value was first calculated for urban areas as reported in Figure 4. These areas should have a stable trend during the year. The value is the mean of pixels falling completely inside the area of the urban element (i.e. rooftop) as depicted in Figure 4.
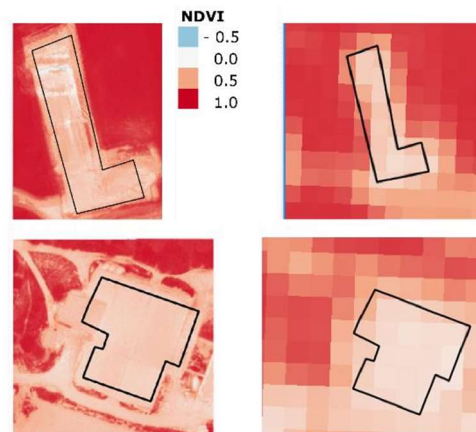

Figure 4. Comparison between NDVI calculated using RPAS images with a resolution of 20 cm/pixel (left) and Sentinel 2 images with a resolution of 10 m/pixel (right)

NDVI values calculated with band 7 of Sentinel 2 are higher than NDVI values obtained with using the band 8 (Figure 5).
Furthermore, the NDVI from the Satellite imagery exceed the NDVI from RPAS. The spatial resolution of 10 meters is sufficient to recognize the buildings, but it is affected by the noise of neighbour green areas, in particular using the band 7 with a resolution of 20 meters. The images were acquired at different time, so it is not possible to calculate the differences. The graphic comparison between satellite and RPAS highlight a difference of 0.15.

Regarding PP, only two areas in Piciacio site (355 and 360) have NDVI values higher than 0.70 as shown in Figure 5. The NDVI, which has been calculated in the area 355 using the band 8 of Sentinel 2, ranges between 0.66 and 0.80 (Figure 5). The minimum value is reached during the summer season in July and August. The NDVI trend, which has been calculated using RPAS, is similar to satellite ones. Nevertheless, since 19th July the RPAS NDVI exceeds the Satellite NDVI. The NDWI and SAVI trend are similar to the NDVI ones. NDWI maximum value, reached in July, is 0.65. The minimum NDWI value, reached in August, is 0.42. The NDBI has a different behaviour reaching the maximum

of -0.13 during the summer. In the springs and autumn, the minimum values are stable around -0.38.
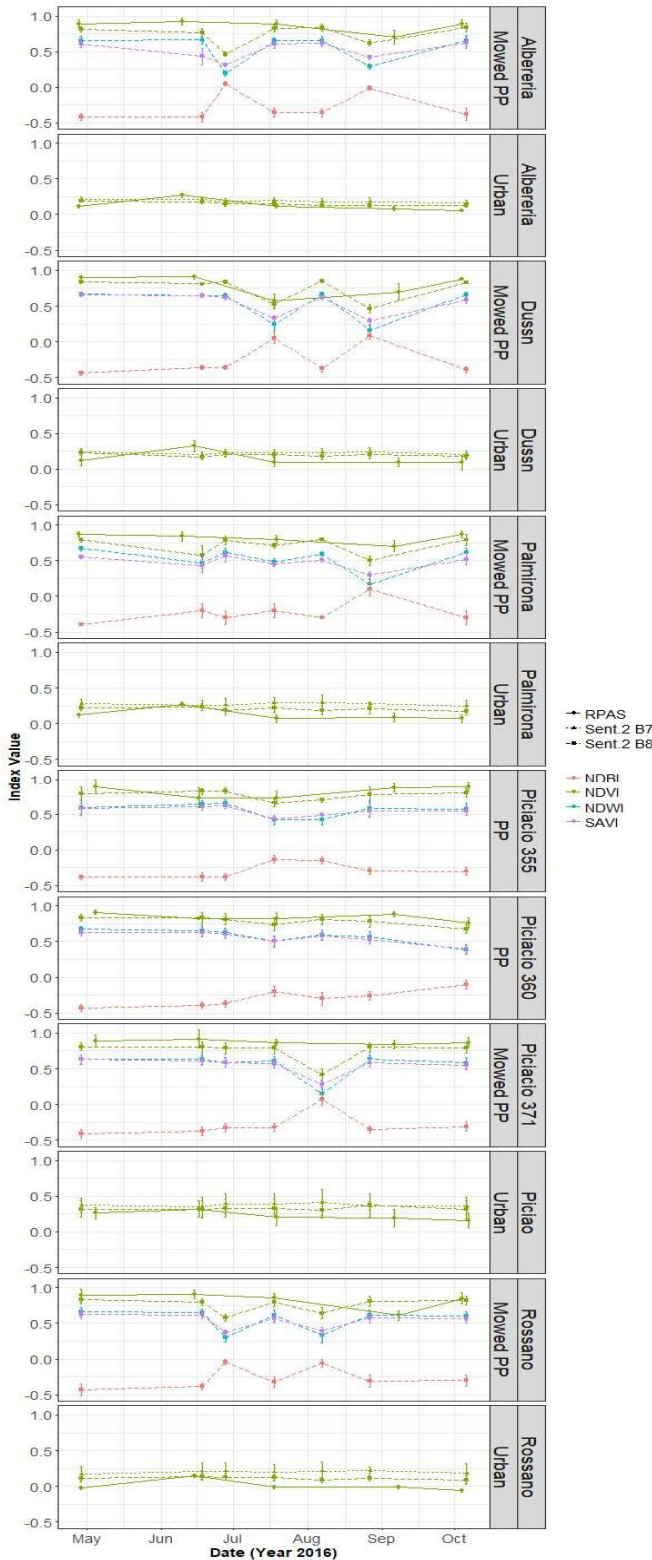

Figure 5. Mean values of indices inside areas with different classes – standard deviation is reported in error bars

The NDVI, calculated in Piciacio site at area 360 with Sentinel 2 band 8, ranges between 0.74 and 0.83 in Figure 5, and the minimum value is reached in July. The NDVI, which has been

calculated using RPAS, exceed the NDVI calculated using Satellite. RPAS shows a stable trend around 0.82, whereas the satellite has values around 0.74. The NDWI trend is similar to NDVI. The minimum value is 0.42, and it was registered in July and August. The SAVI is similar to NDWI trend, and the minimum value is 0.50. The NDBI ranges between -0.40 in spring and 0 in autumn. In summer the average values are -0.20. The mowed PP class has been recognized in each testing areas as shown in Figure 5.

Figure 6. Mowed PP class in each testing area

The NDVI has been calculated using Sentinel-2 in the Piciacio study site in area 371. It reaches a negative peak of 0.42 as shown in Figure 5. The SAVI and NDWI are 0.15 and 0.28, whereas NDBI is positive. In the literature, positive values indicate urban areas or barren land. Considering, the low values of NDVI and SAVI and positive values for NDBI the cover is thin, and probably the imagery were acquired in the same period of the mowing Instead, the peak can not be recognized using the RPAS. Indeed, there is not a temporal overlap between the peak and the RPAS imagery.

The NDVI calculated in Albereria site has two negative peaks. The first one is at the end of June, and NDVI is 0.46. The second one is at the end of August, and NDVI is 0.62 as shown in Figure 5. In June, the SAVI is around than 0.3, and NDWI is around 0.2. NDBI assumes positive values, which confirms the mowing. In August cutting of the pasture (i.e. mowed PP class) is related to a negative peak, where NDVI is 0.62, SAVI 0.41, NDWI 0.29, and NDBI -0.02. NDBI values near zero has been interpreted as vegetation growth.

RPAS imagery in two cases does not recognize the mowing of pasture grass because the two flights were done one month before and one month later, as Figure 5 – Albereira area and Piciacio 371 area.

In the area Palmirona, between June and September, the NDVI trend is not stable as shown in Figure 5. In the middle of June the NDVI value is 0.59. NDWI and SAVI range between 0.5 and 0.5, whereas NDBI is -0.23. Probably, mowing has occurred between 10th and 18th of June.

In July, NDVI is decreasing from 0.78 to 0.71. Then, it increases to 0.80. SAVI and NDWI range between 0.48 and 0.61, and NDBI reachs the peak at -0.18. The High NDVI values, which are above 0.70, but instable, coupled with the other indices suggests it can be a stress of vegetation. Nevertheless, between 28th of June and 18th of July, there are no data to exclude mowing activity.

In August, the absence of vegetation is clear as shown by low NDVI, NDWI and SAVI and NDWI values. NDVI is 0.50, NDWI is 0.17, and NDBI is positive. This highlights the presence of dry vegetation or barren land. RPAS NDVI is stable, and in September, it is decreasing.

In Rossano area, the average value for NDVI calculated using Satellite is 0.8 as shown in Figure 5. In July and August, the NDVI reaches the minimum of 0.58 and 0.64. The other indices have the same trend, and NDBI ranges between -0.04 and -0.06. Consequently, considering indices values, the PP has been probably mowed. Instead, in the same period, NDVI derived from RPAS imagery showed a decrease in September. The NDVI in September is 0.61 and it is similar to satellite values registered in July and August. On one hand, it can suggest that pasture grass was cut, on the other hand, there are no satellite data to confirm this hypothesis.

In the Dussin area, the indices fall in July and August. In both dates, it is clear that the steep decrease of NDVI going to values of 0.52 and 0.57. A similar trend has been found for NDWI, SAVI and NDBI. In July and August, NDWI values are 0.24 and 0.16, SAVI values are 0.33 and 0.29, and NDBI values are 0.05 and 0.09 as shown in Figure 5. This trend has been detected by both Sentinel-2 and RPAS data.

The minimum values for the indices have been summarized in the following tables Table 1 and Table 2.

PP	Piciacio 355 min peak	Piciacio 360 min peak	Average
RPAS NDVI	0.73	0.76	0.75
SAT. NDVI	0.66	0.74	0.70
SAT. NDWI	0.42	0.50	0.46
SAT. SAVI	0.44	0.50	0.47
SAT. NDBI	-0.13	-0.20	-0.17

Table 1. Minimum and average values used to set the PP threshold

	Average all areas
RPAS NDVI	0.57
SAT. NDVI	0.53
SAT. NDWI	0.26
SAT. SAVI	0.35
SAT. NDBI	0.02

Table 2. Minimum and average values used to set the threshold for the Mowed PP class

Then, the PP class average has been compared with an average of the Mowed PP class (Table 1 and Table 2) to set classification threshold as shown in the table below.

	Mowed	Probably Mowed	PP
NDVI SAPR	< -0.57	0.57 - 0.75	> 0.75
NDVI	< 0.53	0.53 - 0.70	> 0.70
NDWI	< -0.26	0.26 - 0.46	> 0.46
SAVI	< -0.35	0.35 - 0.47	> 0.47
NDBI	> 0	-0.25 - 0	< -0.25

Table 3. Threshold defined according to tables above

CONCLUSION

In this paper, we report results on a comparison of NDVI, NDWI, SAVI and NDBI in urban areas, PP and mowed PP. NDVI has been calculated using RPAS imagery and Sentinel 2 imagery. NDWI, SAVI and NDBI have been calculated using Satellite imagery.

In the urban areas, NDVI has been calculated using 20 centimetre GSD RPAS imagery and band 7 and 8 of Sentinel 2. Band 7 has 20 meters of GSD, and 8 has 10 of GSD. The NDVI calculated using RPAS imagery is slightly higher than Sentinel 2. The two dataset do not overlap perfectly in terms of timeline, so we can not calculate the difference analytically. Nevertheless, the difference derived from the graph is 0.15. Finally, the band 8 of Sentinel 2 is more suitable than the 7 because the spatial resolution is higher.

In this study, two PP have been recognized. NDVI values exceed 0.65 also during the summer when water stress can occur. The values in the mowed PP range between 0.4 and 0.60. Therefore, using Sentinel 2 a conservative threshold has been set at 0.70. Using RPAS imagery, the threshold is 0.75.

The information derived from satellite's NDVI and from RPAS's NDVI can be temporally integrated, such as in the parcel Dussin 13 and Rossano 503. In Dussin 13 there is a steep decrease in NDVI recorded using both sensors. In Rossano 503 NDVI from RPAS's imagery detects a probably mowed PP.

The NDWI has been calculated with the band 12 of Sentinel 2 for assessing water stress. The PP has a minimum value of 0.42, whereas the value in mowed PP ranges between 0.15 and 0.47. These values are comparable with 0.4 green vegetation and 0.15

for the dry vegetation found by Gao, 1996. SAVI does not add information as it is highly correlated to NDWI.

The NDBI has negative values for green vegetation. According to the growing rate, the values for mowed PP ranges between -0.23 and 0.0. In absence of vegetation or sparse vegetation, the index has positive values. The threshold that separates PP and mowed PP has been set at -0.25.

This information has several applications that are important in land monitoring. The immediate application is to detect mowing in PP, which is a delicate matter as variance of NDVI can be from low synthetic activity and thus be low, and pastures with mowed grass will have low values of NDVI for a short time, as renovation of vegetation will not take more than some weeks, depending on season of course. Other applications, which are important, an area related to anthropic impact (Piragnolo et al., 2014) which is the focus of creating permanent pastures, to limit anthropic impact in ecological aspects.

REFERENCES

Ali, I., Cawkwell, F., Dwyer, E., Barrett, B., Green, S., 2016. Satellite remote sensing of grasslands: from observation to management. Journal of Plant Ecology, 9, 649–671. doi:10.1093/jpe/rtw005.

Baluja, J., Diago, M.P., Balda, P., Zorer, R., Meggio, F., Morales, F., Tardaguila, J., 2012. Assessment of vineyard water status variability by thermal and multispectral imagery using an unmanned aerial vehicle (UAV). Irrigation Science, 30, 511–522.

Bastin, G., Scarth, P., Chewings, V., Sparrow, A., Denham, R., Schmidt, M., O'Reagain, P., Shepherd, R., Abbott, B., 2012. Separating grazing and rainfall effects at regional scale using remote sensing imagery: A dynamic reference-cover method. Remote Sensing of Environment, 121, 443–457.

Bendig, J., Yu, K., Aasen, H., Bolten, A., Bennertz, S., Broscheit, J., Gnyp, M.L., Bareth, G., 2015. Combining UAV-based plant height from crop surface models, visible, and near infrared vegetation indices for biomass monitoring in barley. International Journal of Applied Earth Observation and Geoinformation, 39, 79–87. doi:10.1016/j.jag.2015.02.012.

Bocci, M., Corticelli, S., Mariani, M.C., Masi, S., Cavallo, M.C., Olio, N.D., Ligabue, M., Vissani, M., 2011. Mappatura dei prati stabili nel comprensorio del Parmigiano-Reggiano mediante telerilevamento, in: Atti 15a Conferenza Nazionale ASITA - Reggia Di Colorno 15-18 Novembre 2011. pp. 379–389.

Diaz-Varela, R.A., Zarco-Tejada, P.J., Angileri, V., Loudjani, P., 2014. Automatic identification of agricultural terraces through object-oriented analysis of very high resolution DSMs and multispectral imagery obtained from an unmanned aerial vehicle. Journal of Environmental Management, 134, 117–126. doi:10.1016/j.jenvman.2014.01.006.

Blanco, L.J., Ferrando, C. a., Biurrun, F.N., 2009. Remote Sensing of Spatial and Temporal Vegetation Patterns in Two Grazing Systems. Rangeland Ecology & Management, 62, 445–451. doi:10.2111/08-213.1.

ESA, Copernicus Open Access Hub https://scihub.copernicus.eu/ (4 January 2018).

Förster, M., Schmidt, T., Schuster, C., Kleinschmit, B., 2012. Multi-temporal detection of grassland vegetation with RapidEye imagery and a spectral-temporal library. International Geoscience and Remote Sensing Symposium (IGARSS), 4930–4933. doi:10.1109/IGARSS.2012.6352506.

Gao, B.C., 1996. NDWI - A normalized difference water index for remote sensing of vegetation liquid water from space. Remote Sensing of Environment, 58, 257–266. doi:10.1016/S00344257(96)00067-3.

Herwitz, S.R., Johnson, L.F., Dunagan, S.E., Higgins, R.G., Sullivan, D. V., Zheng, J., Lobitz, B.M., Leung, J.G., Gallmeyer, B. a., Aoyagi, M., Slye, R.E., Brass, J. a., 2004. Imaging from an unmanned aerial vehicle: Agricultural surveillance and decision support. Computers and Electronics in Agriculture, 44, 49–61.
Huete, A.R., 1988. A soil-adjusted vegetation index (SAVI). Remote Sensing of Environment, 25, 295–309.

Li, F., Zheng, J., Wang, H., Luo, J., Zhao, Y., Zhao, R., 2016. Mapping grazing intensity using remote sensing in the Xilingol steppe region, Inner Mongolia, China. Remote Sensing Letters, 7, 328–337. doi:10.1080/2150704X.2015.1137987.

Morel, J., Todoroff, P., Bégué, A., Bury, A., Martiné, J.F., Petit, M., 2014. Toward a satellite-based system of sugarcane yield estimation and forecasting in smallholder farming conditions: A case study on reunion island. Remote Sensing, 6, 6620–6635.

O'Connor, B., Dwyer, E., Cawkwell, F., Eklundh, L., 2012. Spatio-temporal patterns in vegetation start of season across the island of Ireland using the MERIS Global Vegetation Index. ISPRS Journal of Photogrammetry and Remote Sensing, 68, 79–94. doi:https://doi.org/10.1016/j.isprsjprs.2012.01.004.

Pérez-Ortiz, M., Peña, J.M., Gutiérrez, P.A., Torres-Sánchez, J., Hervás-Martínez, C., López-Granados, F., 2016. Selecting patterns and features for between- and within- crop-row weed mapping using UAV-imagery. Expert Systems with Applications, 47, 85–94. doi:10.1016/j.eswa.2015.10.043.

Piragnolo, M., Pirotti, F., Guarnieri, A., Vettore, A., Salogni, G., 2014. Geo-Spatial Support for Assessment of Anthropic Impact on Biodiversity. ISPRS International Journal of GeoInformation, 3, 599–618. doi:10.3390/ijgi3020599

Pirotti, F., Guarnieri, A., Masiero, A., Vettore, A., 2015. Preface to the special issue: the role of geomatics in hydrogeological risk. Geomatics, Natural Hazards and Risk, 6, 357–361.

Pirotti, F., Neteler, M., Rocchini, D., 2017. Preface to the special issue "Open Science for earth remote sensing: latest developments in software and data." Open Geospatial Data, Software and Standards, 2, 26. doi:10.1186/s40965-017-0039-y

Quadratic, Monitoring crop fields soil moisture (NDWI) using Sentinel-2 temporal series http://www.quadratic.be/en/le-suivide-letat-hydrique-ndwi-des-cultures-par-les-series-temporellessentinel-2/ (4 January 2018).

Rouse, J.W., Haas, R.H., Schell, J.A., Deering, D.W., 1973. Monitoring the vernal advancement and retrogradation (green wave effect) of natural vegetation. Progress Report RSC 1978-1, 112.

Rutzinger, M., Höfle, B., Lindenbergh, R., Oude Elberink, S., Pirotti, F., Sailer, R., Scaioni, M., Stötter, J., Wujanz, D., 2016. Close Range Sensing Techniques in Alpine Terrain. ISPRS Annals of Photogrammetry, Remote Sensing and Spatial Information Sciences, III-6, 15–22.

Saornil, J., Förster, M., Kleinschmit, B., 2008. GIS and Remote Sensing for Natura 2000 Monitoring in Mediterranean Biogeographic Region.

Schmidt, M., Tindall, D., Speller, K., Scarth, P., Dougall, C., 2010. Ground cover management practices in cropping and improved pasture grazing systems:ground cover monitoring using remote sensing. Final Report. State of Queensland.
Sugiura, R., Noguchi, N., Ishii, K., 2005. Remote-sensing technology for vegetation monitoring using an unmanned helicopter. Biosystems Engineering, 90, 369–379.

Sentinel-Hub, NDII index http://www.sentinelhub.com/eoproducts/ndwi-normalized-difference-water-index (4 January 2018).

Tokekar, P., Hook, J. Vander, Mulla, D., Isler, V., 2013. Sensor planning for a symbiotic UAV and UGV system for precision agriculture. IEEE International Conference on Intelligent Robots and Systems, 5321–5326. doi:10.1109/IROS.2013.6697126.

Torres-Sánchez, J., López-Granados, F., Peña, J.M., 2015. An automatic object-based method for optimal thresholding in UAV images: Application for vegetation detection in herbaceous crops. Computers and Electronics in Agriculture, 114, 43–52.
Tucker, C.J., 1979. Red and photographic infrared linear combinations for monitoring vegetation. Remote Sensing of Environment, 8, 127–150. doi:10.1016/0034-4257(79)90013-0.

Turner, D., Lucieer, A., Watson, C., 2010. Development of an Unmanned Aerial Vehicle (UAV) for hyper resolution vineyard mapping based on visible, multispectral, and thermal imagery. Proceedings of 34th International Symposium on Remote Sensing of Environment, 4.

Zha, Y., Gao, J., NI, S., 2003. Use of normalized difference builtup index in automatically mapping urban areas from TM imagery. International Journal of Remote Sensing, 24, 583–594.

Xu, B., Yang, X.C., Tao, W.G., Qin, Z.H., Liu, H.Q., Miao, J.M., Bi, Y.Y., 2008. MODIS-based remote sensing monitoring of grass production in China. International Journal of Remote Sensing, 29, 5313–5327. doi:10.1080/01431160802036276

4. Paper III: Benchmark of machine learning methods for classification of a Sentinel-2 image

BENCHMARK OF MACHINE LEARNING METHODS FOR CLASSIFICATION OF A SENTINEL-2 IMAGE

F. Pirotti [a,b], F. Sunar [c], M. Piragnolo[a,b]

[a] CIRGEO, Interdepartmental Research Center of Geomatics, University of Padua, Viale dell'Università 16, 35020 Legnaro, Italy (francesco.pirotti, marco.piragnolo)@unipd.it
[b] TESAF Department, University of Padua, Viale dell'Università 16, 35020 Legnaro, Italy
[c] Istanbul Technical University, Civil Engineering Fac., Geomatics Engineering Dept., 34469 Maslak Istanbul, Turkey
fsunar@itu.edu.tr

Commission VII, WG VII/4

KEY WORDS: Machine learning, Sentinel-2, Remote sensing, Neural nets, Agriculture, Land cover, Classification

ABSTRACT:

Thanks to mainly ESA and USGS, a large bulk of free images of the Earth is readily available nowadays. One of the main goals of remote sensing is to label images according to a set of semantic categories, i.e. image classification. This is a very challenging issue since land cover of a specific class may present a large spatial and spectral variability and objects may appear at different scales and orientations.

In this study, we report the results of benchmarking 9 machine learning algorithms tested for accuracy and speed in training and classification of land-cover classes in a Sentinel-2 dataset. The following machine learning methods (MLM) have been tested: linear discriminant analysis, k-nearest neighbour, random forests, support vector machines, multi layered perceptron, multi layered perceptron ensemble, ctree, boosting, logarithmic regression. The validation is carried out using a control dataset which consists of an independent classification in 11 land-cover classes of an area about 60 km2, obtained by manual visual interpretation of high resolution images (20 cm ground sampling distance) by experts. In this study five out of the eleven classes are used since the others have too few samples (pixels) for testing and validating subsets. The classes used are the following: (i) urban (ii) sowable areas (iii) water (iv) tree plantations (v) grasslands.

Validation is carried out using three different approaches: (i) using pixels from the training dataset (train), (ii) using pixels from the training dataset and applying cross-validation with the k-fold method (kfold) and (iii) using all pixels from the control dataset. Five accuracy indices are calculated for the comparison between the values predicted with each model and control values over three sets of data: the training dataset (train), the whole control dataset (full) and with k-fold cross-validation (kfold) with ten folds. Results from validation of predictions of the whole dataset (full) show the random forests method with the highest values; kappa index ranging from 0.55 to 0.42 respectively with the most and least number pixels for training. The two neural networks (multi layered perceptron and its ensemble) and the support vector machines - with default radial basis function kernel - methods follow closely with comparable performance.

1. INTRODUCTION

Thanks to space agencies, e.g. ESA and USGS, a large bulk of free digital images of the Earth surface is readily available nowadays for download by anyone with internet access. As a part of the European Copernicus program, the recently launched Sentinel-2 satellite provides remotely sensed data of the Earth features for the key operational services related to environment and security on a regional to global scale; and is now available/ready for its scientific and commercial exploitation.

One of the main goals of remote sensing is to label images according to a set of semantic categories, i.e. image classification. This is a very challenging issue since land cover of a specific class may present a large spatial and spectral variability and objects may appear at different scales and orientations. However, the increased availability, not only from satellite sensors, but also from distributed participatory sensors (Chen et al., 2015), has pushed for faster and better algorithms for classification of the available images. Within this context, the machine learning methods have developed at fast pace in the past years due to the growing amount of data available and the bigger size of the data itself. Doubtless, successful development of machine learning methods and their correct application for the data obtained from the new

advanced sensors will benefit all fields where land-cover is a necessary information in planning and decision making. In the urban context, fitting models can help to contribute to the "smart-city" paradigm, e.g. by monitoring land-surface temperature (Scarano, 2015) or providing data for anthropic impact assessment in urban areas and outside urban areas (Akın et.al., 2015; Piragnolo et al., 2014). In environmental context, remote sensing provides a global view of the Earth's phenomena and all the variables which are necessary to assess and predict its dynamics. One important example is the estimation of the biomass for carbon source/sink (Pirotti et al., 2014) that uses various remote sensing data due to the necessary global scale of monitoring (Pirotti, 2010). Another critical aspect is the risk monitoring at various scales, ranging from subsidence of the Earth crust to fire and landslides (Scaioni et al., 2014). However, for a range of products dedicated to accurate thematic mapping in these applications such as mentioned above, the development and benchmarking of the machine learning algorithms for the new satellite missions such as Sentinel-2 satellite need to be validated and demonstrated in collaboration with national and international users. The goal of this paper is to analyse the performance of the different machine learning algorithms for land-cover mapping using a Sentinel-2 image. The novelty resides in discussing not only a typical assessment of accuracy from a

classification step, but a comparison of three typical methods for accuracy assessment: (i) comparing against training areas without cross validation, (ii) comparing against training areas using K-fold cross validation and (iii) comparing against a much bigger independent dataset. Several accuracy metrics are extracted and all results are cross-compared to investigate on common pitfalls in the evaluation of the classification results. Therefore, our study performs a benchmarking of different classification algorithms highlighting the adequacy and efficiency of the Sentinel-2 data for land cover mapping.

2. STUDY AREA

The study area is located at south-east of city of Padova, in the Italian Veneto Region (Figure 1). The area is approximately 11 km in the East-West axis and 16 km in the North-South. The extension of the data polygons is approximately 60 km2. The area is roughly composed of urban areas, grassland, and crop sowable area.
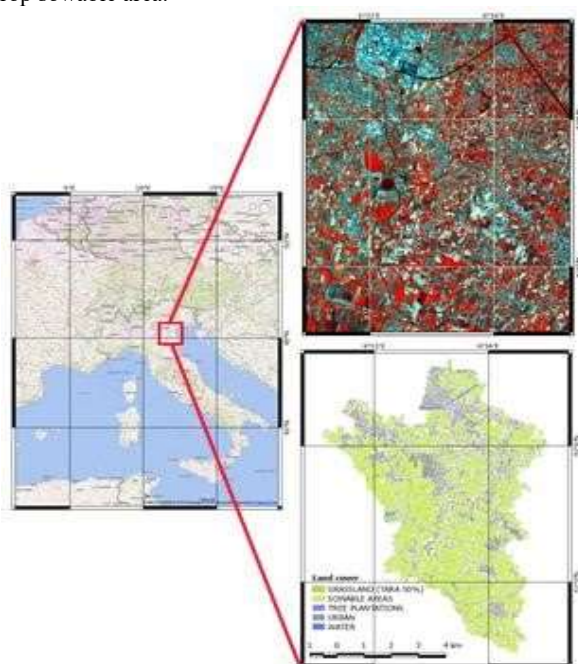

Figure 1. The satellite image (above) and land use map (below) of the study area.

3. MATERIALS AND METHODS

3.1. Satellite images – Sentinel-2

The Sentinel-2A satellite successfully launched on 23 June 2015, is becoming an important image data source for a wide spectrum of applications reaching from agriculture to forestry, environmental monitoring to urban planning. The reason is to be found in the following sensor features. A combination of different spatial resolutions (10 to 60m) with novel spectral capabilities (e.g., three bands in the 'red-edge' which provide key information on the state of vegetation plus two bands in the SWIR) – see Table 1. Wide coverage (swath width of 290 km) and minimum five-day global revisit time (with its twin, Sentinel2B, to be launched in 2016) (Malenovský et. al., 2012). The satellite's orbit is Sun-synchronous, at 786 km altitude, 98.5° inclination. Temporal resolution is 10 days with one satellite and 5 days with 2 satellites. In this study, the

Sentinel-2 satellite data dated on 13th August 2015, is used to assess the three methods for accuracy assessment proposed.

Band	Central Wavelength (nm)	Bandwidth (nm)	Spatial resolution (m)
Band 1	443	20	60
Band 2	490	65	10
Band 3	560	35	10
Band 4	665	30	10
Band 5	705	15	20
Band 6	740	15	20
Band 7	783	20	20
Band 7	783	20	20
Band 8	842	115	10
Band 8A	865	20	20
Band 9	945	20	60
Band 10	1375	30	60
Band 11	1610	90	20
Band 12	2190	180	20

Table 1. Band description of Sentinel-2 sensor.

3.2. Classification methods

Supervised classification considers a set of observations S = {x1, x2, …, xn} - sometimes referred to as features, attributes, variables or measurements - for each sample of an area with known class C. This set is called the training set and is usually determined manually by setting regions of interest (ROI). The classification problem is then to find a good predictor for the class C of any sample of the same distribution (not necessarily from the training set) given observation S (Venables and Ripley, 2002). To find good predictors, various machine learning methods are used. The machine learning methods (MLM) tested in this study are given below:

1. Linear Discriminant Analysis (*lda*),
2. K-nearest Neighbour (*kknn*),
3. Random Forests (*randomForest*),
4. Support Vector Machines (*svm*),
5. Multi Layered Perceptron (*mlp*),
6. Multi Layered Perceptron Ensemble (*mlpe*),
7. Ctree (*ct*),
8. Boosting (*b*), 9. Logistic Regression (*lr*).

A brief explanation of each method is given below together with some references for further reading:
- Linear discriminant analysis is similar to principal component analysis, where finding the best linear combination of variables to best explain the data is the goal of the process (Venables and Ripley, 2002).
- K-nearest neighbour is a popular technique which uses kernel functions to weight the neighbours according to their distances. As a matter of fact, not only kernel functions, but every monotonic decreasing function will work. The number of neighbours used for the "optimal" kernel should be:

$$\left[\left(\frac{2(d+4)}{d+2} \right)^{\left(\frac{d}{d+4} \right)} k \right]$$

(1)

where: d is the distance and k is the number that would be used for unweighted classification, a rectangular kernel. See (Samworth, 2012) for more details.

- Random forests is a very well-performing algorithm which grows many classification trees. To classify a new object from an input dataset, put the set of observations (S) down each of the trees in the forest. Each tree gives a classification, and we say the tree "votes" for that class. The forest chooses the classification having the most votes (over all the trees in the forest). Each tree is grown with specific criteria, which are thoroughly reported in (Breiman and Cutler, 2015). The main features of the random forests method that makes it particularly interesting for digital image analysis are that it is unexcelled in accuracy among current algorithms, it runs efficiently on large data sets (typical among digital images to have a large number of observations), it can handle thousands of input variables without variable deletion and it gives estimates of what variables are important in the classification. Also generated forests can be saved for future use on other datasets. For more reading (Breiman, 2001; Yu et al., 2011).
- Support vector machines is another popular MLM which has been particularly applied in remote sensing by several investigators (Plaza et al., 2009). It uses hyper-planes to separate data which have been mapped to higher dimensions (Cortes and Vapnik, 1995). A kernel is used to map the data. Different kernels are used depending on the data. In this study, the radial basis function kernel is applied.
- Multi layered perceptron and multi layered perceptron ensemble are two neural networks, differing on the fact that the latter method uses average and voting techniques to overcome the difficulty to define the proper network due to sensitivity, overfitting and underfitting problems which limit generalization capability. A multi layered perceptron is a feedforward artificial neural network model that maps sets of input data onto a set of appropriate outputs. It consists of multiple layers of nodes in a directed graph, where each layer is fully connected to the next. Each node is a processing element with a nonlinear activation function. It utilizes supervised learning called backpropagation for training the network. This method can distinguish data that are not linearly separable (Cybenko, 1989; Atkinson and Tatnall, 1997; Benz et al., 2004).
- Ctree uses conditional inference trees. The trees estimate a regression relationship by binary recursive partitioning in a conditional inference framework. The algorithm works as follows: 1) Test the global null hypothesis of independence between any of the input variables and the response (which may be multivariate as well). Stop if this hypothesis cannot be rejected. Otherwise select the input variable with strongest association to the response. This association is measured by a p-value corresponding to a test for the partial null hypothesis of a single input variable and the response. 2). Implement a binary split in the selected input variable. These steps are repeated recursively (Hothorn et al., 2006).
- Boosting consists of algorithms which iteratively finding learning weak classifiers with respect to a distribution and adding them to a final strong classifier. When they are added, they are typically weighted in some way that is usually related to the weak learners' accuracy. In this study, the AdaBoost.M1 algorithm is used (Freund and Schapire, 1996).
- Logistic regression method is also being applied in remote sensing data classification (Cheng et al., 2006). It fits multinomial log-linear models via neural networks.

3.3. Classification

Our total dataset consists in approximately 60 km^2 therefore, taking as measuring unit the pixel size 10 x 10 m, 6x10^5 pixels. For each pixel we have information on its land-cover class due to manual interpretation which was provided as polygons with landcover classes (Figure 1 – bottom left). Because the study requires numerous runs with different combinations of MLM and size of training data, to limit computation time while keeping statistic robustness, we took a smaller subset of the total number of pixels. Pseudo-random stratified sampling was used to choose 20% of the pixels, which gave us 1.2x10^5 pixels with known classes to work with, hereafter defined as our control dataset. The sampling is "pseudo-random stratified" because two criteria were used to pick "cleaner" pixels. The first criterion consists in choosing only pixels falling completely in a polygon, i.e. no pixels are shared between polygons, thus theoretically decreasing spectral mixing in our control. The second criterion consists in balancing numerosity of pixels per class to avoid having under-represented classes.

The training is then done automatically for each MLM also with stratified random sampling of the control dataset obtained with the aforementioned procedure. Thirty training subsets are picked for each MLM subsetting from 1% to 50% (1200 to 6x10^4 pixels). The same procedure described above is also carried out over a much smaller subset consisting of 4% of the total dataset pixels. This further processing was done to see the impact of a smaller dataset on results, and results are reported as blue points and red points, on figures 2 and 3, for 4% and 20% respectively.

3.4. Validation

The control dataset consists of an independent classification with 11 land-cover classes in the total area (see Figure 1). The class attribution was done by manual visual interpretation of high resolution images (20 cm ground sampling distance) by experts. In this study, only five out of the eleven classes are used since the other classes cover very small areas with the consequence that the samples (pixels) for testing and validating subsets are not frequent enough to be tested significantly. The classes used are the following: (i) urban, (ii) sowable areas, (iii) water, (iv) tree plantations, and (v) grasslands. Five accuracy indices are calculated:

- Classification accuracy rate (ACC) [0-100]
- Classification error (CE) [0-100]
- Balanced error rate (BER) [0-100] - Kappa index (KAPPA) [0-100]
- Cramer's V (CRAMERV) [0-1]

Validation is carried out using three different approaches: (i) using pixels from the training dataset (train), (ii) using pixels from the training dataset and cross-validated via k-fold cross validation with ten folds of the training set (kfold) and (iii) using all pixels from the control dataset (all). The former will give the least independent validation whereas the latter will provide the most independent validation. As described in the previous section, since multiple trials were tested for the benchmarking speed and accuracy depending on the size of the training samples, the number of pixels used in the first two methods range from 1200 to 6x10^4 pixels; whereas in the last method whole control dataset was used, i.e. 1.2x10^5 pixels.

4. RESULTS AND DISCUSSION

As reported in the previous section, validation has been done using three sets of data. The validation against the training set (train) is not reported in a figure, because it is not cross-validated in any way and not independent. As a matter of fact, as expected, the accuracies from train validation were much over-estimated when compared to the other methods; i.e. for one of the MLM method, RF, the accuracy was 100%, as the decision trees model the training data perfectly (with decisions) and thus validation against training does not have any sense.

The k-fold cross-validation and the validation against the full dataset are reported in Figure 2 and Figure 3, respectively.
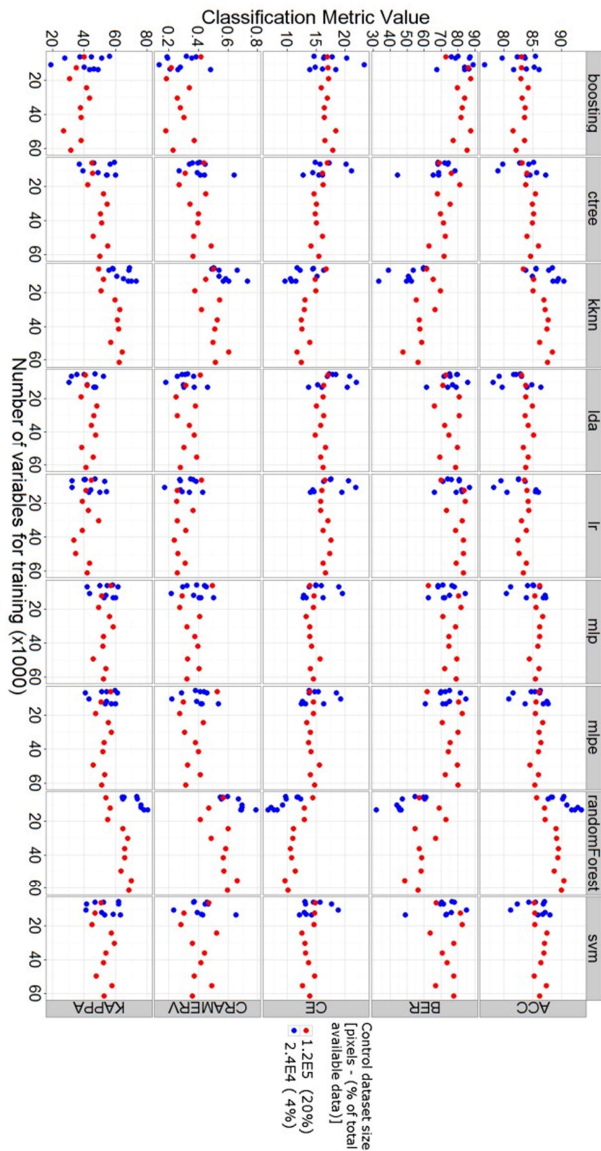
Figure 2. Accuracy metrics of k-fold cross validation over the training set.

4.1. Best performing classifier

The first question that needs to be asked is: what is the best classifier? As can be seen in Figure 2, the random forests (RF)

performs better than the others, however there are several points that should be made. First of all, RF keeps the title of "best performer" when there are enough training variables. As can be seen in both plots, below 20 x103 pixels for training RF tends to be as accurate, if not less, than other MLM.

The two MLM based on neural networks (MLP and MLPE) seem to perform better than RF when considering smaller number of pixels for training. This is particularly clear from the validation results from the full independent dataset (Figure 3), where RF drops. RF also gets the title of best performer when comparing accuracies with the k-fold cross validation, keeping the title also at lower number of training pixels. A final remark is that the neural networks seem the most robust performers also with little training data. This can be inferred from observing how the accuracy (ACC) and kappa index (KAPPA) are more constant than the other classifiers, both for the full validation and for the k-fold validation. This is an important characteristic since more training data means more computation time and more manual work for determining the training areas over the image.
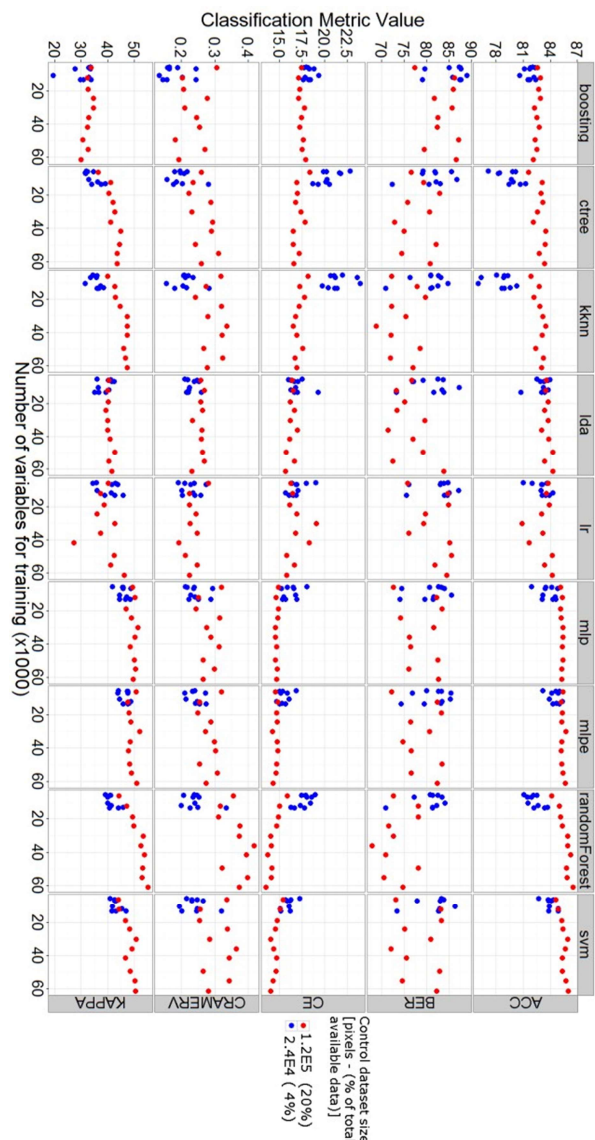

Figure 3. Accuracy metrics of results over the full independent dataset.

4.2. K-fold versus full validation

K-fold does have a small drawback when compared against validation from the full dataset. It overestimates accuracy when using the 2% of total polygons (blue dots) as opposed to the 10% of total polygons (red dots). This is explained by the smaller set used for training when using 2% of the available pixels as opposed to 10%. K-fold cross-validation uses available training data to assess accuracy, simulating independent sets of data by sampling from the training data and applying the model to it. Therefore, a smaller set will overestimate accuracy as opposed to a larger training set, which has more variance. It is trivial to state that validation against the full dataset is more robust. This type of overestimation of accuracy is observed in RF and KKNN, but not in the other classifiers.

4.3. Processing speed

Each combination of MLM and number of pixels used for training were also benchmarked for its speed in processing (Figure 4). This benchmark was performed by running the MLMs with R cran rminer package (Cortez, 2010) on a workstation with 1 Intel® Xeon® Six-Core Processor X5660 (2.80 GHz, 12 MB cache, 1333 MHz memory), 12 Gb RAM running Windows©7 64 bits.
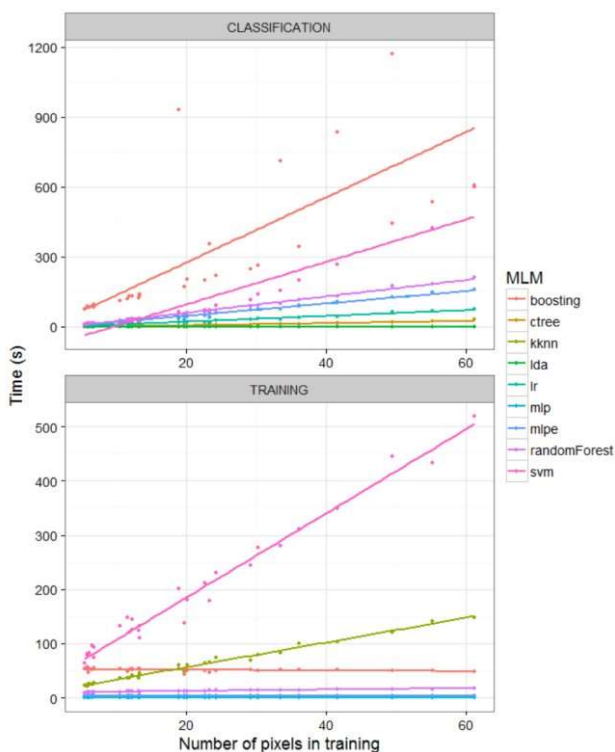

Figure 4. Benchmark results of processing speeds for each MLM with different number of pixels used in the training phase.
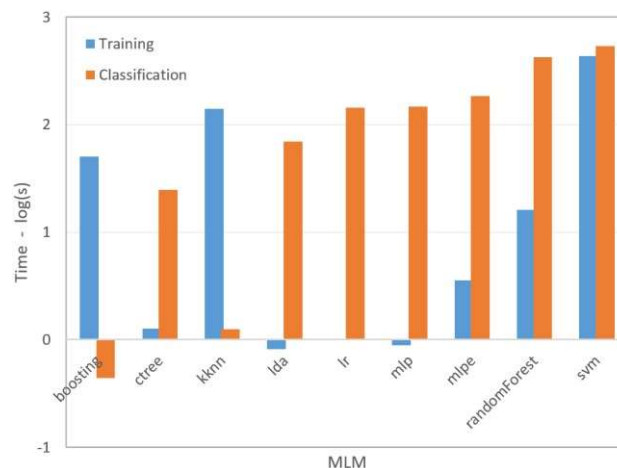

Figure 5. Processing speed of different MLMs for training and classification using the highest number of pixels for training (6x104).

This type of benchmark is to be considered for testing relative performance issues between MLMs in this particular case, and not an indicator for a final conclusion on speed of the algorithms as they are influenced by many factors which have not been monitored in this study.

As shown n Figure 5, a group of classifiers are much faster in the training phase, especially when the highest number of training pixels – i.e. 6x104 pixels, are used. In training, the faster MLMs are lda, lr, ctree, and mlp. In the classification phase only boosting and kknn, followed by ctree, are significantly faster. The more complex methods, randomForest and svm, require longer processing times for both classification and training.

5. CONCLUSIONS

In this study, the benchmarking of 9 machine learning algorithms is carried out for accuracy and speed in training and classification of a Sentinel-2 dataset for land-cover mapping. Some interesting points which are worth reporting are outlined as below:

- Overall, the RF is among the best performing method for the classification, i.e., Kappa index ranging from 0.55 to 0.42 respectively with the most and least number pixels for training. - Next, the neural networks (mlp and mlpe) follow closely to randomForest and also have an important added value of keeping a high accuracy with smaller training datasets, as opposed to randomForest, i.e., drops in accuracy with a smaller number of training data.
- The support vector machines also follow close, and it can be said that there are various methods to improve performance of SVM which have not been investigated in this study.
- Although many factors which have not been monitored in this study, affect the speed of the algorithms used, in general, the more complex methods, such as randomForest and svm, showed that they require longer processing times for both classification and training phases.

As a final remark, it might be the case that an optimized SVM over the same Sentinel 2 data used might lead to have an improved result; hence, it is thought that it will be an interesting topic for future investigations.

6. REFERENCES

Akın, A., Sunar, F., Berberoğlu, S., 2015. Urban change analysis and future growth of Istanbul, *Environmental Monitoring and Assessment*, 187(8), 1-15.

Atkinson, P.M., Tatnall, A.R.L., 1997. Introduction Neural networks in remote sensing. *International Journal of Remote Sensing*, 18, 699–709.

Benz, U.C., Hofmann, P., Willhauck, G., Lingenfelder, I., Heynen, M., 2004. Multi-resolution, object-oriented fuzzy analysis of remote sensing data for GIS-ready information. *ISPRS Journal of Photogrammetry and Remote Sensing*.

Breiman, L., 2001. Random forests. *Machine Learning*, 45, 5–32.

Breiman, L., Cutler, M.E.J., 2015. Random forests [WWW Document].
URL,https://www.stat.berkeley.edu/~breiman/RandomForests/c c_home.htm (accessed 7 November 2015).

Chen, J., Dowman, I., Li, S., Li, Z., Madden, M., Mills, J., Paparoditis, N., Rottensteiner, F., Sester, M., Toth, C., Trinder, J., Heipke, C., 2015. Information from imagery: ISPRS scientific vision and research agenda. *ISPRS Journal of Photogrammetry and Remote Sensing.*

Cheng, Q.C.Q., Varshney, P.K., Arora, M.K., 2006. Logistic Regression for Feature Selection and Soft Classification of Remote Sensing Data, IEEE Geoscience and Remote Sensing Letters.

Cortes, C., Vapnik, V., 1995. Support-vector networks. *Machine Learning*, 20, 273–297.

Cortez, P., 2010. Data Mining with Neural Networks and Support Vector Machines Using the R/rminer Tool. *10th Industrial Conference*, ICDM 2010, 6171, 572–583.

Cybenko, G., 1989. Correction: Approximation by Superpositions of a Sigmoidal Function. *Mathematics of Control, Signals, and Systems*, 2, 303–314.

Freund, Y., Schapire, R.R.E., 1996. Experiments with a New Boosting Algorithm. *International Conference on Machine Learning*, 148–156.

Hothorn, T., Hornik, K., van de Wiel, M. a, Zeileis, A., 2006. A Lego System for Conditional Inference. *The American Statistician*, 60, 257–263.

Malenovský, Z., H. Rott, J. Cihlar, M. E. Schaepman, G. GarcíaSantos, R. Fernandes, M. Berger, 2012. Sentinels for science: Potential of Sentinel-1, -2, and -3 missions for scientific observations of ocean, cryosphere, and land, *Remote Sensing of Environment*, Volume 120, P.91–101.

Piragnolo, M., Pirotti, F., Guarnieri, A., Vettore, A., Salogni, G., 2014. Geo-Spatial Support for Assessment of Anthropic Impact on Biodiversity. *ISPRS International Journal of GeoInformation*, 3, 599–618.

Pirotti, F., 2010. IceSAT/GLAS Waveform Signal Processing for Ground Cover Classification: State of the Art. *Italian Journal of Remote Sensing*, 13–26.

Pirotti, F., Laurin, G., Vettore, A., Masiero, A., Valentini, R., 2014. Small Footprint Full-Waveform Metrics Contribution to the Prediction of Biomass in Tropical Forests. *Remote Sensing*, 6, 9576–9599.

Plaza, A., Benediktsson, J.A., Boardman, J.W., Brazile, J., Bruzzone, L., Camps-Valls, G., Chanussot, J., Fauvel, M., Gamba, P., Gualtieri, A., Marconcini, M., Tilton, J.C., Trianni, G., 2009. Recent advances in techniques for hyperspectral image processing. *Remote Sensing of Environment*, 113, S110–S122.

Samworth, R.J., 2012. Optimal weighted nearest neighbour classifiers. *Annals of Statistics*, 40, 2733–2763.

Scaioni, M., Longoni, L., Melillo, V., Papini, M., 2014. Remote sensing for landslide investigations: An overview of recent achievements and perspectives. *Remote Sensing*, 6(10), 96009652.

Scarano M., 2015. On the relationship between the urban parameters sky view factor, normalized difference vegetation index and vegetation fraction and the land surface temperature derived by Landsat-8 in Bari, Italy. *Bollettino SIFET*, 2, pp.1-9.

Tarantino E., 2012. Monitoring spatial and temporal distribution of Sea Surface Temperature with TIR sensor data. *Italian Journal of Remote Sensing*, 44, pp.97-107.

Venables, W.N., Ripley, B.D., 2002. Modern Applied Statistics with S. *Issues of Accuracy and Scale*, 868.

Yu, X., Hyyppä, J., Vastaranta, M., Holopainen, M., Viitala, R., 2011. ISPRS Journal of Photogrammetry and Remote Sensing Predicting individual tree attributes from airborne laser point clouds based on the random forests technique. *ISPRS Journal of Photogrammetry and Remote Sensing*, 66, 28–37.

5. Paper IV: Open source R for applying machine learning to RPAS remote sensing images

ORIGINAL ARTICLE **Open Access**

CrossMark

Open source R for applying machine learning to RPAS remote sensing images

Marco Piragnolo[*], Andrea Masiero and Francesco Pirotti

Abstract

The increase in the number of remote sensing platforms, ranging from satellites to close-range Remotely Piloted Aircraft System (RPAS), is leading to a growing demand for new image processing and classification tools. This article presents a comparison of the Random Forest (RF) and Support Vector Machine (SVM) machine-learning algorithms for extracting land-use classes in RPAS-derived orthomosaic using open source R packages. The camera used in this work captures the reflectance of the Red, Blue, Green and Near Infrared channels of a target. The full dataset is therefore a 4-channel raster image. The classification performance of the two methods is tested at varying sizes of training sets. The SVM and RF are evaluated using Kappa index, classification accuracy and classification error as accuracy metrics. The training sets are randomly obtained as subset of 2 to 20% of the total number of raster cells, with stratified sampling according to the land-use classes. Ten runs are done for each training set to calculate the variance in results. The control dataset consists of an independent classification obtained by photointerpretation. The validation is carried out(i) using the K-Fold cross validation, (ii) using the pixels from the validation test set, and (iii) using the pixels from the full test set.
Validation with K-fold and with the validation dataset show SVM give better results, but RF prove to be more performing when training size is larger. Classification error and classification accuracy follow the trend of Kappa index.
Keywords: Remote sensing, R software, Machine learning, Random forest, Support vector machine, RPAS, Land use classification

Background

The increase in the number of remote sensing platforms, ranging from satellites to close-range Remotely Piloted Aircraft System (RPAS), is causing a growing demand for new tools for image processing and classification. Classification is applied in many research fields such as geomorphology, environmental analyses, land use, fragmentation of habitats and risk assessment [1, 2] just to name a few. In particular, RPAS are applied to fields that benefit from close-range sensing, such as 3D modelling of cultural heritage and archaeology, environmental sciences, precision forestry and precision agriculture [3–7]. Imagery collected from remote sensing platforms is commonly classified using conventional remote sensing techniques supplied by available software in the market. In remote sensing literature, there are two main classification approaches, pixel-based and object-

based. The pixel-based methods can be divided into unsupervised and supervised. The unsupervised classifiers cluster pixels in a number of classes based on statistical information from the image. The process is automatic and the user can only set the number of clusters. The supervised classifiers are based on training areas inserted by an operator, which define a spectral signature for each class. The object-based classifiers defined an object using geometric information, contextual information and texture information. Machine learning techniques are classification/regression methods for analysing data. They can be used for supervised and unsupervised classification. They use algorithms that learn from previous computation, and they were recently applied in investigations regarding cotton crop [8], variable-rate fertilization [9], classification of invasive weed species [10], detecting landing sites [11, 12], geological mapping [13], Land Use/Land Cover (LULC) classification [14–18].

* Correspondence: marco.piragnolo@phd.unipd.it
CIRGEO, Interdepartmental Research Center of Geomatics, University of Padua, Viale dell'Università 16, 35020 Legnaro, Italy

Springer Open

Recent developments in technology have pushed for a fast increase in using RPAS – commonly referred to as "drones" for observation of the earth surface. The challenge of processing imagery obtained from RPAS resides in the increase of the size of datasets, which is due to increasing resolution of images and the ability of RPASs to collect hundreds of images in each flight. A novel approach using machine learning might provide faster and more accurate results than typical supervised classification of such images. The goal of this work is to benchmark the performance of two machine learning algorithms for classifying an RPAS-derived orthomosaic using open source R packages. The algorithms are Random Forest (RF) and Support Vector Machine (SVM). They are evaluated using three accuracy metrics, Kappa index, classification accuracy and classification error.

Material and methods

The RPAS images have been acquired in a testing area inside the Campus of Agripolis at University of Padova in the city of Legnaro (Italy). The size of the area is 241 m × 508 m. It contains heterogeneous land-cover, including bare ground, vegetation and urban features. The ground-truth is defined by direct observation. Eighteen ground control points (GCP) were defined in the area for orientation of the photogrammetric image block. The coordinates were collected with GNSS in Real Time Kinematic mode; the root mean square error (RMSE) of measures resulted between 0.008 and 0.011.

The RPAS flight was performed in November 2015 using a camera with Red, Blue, Green and Near Infrared camera (RGBI) carried by the SenseFly EBee fixed wing platform. The average ground sampling distance (GSD) was 4.5 cm on the ground at a flight altitude of 150 m. The images have been processed using Agisoft Photoscan. The result is an ortho-rectified mosaic of images, with an RMSE of

0.393 pixel. The final GSD, or spatial resolution, is 6 cm, so the final dimensions are 4020 X 8466 pixels, and the storage size is 48.9 MB. To reduce the computation time, the full dataset was resampled using the nearest neighbour algorithm to a cell size of 30 cm. The nearest neighbour algorithm preserves the radiometric values of cells. Then, the orthomosaic is clipped to a final dimension of 801 × 529 pixels, storage size of 1.21 MB (Fig 1). The RF and SVM machine learning methods were tested on the clipped image, using the R/rminer package [19] available in The Comprehensive R Archive Network repository [20].

The R/rminer package, version 1.4.1 for R is an aggregator of 14 classification and 15 regression methods. It also includes methods for determining common accuracy metrics over results [21, 22]. Two algorithms, Support Vector Machine (SVM) and Random Forest (RF) have been compared in this study. The SVM uses a separating hyperplane as a predictor. A decision plane divides dataset into two groups. Hence, the set of objects has different class memberships, and data are transformed in classes by using a mathematical function called kernel [23]. The RF classifier consists of a collection of trees. It samples randomly the original dataset, and defines decision trees using bootstrap aggregating. Bootstrap is a statistical technique that allows approximating statistics (e.g. average, variance, confidence interval) of data from the data itself. It is used when the distribution of the original dataset is not known before-hand. A complete tree with all branches is grown for each sample, and the predictors are applied to each branch [24]. Finally, the best variable obtained from the predictor is chosen, and predictions are aggregated in a new sample. Consequently, a new sample is predicted, and the estimation of errors can be calculated at the level of iteration and aggregation [25, 26]. In this study, RF and SVM have been trained using a subset of 2 to 20% of the

Fig. 1 Clipped testing area: true colour image (left), false colour infrared image (right)

total number of raster cells. For each percentage, ten training sets were extracted using stratified random sampling. This allowed to assess the variance from accuracy results for each size of training set. The control dataset is an independent classification based on photo interpretation as shown in Fig. 2. The classes for LULC are: (i) broadleaf, (ii) building, (iii) grass, (iv) headland access path, (v) road, (vi) sowed land, (vii) vegetable.

The framework of the benchmarking process is illustrated in Fig. 3. Each class in the area is represented differently in terms of number of pixels (i.e. area). Therefore, the number of pixels we sampled for training was proportional to the class area (i.e. stratified sampling). Pixels falling across two polygons, thus mixing two different classes, were discarded to limit using pixels with mixed spectral signature. For each set of stratified samples, ten different training sets and ten validation sets have been created. The training set is used to fit the model and to apply it for classification of the image. The validation dataset is the difference between the full set and the training set.

The framework trains and tests each of the two methods (RF and SVM) fitting the model and applying K-fold cross-validation. The K-fold cross-validation technique splits the data in K (10) sets (folds) of equal size. K − 1 subsamples are used as training test set, and a single subsample is used for validation. The procedure is repeated K times, but each subset is used only once for the validation.
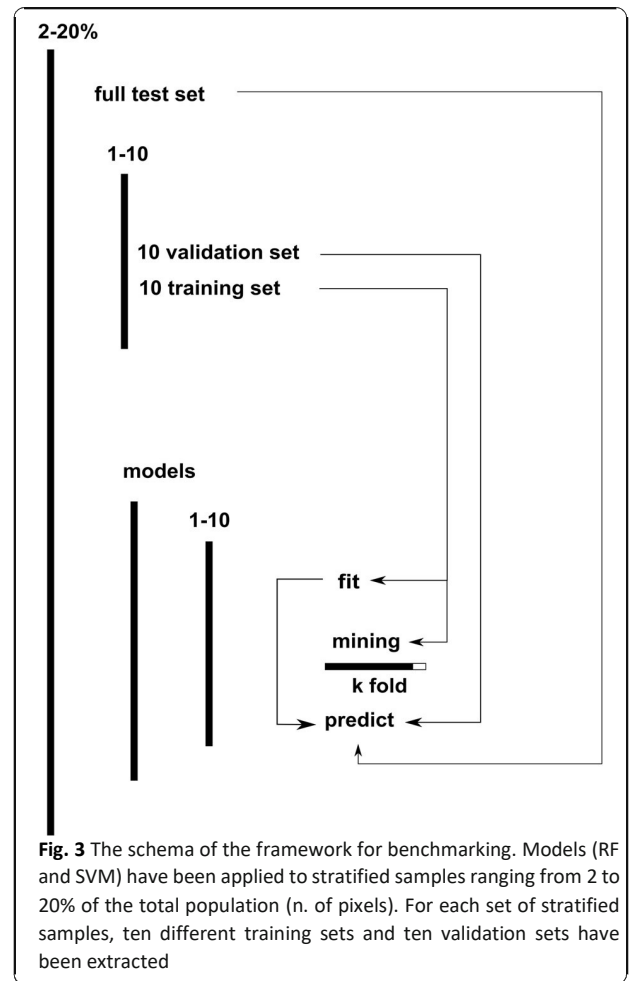

Fig. 3 The schema of the framework for benchmarking. Models (RF and SVM) have been applied to stratified samples ranging from 2 to 20% of the total population (n. of pixels). For each set of stratified samples, ten different training sets and ten validation sets have been extracted
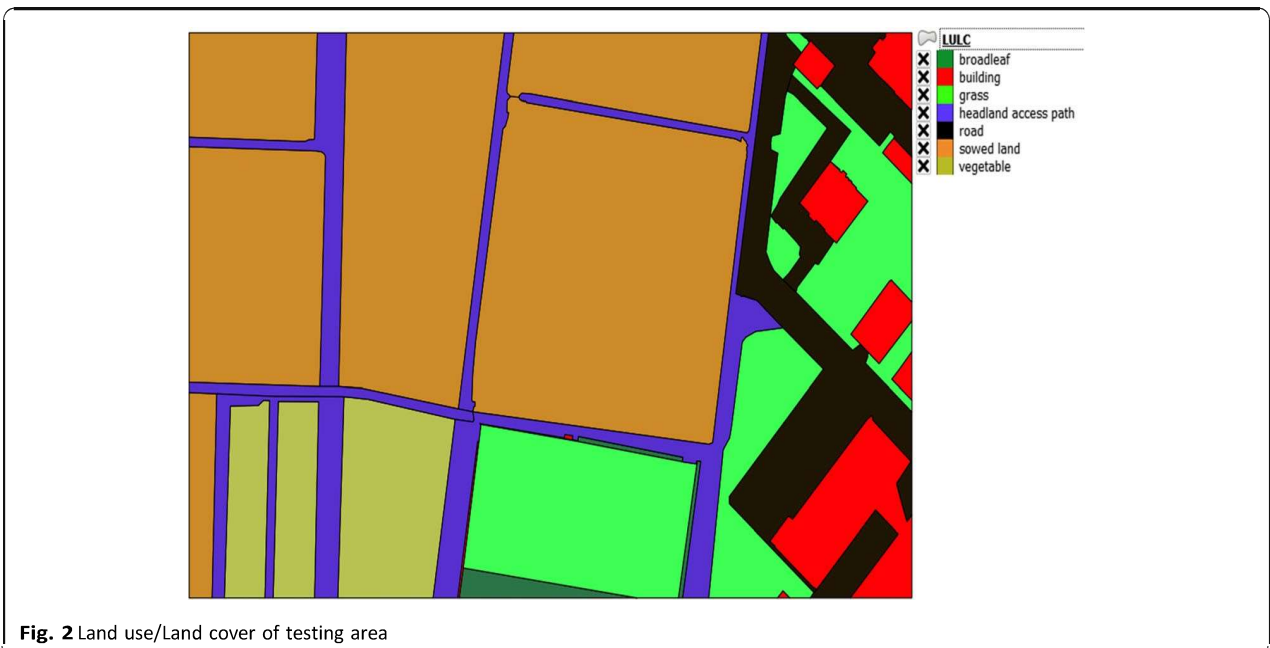

Fig. 2 Land use/Land cover of testing area

The accuracy metrics used for comparing results are the Kappa index, the classification accuracy and the classification error. Their values range from 0 to 100, and they are estimated with three different approaches, (i) using pixels from the training test set and applying KFold cross validation, (ii) using pixels from the validation test set, and (iii) using pixels from the full test set.

Results and discussion

The accuracy metrics are reported in three boxplots (Figs. 4, 5, 6) which represent respectively the Kappa index (K), the classification accuracy rate (Acc) and the classification error rate (CE). The last two are the inverse of each other. All metrics range from 0 to 100. The boxplots show the variance calculated from the ten runs for each
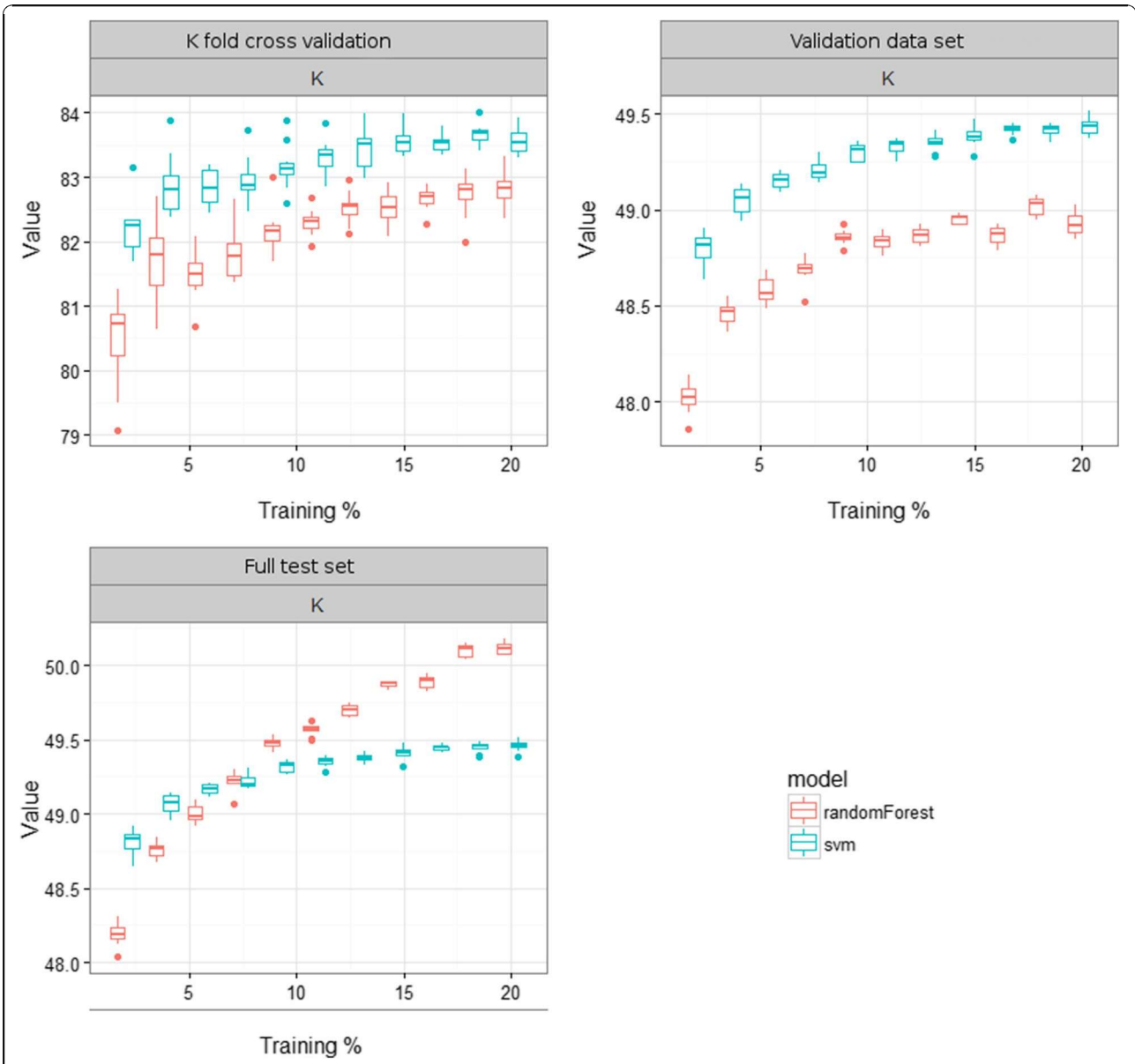
Fig. 4 Boxplot of Kappa index (percentage value) calculated for K-fold cross-validation, full test set and validation dataset ranging from 2 to 20% of the total population (n. of pixels)

training size. Figure 4 reports Kappa index calculated for K-fold test set, validation test set and full test sets. Comparing the boxplots of the three validation methods, it is clear how their values grow proportionally with the training subset size from 2% to 20%. The variance decreases with the increase of the training subset size. In the K-fold cross validation test set, the results range from 80 to 84, and the SVM performs better than RF. Using the validation test set, the results are similar, but values are,

as expected, lower, ranging from 48 to 49.5. In addition, in this case the SVM is better in comparison with RF. When validating against the full test set, the RF returns a better result than SVM when training with more than 10% of the full test set. The Kappa values range from 48 to 51. RF rises gradually from 48.5 to 50.5, whereas the SVM remains stable around 49.5.

Figure 5 shows the classification accuracy for K-fold test set, validation test set and full test sets. Likewise, the
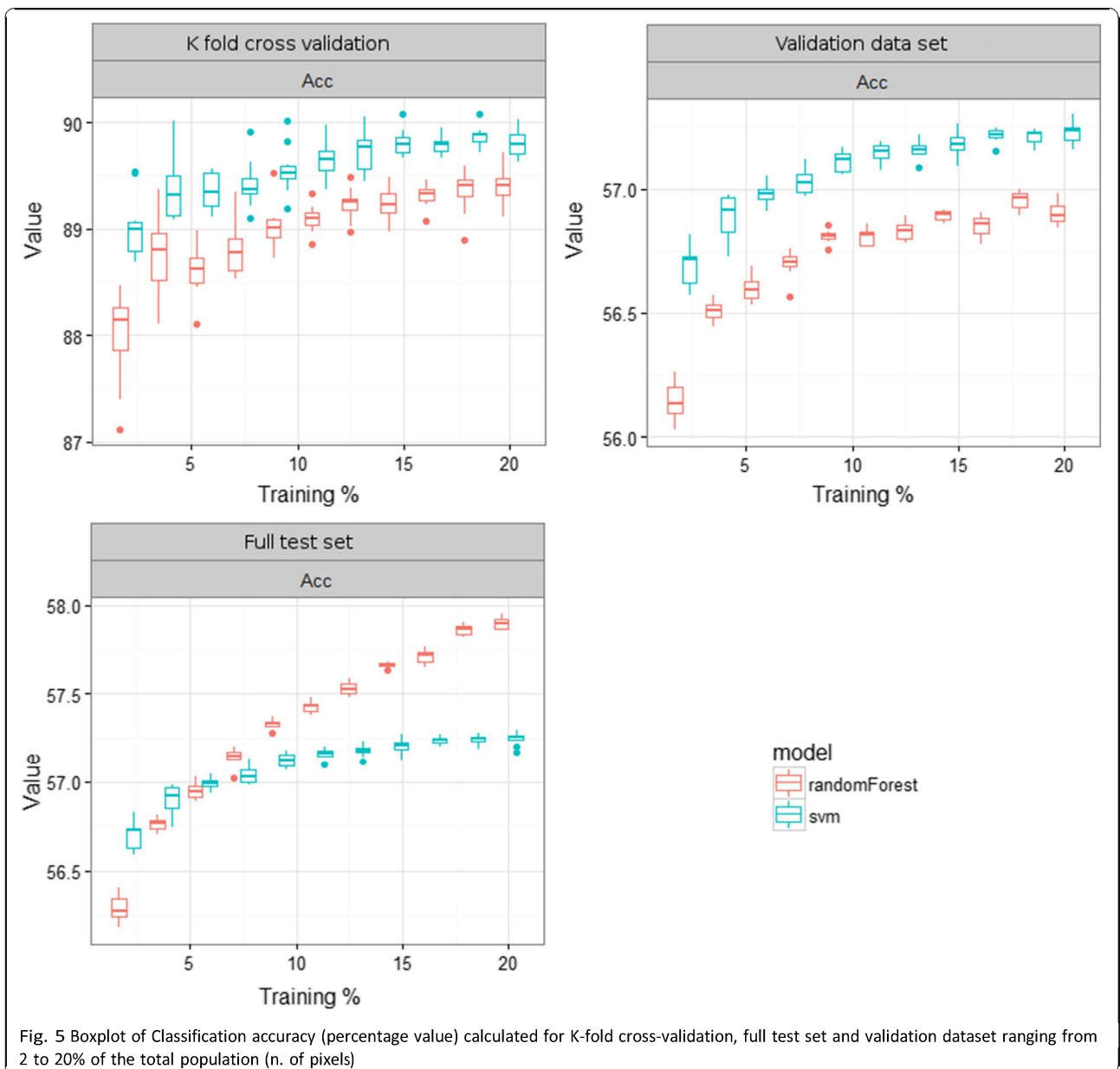

Fig. 5 Boxplot of Classification accuracy (percentage value) calculated for K-fold cross-validation, full test set and validation dataset ranging from 2 to 20% of the total population (n. of pixels)
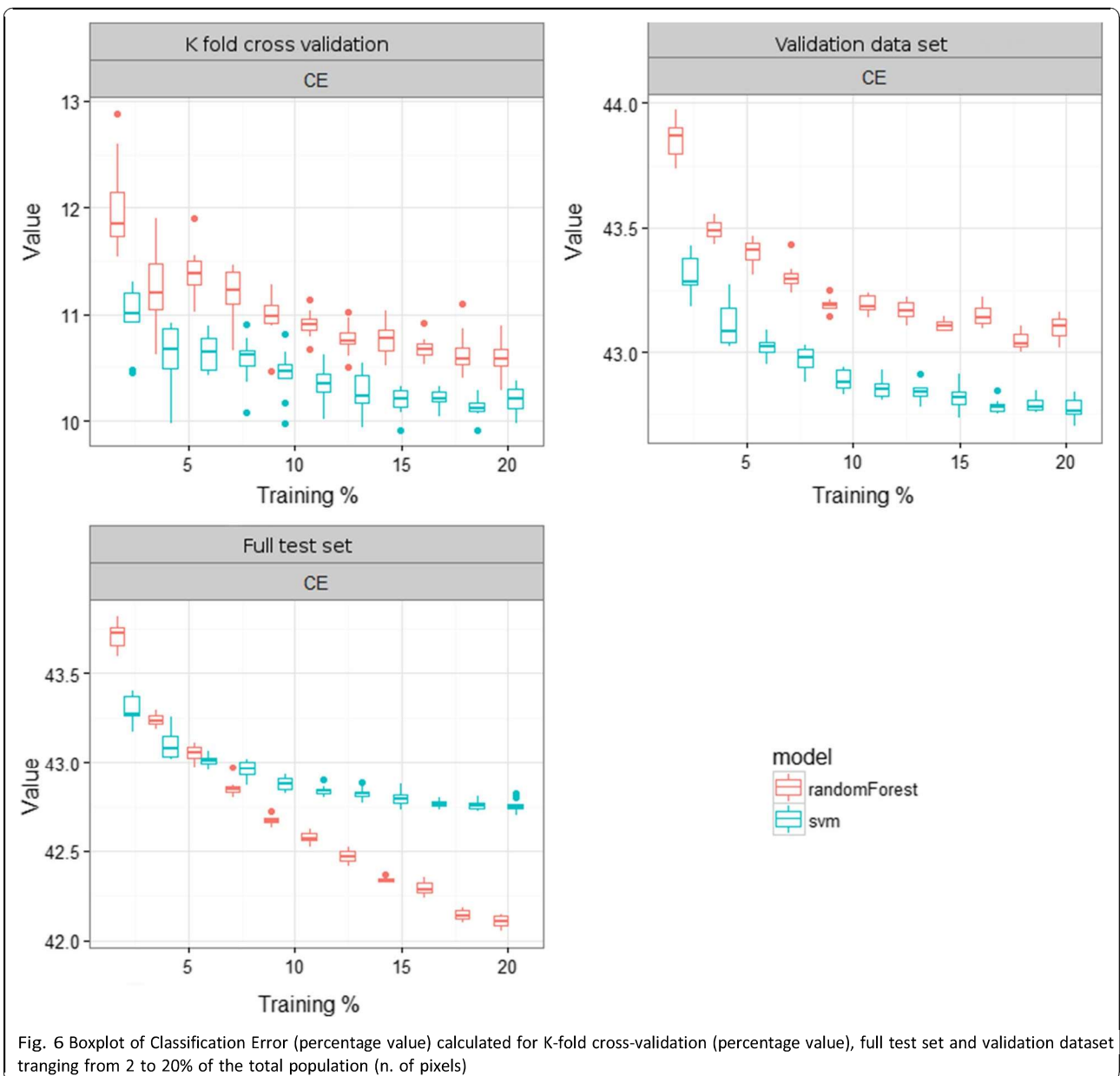
Fig. 6 Boxplot of Classification Error (percentage value) calculated for K-fold cross-validation (percentage value), full test set and validation dataset tranging from 2 to 20% of the total population (n. of pixels)

accuracy trend is similar the K index trend, and a gradual improvement in accuracy is related to an increasing training percentage. Indeed, using K-fold cross validation test set, the SVM gets a better result than RF. In this case, the score is over 88 whereas using a validation test the score ranges from 56 to 58. Using a full test set, the RF has better results than SVM, and the score ranges from 56 to 58. The RF rises gradually from 56 to 58, whereas SVM remains stable between 57 and 57.5.

Figure 6 illustrates a decreasing trend for classification error in the three dataset. In the K-fold cross validation test set, the SVM has less error that RF with variations of 0.5. Likewise, the validation test set has a decreasing trend, and the score ranges between 42 and 44. Using the full test set, errors range from 42 to 43.5, but the RF and SVM have a similar score using less than 5% of the pixels as training. Using a set for training of more than 5% of the total pixels, the RF and SVM results have some differences. The RF has a decreasing trend, and it reaches the minimum around 42, whereas SVM remains steady at 42.7.

Results by no means intend to prove one classifier better than another. Classifiers behave differently depending on several factors, and results prove exactly this point. Figure

4 is the most informative, where the first two validation methods show a better performance by SVM, but validation against the full test set provides a different result. The comparison of results from three different validation methods provides added insights on the behaviour that operators can expect from the two classifiers. Also, another informative aspect from the plots is the added value from using larger training sets. This is an important aspect, as bigger training sets require more computing time, and relative expenditure in terms of energy. Knowing the range of improvement over a growing training size can support decision in future classification procedures.

Another source for discussion is the definition of classes and their identification over the image. This, of course, has a certain degree of subjectivity depending on the operator who manually defines these areas with polygons. Also, the inevitable aspect of inter-class and intra-class spectral mixtures has to be accounted for.

Border pixels were removed in this study to limit mixing, but this operation does not remove the problem completely. Nevertheless, the results show significant relative differences correlated to the size of training sets. This is something to consider as supportive information when using such methods.

Conclusions

This paper compared accuracy metrics of two machine learning algorithms, SVM and RF, using three validation methods and testing different sizes of training sets. As expected, accuracy was better when a bigger training size is used, but this trend is not linear. This is particularly evident when the validation is done against the full test set. SVM gets better results with smaller training sets, whereas RF becomes better at training sizes larger than 7–8% of the total. Validation with K-fold and with the validation dataset showed SVM give better results, but RF proved to be more performing when training size is larger. Classification error and classification accuracy followed the trend of Kappa index.

Future investigations will limit mixing by careful selection of single pixels for both training and validation. This will decrease the size of the sets, but will increase the purity of pixel class and provide better insight on the behaviour of the machine learning methods. Available multi-spectral imagery benchmarking datasets will be considered also for further testing, for example the MUULF Gulfport dataset [27]. The focus of future studies will test more machine learning methods including multiple runs with different combinations of training and test sets, to improve on results from this study and from [16].

Authors' contributions

MP collected the data, developed the methodology, performed the analysis, and wrote the manuscript. AM reviewed the manuscript. FP designed the study, developed the methodology, and reviewed the manuscript.

Competing interests

The authors declare that they have no competing interests.

References

1. Pirotti F, Guarnieri A, Vettore A. Collaborative Web-GIS design: a case study for road risk analysis and monitoring. Trans GIS. 2011;15:213–26.
2. Van Asselen S, Verburg PH. Land cover change or land-use intensification:
Simulating land system change with a global-scale land change model. Glob Chang Biol. 2013;19:3648–67.
3. Berni JAJ, Zarco-Tejada PJ, Suárez L, Fereres E, Suarez L, Fereres E. Thermal and narrowband multispectral remote sensing for vegetation monitoring from an unmanned aerial vehicle. IEEE Trans Geosci Remote Sens. 2009;47(3):722–38.
4. Herwitz SR, Johnson LF, Dunagan SE, Higgins RG, Sullivan D V, Zheng J, et al. Imaging from an unmanned aerial vehicle: Agricultural surveillance and decision support. Comput Electron Agric. 2004;44(1):49–61.
5. Hunt ER, Dean Hively W, Fujikawa SJ, Linden DS, Daughtry CST, McCarty GW. Acquisition of NIR-green-blue digital photographs from unmanned aircraft for crop monitoring. Remote Sens. 2010;2(1):290–305.
6. Lelong CCD, Burger P, Jubelin G, Roux B, Labbé S, Baret F. Assessment of unmanned aerial vehicles imagery for quantitative monitoring of wheat crop in small plots. Sensors. 2008;8(5):3557–85.
7. Remondino F, Barazzetti L, Nex F, Scaioni M, Sarazzi D. UAV photgrammetry for mapping and 3D modeling – current status and future perspectives. In: Int Arch Photogramm Remote Sens Spat Inf Sci. 2011;38:14–16.
8. Papageorgiou EI, Markinos AT, Gemtos TA. Fuzzy cognitive map based approach for predicting yield in cotton crop production as a basis for decision support system in precision agriculture application. Appl Soft Comput. 2011;11(4):3643–57. https://doi.org/10.1016/j.asoc.2011.01.036.
9. Zheng YJ, Song Q, Chen SY. Multiobjective fireworks optimization for variable-rate fertilization in oil crop

production. Appl Soft Comput. 2013; 13(11):4253–63. http://dx.doi.org/10.1016/j.asoc.2013.07.004.

10. Hung C, Xu Z, Sukkarieh S. Feature learning based approach for weed classification using high resolution aerial images from a digital camera mounted on a UAV. Remote Sens. 2014;6(12):12037–54.

11. Guo X, Denman S, Fookes C, Mejias L, Sridharan S. Automatic UAV forced landing site detection using machine learning. In: 2014 Int Conf Digit Image Comput Tech Appl (DICTA), Wollongong, NSW, Australia, 25-27 November 2014. 2014. doi:10.1109/DICTA.2014.7008097.

12. Anthony D, Basha E, Ostdiek J, Ore J, Detweiler C. Surface Classification for Sensor Deployment from UAV Landings. In: 2015 IEEE Int Conf Robot Autom (ICRA), Seattle, WA, USA, 26-30 May 2015. 2015. doi:10.1109/ICRA. 2015.7139678.

13. Cracknell MJ, Reading AM. Geological mapping using remote sensing data: A comparison of five machine learning algorithms, their response to variations in the spatial distribution of training data and the use of explicit spatial information. Comput Geosci. 2014;63:22–33.

14. Foody GM, Mathur A. A relative evaluation of multiclass image classification by support vector machines. IEEE Trans Geosci Remote Sens. 2004;42(6): 1335–43.

15. Pal M. Random forest classifier for remote sensing classification. Int J Remote Sens. 2005;26(1):217–22.

16. Pirotti F, Sunar F, Piragnolo M. Benchmark of Machine Learning Methods for Classification of a Sentinel-2 Image. In: Int Arch Photogramm Remote Sens Spat Inf Sci XLI-B7:335–34. 2016. doi:10.5194/isprs-archives-XLI-B7-335-2016.

17. Song X. Comparison of artificial neural networks and support vector machine classifiers for land cover classification in Northern China using a SPOT-5 HRG image. Int J Remote Sens. 2012;33(10):3301–20. doi:10.1080/ 01431161.2011.568531.

18. Waske B, Benediktsson JA, Árnason K, Sveinsson JR. Mapping of hyperspectral AVIRIS data using machine-learning algorithms. Can J Remote Sens. 2009; 35(Suppl. 1):S106–S116.

19. Cortez P. rminer: Data Mining Classification and Regression Methods. 2016. Available from: https://cran.r-project.org/package=rminer. Accessed 27 June 2017.

20. Cortez P. Package "rminer" 2016. In: rminer: Data Mining Classification and Regression Methods. 2016. https://cran.r-project.org/web/packages/rminer/ rminer.pdf. Accessed 27 June 2017.

21. Cortez P. Data Mining with Neural Networks and Support Vector Machines Using the R/rminer Tool. In: Perner P. (eds) Advances in Data Mining.

Applications and Theoretical Aspects. ICDM 2010. Lecture Notes in Computer Science, vol 6171. Springer, Berlin, Heidelberg. 2010. https://link.springer.com/ chapter/10.1007/978-3-642-14400-4_44. Accessed 27 June 2017.

22. Cortez P. A tutorial on using the rminer R package for data mining tasks, Teaching Report. Department of Information Systems, ALGORITMI Research Centre, Engineering School, University of Minho, Guimar˜aes, Portugal. 2015.

23. Cortes C, Vapnik V. Support-Vector Networks. Mach Learn. 1995;20:273–97.

24. Shi T, Horvath S. Unsupervised Learning With Random Forest Predictors. J Comput Graph Stat. 2006;15:118–38. http://www.tandfonline.com/doi/abs/ 10.1198/106186006X94072. Accessed 27 June 2017.

25. Breiman L. Random forests. Machine Learning. 2001;45(1):5–32. doi:10.1023/ A:1010933404324.

26. Liaw A, Wiener M. Classification and Regression by randomForest. R News. 2/3(December). 2002;18–22.

27. Gader P, Zare A, Close R, Aitken J, Tuell G. MUUFL Gulfport Hyperspectral and LiDAR Airborne Data Set. Univ. Florida, Gainesville, FL, USA, Tech. Rep. REP-2013-570. 2013. https://github.com/GatorSense/MUUFLGulfport. Accessed 27 June 2017.

6. Paper V: Benchmark of machine learning for planning the wood harvesting operations

BENCHMARK OF MACHINE LEARNING FOR PLANNING WOOD HARVESTING OPERATIONS

M. Piragnolo[a], S. Grigolato[a], F. Pirotti[a]

[a] TESAF Department, University of Padua, Viale dell'Università 16, 35020 Legnaro, Italy
(marco.piragnolo@.phd.unipd.it)

Abstract

In the last decades, the interest in forest planning has been renewed with the use of high-resolution data and with the use of advanced spatial analysis techniques (Baskent and Keles, 2005; Li et al., 2007). The spatial analysis has also been applied successfully to wood harvesting and wood transportation both at the tactical and operational level. However, planning wood harvesting operations in complex situations, such as steep terrain, and low density of forest road network is challenging. To study, biomass and morphological aspect of harvesting site, the laser identification detection and ranging (LIDAR) is a common technology applied in forestry. Moreover, the usage of LIDAR and sophisticated classification methods, such as machine learning, can take advantage of a rich data set. Indeed, the machine learning is increasing in forestry, geomorphology. It can be effective using spatial data, such digital elevation model (DEM), altitude, slope, and the distance from the roads. For these reasons, the goal of the work is to support a decision-maker, using the machine learning approach based on morphological information, to identify the suitable areas for two classes of forestry machines, the skyline and the forwarder. Moreover, the innovation consists of simulating the choices of a worker during the forestry operations considering the accessibility of the area rather than estimate the morphological aspects, such as slope or roughness. The algorithms tested are conditional inference trees (Ctree), k-nearest neighbors (KNN), linear discriminant analysis (LDA), logistic regression (LR), multi-layered perceptron (MLP), multi-layered perceptron ensemble (MLPE), naive, naivebayes (NB), and random forest (RF). The metrics assessed through k-fold cross-validation are kappa (K), accuracy (ACC) and classification error (CE), and the execution time. Finally, a sensitivity analysis (SA) has been done to study the contribution of each input for the classification. The benchmark shows the RF has the best performance in terms of K 91.85%, but it is the slower in comparison to the KNN and the Ctree. However, the KNN process has a high accuracy

of 87.07%, and the processing is very fast. Finally, the Ctree is fastest, but it has the lower accuracy of 77.93%. The SA evidences the input relative importance for the RF, the KNN and the Ctree, where the accessibility of the harvesting site, have higher relative importance rather than the morphological aspect. Indeed, the slope and the roughness are less important for the classification.

1. Introduction

In the last decades, the interest in forest planning has been renewed with the use of high-resolution data and with the use of advanced spatial analysis techniques (Baskent and Keles, 2005; Li et al., 2007). Spatial analysis has also been applied successfully to wood harvesting and wood transportation both at the tactical and operational level (Grigolato et al., 2017). However, planning wood harvesting operations in complex situations, such as in wet-area (Murphy et al., 2007), roughness terrain (Duka et al., 2017), steep terrain (Bont et al., 2012; Kuhmaier and Stampfer, 2010) and low density of forest road network (Cavalli and Grigolato, 2010; Najafi and Richards, 2013) is challenging. Considering the wood harvesting operations, the main working phases are felling, tree processing, yarding, loading and hauling. Generally, in term of transportation, wood harvesting can be split into primary transportation and haul (or secondary transportation) (Owende, 2004). The primary transportation consists of extract log from the stump site to the first road along which logs are loaded into a truck for long transportation to the final wood processing sites. In the context of primary transportation, steep slope terrain together with a widespread terrain roughness force the choice of forest utilization systems based on highly specialized machines (Mologni et al., 2016). The main forest machines used in very steep slope terrain are an overhead system of the cinch-driven cable such as cable cranes (Proto et al., 2016) and articulated chassis tractors such as forwarders (Strandgard and Mitchell, 2015). The latter present with respect to the first operating limits depending on the slope (usually less than 40%) and the accidentally of the terrain (in particular with the spread of obstacles with a height greater than 50 cm) (Pentek et al., 2008). Recently, the introduction of winch assisted machine systems lets also forwarders to expand to work also in steeper terrain up to 70-80% (Holzleitner et al., 2018; Mologni et al., 2018; Visser and Stampfer, 2015). The usefulness of setting up spatial analysis models able to support forest technicians in the medium-term planning of wood harvesting. The current availability of high-resolution data such as data derived from laser identification detection and ranging (LIDAR) can give an advantage in terms

(In preparation)

of awareness. Certainly, the complexity of the spatial analysis (Grigolato et al., 2017) depends on a large number of variables, data sets and software. In fact, in addition to the slope and accidentally, other variables are the forest growing stock distribution, stand parameters and distance from the forest roads.

Consequently, the geographic information plays an important role in the planner of the forestry operation, and the GIS software can help the decision-maker for the data analysis (Matwin et al., 1995). The information derived from LIDAR and remote sensing data are used for estimate the model vegetation, the canopy, and the biomass estimation (Gleason and Im, 2012; Stojanova et al., 2010). In addition, the combination of LIDAR and machine learning can obtain positive results that exceed the traditional approaches such as the maximum likelihood classifier and linear regression models (Zhao et al., 2011). The machine learning is an automatic method for analysing data that iterates and learns from previous computation taking advantage of a rich data set. For these reasons, the machine learning have been applied in several studies, such as the precision agriculture (Papageorgiou et al., 2011; Zheng et al., 2013), land use / land cover (Pirotti et al., 2016), landslide assessment (Cracknell and Reading, 2014), surface classification (David Anthony et al., 2015). It and it can be effective using spatial data, such as geological maps, lithology, digital elevation model (DEM) (Marjanović et al., 2011), and morphological information e.g. altitude, slope, distance from road (Pradhan, 2013). Finally, studies of machine learning have been conducted with positive results in the different field of research related to marketing, psicology, e.g. for investigating the wine taste preferences, the preferences of the consumer, the marketing areas, and the contraceptive method choice (Cortez et al., 2009; Cortez and Embrechts, 2013).

The goal of the work is to support a decision-maker, using the machine learning approach based on morphological information, to identify the suitable areas for two classes of forestry machines, the skyline and the forwarder. Moreover, the innovation consists of simulating the choices of a worker during the forestry operations. We assume that it is more natural for a worker to focus the attention on the accessibility of the harvesting site rather than estimate the operation limits based on the morphological aspects, such as the slope or the roughness.

2. Materials and methods

The case study area is in the southern part of the Altopiano dei Sette Comuni in the Veneto region in Northern Italy, (Figure 2). The study area is 34.32 km2, and the perimeter is 34.4 km. The Pre-Alps

area is covered by forestry and two types of forestry machine, the forwarder and the skyline, are used in the harvesting sites, which are accessible through a roads network, as shown in Figure 3.
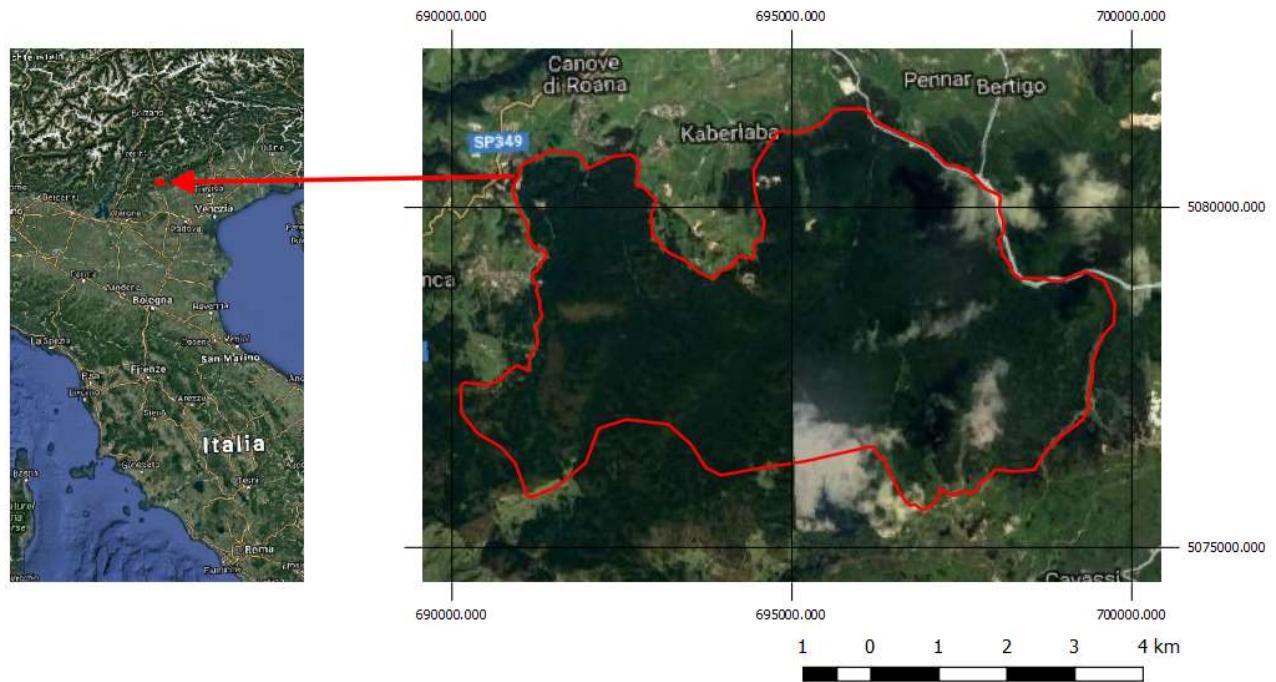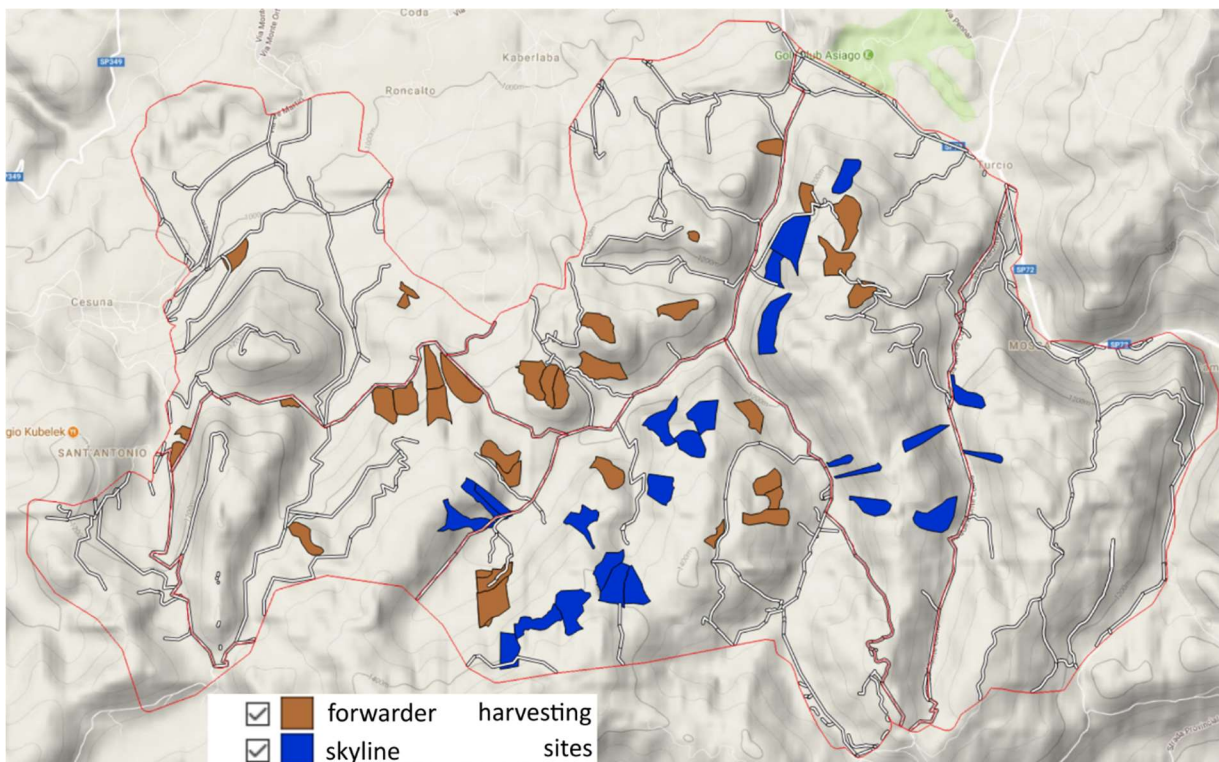

Figure 2 Location of the area of study

Figure 3 Location of the harvesting sites

(In preparation)

The dataset has been built in the R environment, using the digital elevation model (DMT), the canopy height model (CHM), the roads network and the by-products calculated from the previous ones. The DTM and the CHM raster maps have a ground sample distance (GSD) of 1 metre. Based on the DTM, the slope and the roughness map have been calculated. The forestry machines can work only in a specific condition e.g. the forwarder can work with slope lower than 40% and maximum roughness of 70 centimetres. Otherwise, the skyline is preferable. Indeed, it is theoretically possible to classify a land use map using this information. Nevertheless, we have added two layers that are the elevation difference between an arbitrary point and the nearest road, and the distance between the roads. The reason is to simulate the choices of a worker during the forestry operations. In our simulation, a worker is inside the harvesting site. We assume that it is more natural to focus the attention on the accessibility of the area rather than estimate the morphological aspect, such as slope or roughness. Therefore, the worker will try to move easily and fast identifying the minimum elevation difference between two points e.g. the place where he is and the nearest road. Consequently, the nearest road has been recognized starting from an arbitrary DTM cell, which represents the worker position. Then, the road elevation has been extracted, and the elevation difference has been calculated. Concerning the roads distance, it has been calculated by rasterizing the road network using the GSD of the DTM. Finally, the dataset raster stack counts 2150215 pixels, and it is composed of six layers: the DTM, the CHM, the slope, the roughness, the distance from between the roads, and the elevation difference between the cell of the DTM and the nearest cell of the road Table 2. To clarify the terminology, in this work we use "layer" to identify the single raster of the stack, whereas use "input" to identify the raster layer used as input in the sensitivity analysis.

Raster base layer	Vector base layer	Derived raster layer	Raster stack layer
DTM 1 m/pixel	-	-	DTM 1 m m/pixel
		Slope	Slope
		Roughness	Roughness
		Elevation difference from DTM and the nearest road	Elevation difference from DTM and the nearest road
CHM 1 m/pixel	-	-	CHM 1 m m/pixel
-	Road's network	Distance among the roads	Distance among the roads

Table 2 Summary of the layers that compose the raster stack

A prior statistical analysis of the correlation between the layers derived from DTM has been done for assessing potential effect in the classification process. In addition, the big number of the pixel can be time-consuming for the training, the test and the classification phase. Then, to obtain a good result that balance the accuracy and the processing time, a stratified sample of 10% has been done. On one hand, using a number of pixels lower than this threshold the performance is poorly. On the other and, using threshold the accuracy trend is stable. Using more than 10% there is no significant improvement (Piragnolo et al., 2017). The machine learning framework has been tested using a similar approach to the framework described in (Pirotti et al., 2016). Moreover, the subsample has been split into a training set (60%), a validation set (20%) and test set (20%). The training phase uses regions of interest (ROIs) that correspond to two types of harvesting site where forwarder and skyline machines have been used. During the training and the testing phase, the accuracy has been evaluated using three metrics applying the k-fold cross-validation. The metrics are: are kappa (K), accuracy (ACC) and classification error (CE), and the execution time. The k-fold cross-validation split the subset in 10 k-fold, and using k-1 for the training and 1 for the testing, and helps to reduce overfitting problems. Finally, the algorithms tested are conditional inference trees (Ctree), k-nearest neighbors (KNN), linear discriminant analysis (LDA), logistic regression (LR), multi-layered perceptron (MLP), multi-layered perceptron ensemble (MLPE), naive, naivebayes (NB), and random forest (RF).

The Ctree uses a tree to partition recursively the covariate M that influence the variable Y. M is an m-dimensional covariate vector X=(X1…., Xm). The algorithm fits a learning sample, where the learning sample is a random sample composed of n observations vector. Consequently, the algorithm works recursively on the vector. The steps of binary partitioning are: testing the null hypothesis between the m covariate and Y and selecting the covariate Xi with the strongest association with Y. Measuring the associated P-values. Running the algorithm until the hypothesis is accepted. Splitting the variable into two subgroups, and repeating the previous steps. In case of the covariate Xi is missing, a new split can be calculated leading the same division of original split. When the null hypothesis is accepted, the algorithm stops (Hothorn et al., 2015).

The KNN is based on a distance metric. Then, it finds the k nearest neighbours of the sample, and it assigns the sample with a majority vote among the K-nearest Neighbors. The method advantage is to adapt to a new training data set, but the computational request and storage space is significant. The key to avoiding overfitting and the underfitting problem is the right choice of k,

for example, using the standardized Euclidean distance. The steps are: choose the number of k nearest neighbours and a distance metric. Determine the k nearest neighbours. Count the majority vote and assign the class label (Raschka, 2015).

The LDA is an algorithm for solving multi-class classification problems. The LDA is based on the dataset normality assumption and the independence feature assumption. The goal is to find the best variable combination for dividing the space into regions using a linear boundary. (Venables and Ripley, 2002).

The LR is an algorithm for linear and binary classification based on neural network, where the classes are linearly separable. The binary classification is extended to multiclass classification using the One-vs-Rest (OvR) method. The OvR trains one classifier for a class. Then, it assigns a positive value to the class membership, and all other classes are considered as negative values. Iterating n times, where n is the number of classes a specific sample is assigned to a class considering the probability of membership. Logistic regression tries to maximize the likelihoods of the training data (Cheng et al., 2006).

The MLP and the MLPE are neural networks composed of two perceptron layers. The perceptron algorithm has been developed in the 50s, and it is a single layer neural network with a threshold activation function, where the inputs are connected directly output using connected with adaptive weights. The advantage of the perceptron is to find a solution in a finite number of steps as studied by several authors (Arbib, 1987)(Duda and Hart, 1973) (Hand, 1985) (Hertz et al., 1991)(Minsky and Papert, 1988)(Van Der Malsburg, 1986). However, when the dataset is not linearly separable data the learning algorithm cycle to infinite and never terminate. The multi-layer perceptron is a perceptron network composed of layers with adaptive weights. Thus, the input units of the first layer are connected to the output layer through intermediate layers (Atkinson and Tatnall, 1997) (Benz et al., 2004).

The naive and NB algorithm tries to solve the classification problem using a simple and direct way. It could be described as a query that starts from the source to the end of the dataset. The NB uses the probability theorem to classify a normally distributed dataset, where the class feature is independent. Nevertheless, in the case of weak violation of independence assumptions in a small sample, the NB still tend to perform well. In case of strong violation of independence assumptions or non-linear classification, very poor performance is obtained (Raschka, 2014).

The RF is a decision tree based on a bootstrap technique that creates a large number of training sets to compute the statistics. Hence, it draws randomly a sample of size n with no replacement,

(In preparation)

and the value of n controls the bias and the variance. Replacement means an element can appear multiple times in the sample. On one hand, large values of n reduce randomness and increase the overfitting risk, on the other hand, small values of n reduce risk and model performance. Then, a decision tree grows, selecting d feature without replacement, so an element can appear only once in the sample. The tree nodes are split and the procedure is repeated k times. Consequently, the class label is assigned by majority vote to the aggregated classification (Breiman, 2001).

Finally, the trained model has been studied with the sensitivity analysis (SA). The SA is a technique to interpret a black box model, studying the input layers. Indeed, a black box model produces one output (y) using M inputs. Applying the sensitivity samples to the fitted model, the model responses are obtained as stated in the (1) :

$$\hat{y} = P(x) \qquad (1)$$

$\hat{y}$ is the value predicted by the model

$P()$ is the function used to build the predicted value

x is the data sample

Consequently, the input variable $\{x_a : a \in \{1, M\}\}$ ranges through minimum to maximum with L levels. hen, calculating the input sensitivity for each input variable, the relevant input can be identified through the variation of the input level. Indeed, all inputs held at their average value, and one input changes assuming the L value (Kewley et al., 2000). For example, using a One-dimensional SA (1D-SA) with 7 levels, the x_a ranges [0, 1], and the values are $x_{aj} \in (0.0, 0.14, 0.29, 0.57, 0.71, 0.86, 1.0)$. The following formula describes the model (2):

$$\hat{y}_a = \{\hat{y}_{aj} : j \in \{1, \dots, L\} \qquad (2)$$

where:

$\hat{y}_{aj}$ is the x_{aj} response.

The input importance can be calculated using the input sensitivity. The sensitivity measure is calculated using the Average Absolute Distance (AAD) from the median (s_d) proposed by (Cortez and Embrechts, 2013). A relevant input can be identified through the variation of the input level, and a variation of input levels produce output changes. The AAD is a robust method few sensitive to out layers, where a high value indicates high input relevance, as stated in the (3):

$$s_d = \sum_{j=1}^{L} |\hat{y}_{aj} - \widetilde{y_a}| / L \qquad (3)$$

The sensitivity measure is calculated from the responses of x_a, and a high value indicates high relevance. The relative importance (4) is:

$$r_a = \varsigma_a / \sum_{i=1}^{M} \varsigma_i \qquad (4)$$

r_a = relative importance

ς_a = sensitivity for input x_a

The sensitivity values have been plotted using Variable Effect Curve (VEC) that plot input $x$aj versus the $\hat{y}_{aj}$ responses. In the paper, the input variables are the layers of the raster stack previous described. Consequently, I1 is the DTM layer, I2 is the CHM, I3 is the slope, I4 is the roughness, I5 is the distance from DTM and the roads and I6 is elevation difference between a DTM cell and nearest roads cell.

3. Results

A statistical analysis has been done to assess the normality and the correlation among the raster layers, in particular among the DTM and DTM-derived layers. The dataset is not normally distributed as reported in Figure 3 and Table 1. Therefore, we have been applied a not parametric test to study the homogeneity of variance and correlation. The results of Figner-Killeen show all input layers have not homogeneous variance as reported in Table 4. The correlation has been calculated using the Kendall Rank correlation, which is a robust, not parametric test (Croux and Dehon, 2010). The correlations among DTM and respectively the slope, the distance from roads, the elevation difference between the DTM and the roads, and the roughness are reported in Figure 4 and Table 4. A weak correlation has been found between the DTM and the distance from roads. In the other cases, a very weak correlation has been found.
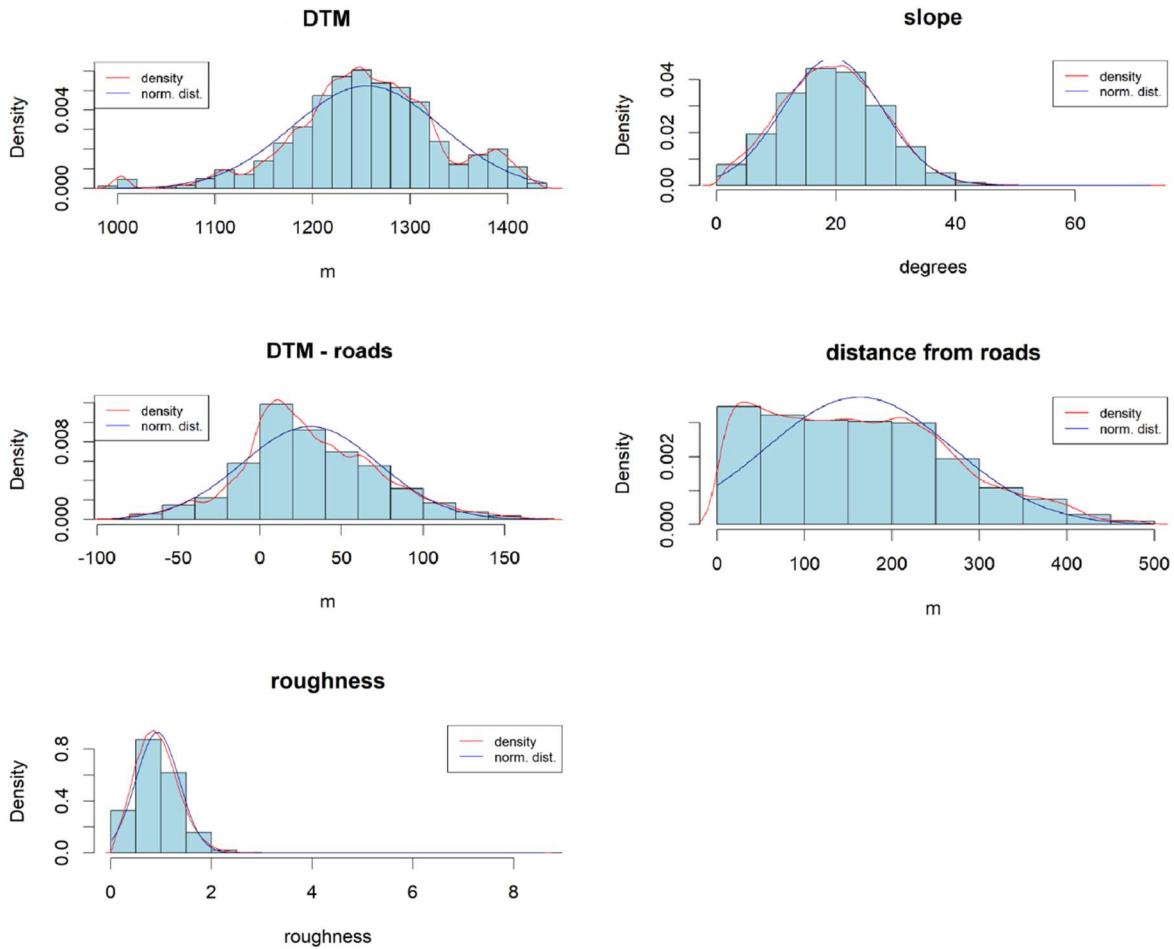
(In preparation)

Figure 4 Normality and density distribution for the raster stack

Normality	DTM	Slope	Distance	DTM-roads	DTM, roguhness
Shapiro-wilk	p-value <2.2e-16	p-value <3.288e-10	p-value <2.2e-16	p-value <2.2e-16	p-value < 2.2e-16
	Not normal	Not normal	Not normal	Not normal	Not Normal
Skewness	-0.3108419	0.1355057	0.5314014	0.3801503	0.9623484
	to the left	to the right	to the right	to the right	to the right
Kurtosis	0.7861781	-0.3649288	-0.3125651	0.3053029	5.141353
	platykurtic	platykurtic	platykurtic	platykurtic	leptokurtic

Table 3 Test for the normality

Homogeneity of Variances	DTM, slope	DTM, distance from roads	DTM, DTM-roads	DTM, roguhness
Figner-Killeen	p-value = 1.644e-08	p-value < 2.2e-16	p-value 0.000797	p-value < 2.2e-16
	Variances not homogenous	Variances not homogenous	Variances not homogenous	Variances not homogenous

Table 4 Homogeneity of variance has been studied with the not parametric test.
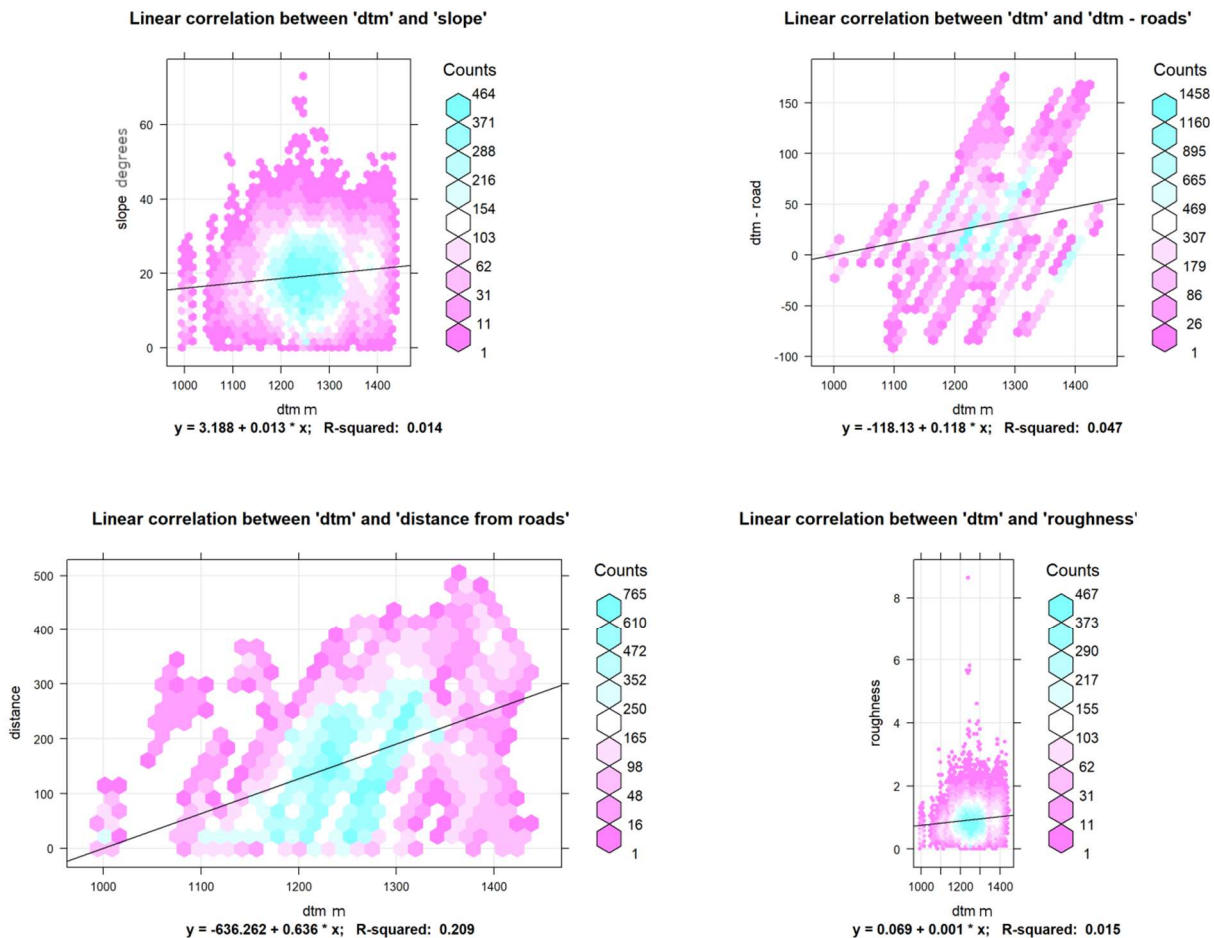
(In preparation)

Figure 5 Scatterplot with hexagon cell to visualize large dataset. The scatterplot shows the very low correlation between DTM and stack's layers.

Correlation	DTM, slope	DTM, distance from roads	DTM, DTM-roads	DTM, roughness
Kendall's rank correlation	p-value < 2.2e-16	p-value < 2.2e-16	p-value < 2.2e-16	p-value < 2.2e-16
	tau 0.06062991	tau 0.3243403	tau 0.1580749	tau 0.06139136
	Very weak correlation	Weak correlation	Very weak correlation	Very weak correlation

Table 5 Correlation between DTM and the levels of the stack has been calculated with two not parametric test.

The correlation has been calculated between the layer of the difference of elevation and the layer of the distance from the roads. The Kendall's rank correlation tau is 0.33 that indicate a weak correlation as reported in Figure 6.
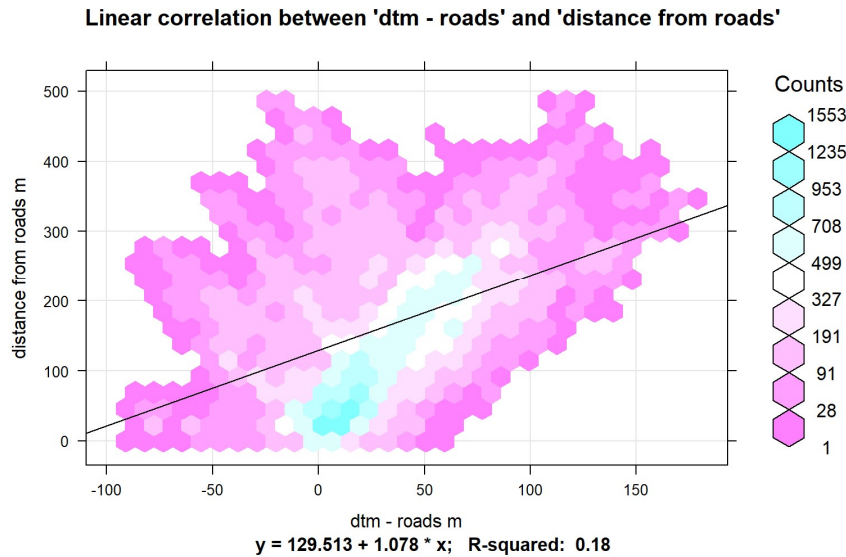
(In preparation)

Linear correlation between 'dtm - roads' and 'distance from roads'

y = 129.513 + 1.078 * x;   R-squared: 0.18

Figure 6 Correlation between the level of the elevation difference (DTM - roads) and the layer of the distance from roads

The statistical analysis evidences weak and very weak correlation, so it reasonable think to a limited effect in the classification process. Consequently, the machine learning has been performed calculating the probability of each pixel to be classified as a forwarder or a skyline. The accuracy metrics of the training ranges between0-100, and they are reported in Table 6 and Figure 7. The three best algorithms in terms of K and process time are the RF, the KNN, and the Ctree, and they have been used for the testing. The K value for RF is 95.49, for KNN is 95.23, and for the Ctree is 84.36. In contrast, the faster algorithm is the KNN, whereas the slower algorithm is the RF.

Model	Task	Time Sec.	K	ACC	CE	Estim. Sec.
RF	prob	292,35	95,49	97,6	2,4	9690,19
KNN	prob	0,01	91,04	95,23	4,77	0,33
Ctree	prob	34,87	84,36	91,7	8,3	1155,8
Mlpe	prob	136,64	63,56	80,6	19,4	4529,05
Mlp	prob	136,76	62,8	80,2	19,8	4533,03
Lr	prob	9,59	54,99	75,95	24,05	317,87
NaiveBayes	prob	0,36	54,65	75,61	24,39	11,93
Lda	prob	0,37	52,04	73,67	26,33	12,26
Naive	prob	0,01	0	52,64	47,36	0,33

Table 6 Accuracy metric for the training set. The table reports also the time estimation for the classification for the full dataset.
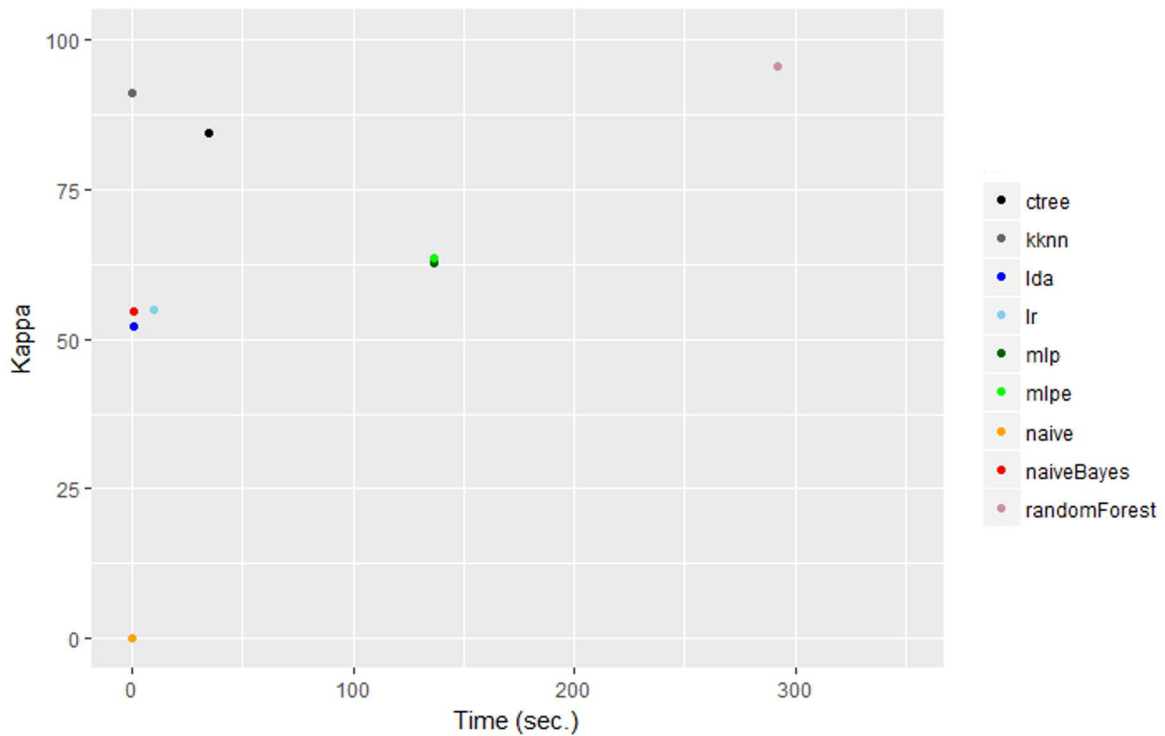
(In preparation)

Figure 7 Plot of the time vs K. Random Forest has the best K score, but it is very slow. In contrast, KNN and Ctree are faster than RF.

The result of machine learning using the test set is reported in the following Table 7 and Figure 8. Likewise, in the training phase, the RF has the higher k, and the Ctree has the lowest k. In comparison to the training phase, the values have has been decreased.

Model	Task	Time	K	ACC	CE
RF	prob	770,2	91,85	95,67	4,33
KKN	prob	57,45	87,07	93,13	6,87
Ctree	prob	50,52	77,93	88,33	11,67

Table 7 Accuracy metric for the test set

Figure 8 Time vs K for the test set

(In preparation)

82

Specifically, the RF is the slower algorithm, but it has a high K score of 91.85. KNN has K of 87.07. In contrast to the training set result, the KNN is slower than the Ctree. The Ctree is the fastest algorithm with a K of 77.93. Finally, the sensitivity analysis has been conducted for the three algorithms using the AAD metric. The AAD metric measures the relative importance of RF inputs as reported in Figure 9. The most important inputs are the elevation difference between the DTM and the roads, then the DTM, and the distance between roads. In contrast, the CHM, the slope and the roughness have less importance.

Relative importance

0.0	0.1	0.2	0.3	0.4

DTM-roads

DTM

Distance roads

CHM

Slope

Roughness

0.0	0.1	0.2	0.3	0.4
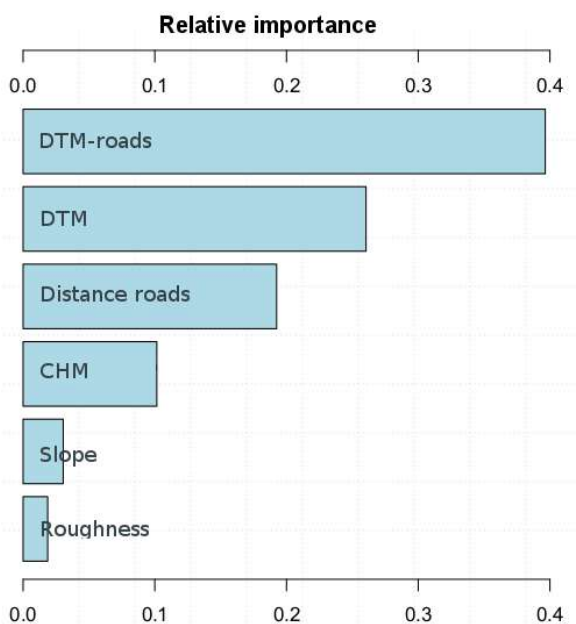
Figure 9 Random Forest relative importance of the input variables. The x-axis reports the AAD metric

To understand the contribution of each input in the classification process, a detailed analysis of the inputs has been done using the VEC plot as a report in Figure 10. The values are summarized in Table 8. The elevation difference, which ranges between negative values and 50 metres, has a high sensitivity in the forwarder class. In contrast, the skyline label is assigned when the elevation difference is greater than 100 metres. Between 0 and 50 metres, the sensitivity is 0.5 for both classes. The DTM has a threshold of 1300 metres that clearly discriminates the forwarder and the skyline classes. The distance from roads affects the forwarder class for values lower than 100 metres. In contrast, the skyline is recognized for values greater than 200 metres. Between 100 and 200 metres, there classification is not clear, and both classes have a value of 0.5. The CHM sets a threshold of 6 metres that discriminates well the forwarder and the skyline classes. The slope of 20 degrees is the threshold that discriminates the forwarder and the skyline. Indeed, the forwarder sensitivity ranges between 0 and 20 degrees, whereas the skyline ranges from 20 degrees to 40

(In preparation)

degrees. The roughness sensitivity can be found for values lower than 1 metre, but the flat trend suggests a low importance of this input for the classification.
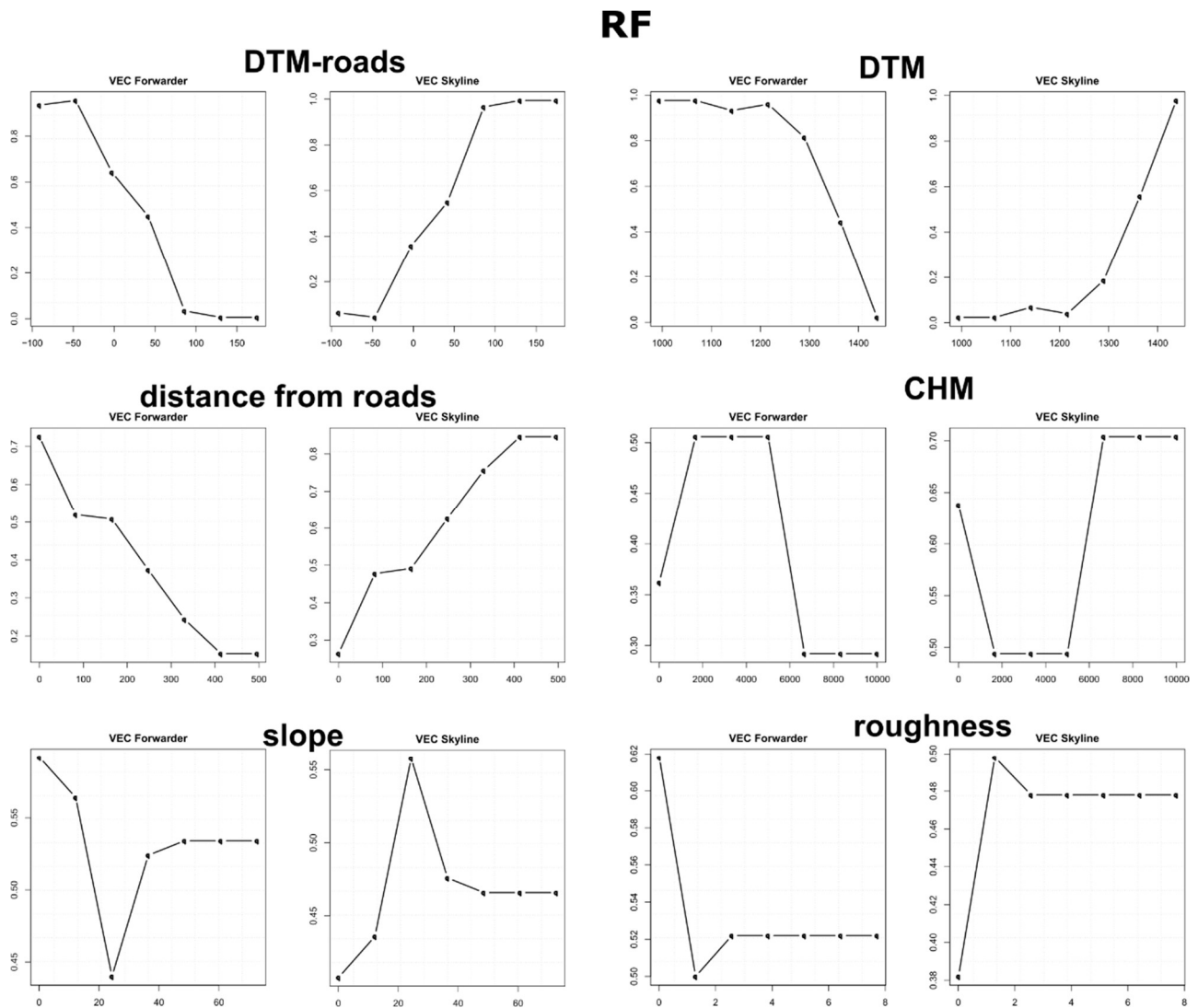

Figure 10 Inputs sensitivity analysis for the two classes of the RF classification. The X-axis reports the input level, and the Y-axis reports the sensitivity value. High input sensitivity occurred when the trend is varying, whereas a flat trend suggests low sensitivity.

Input	Forwarder Sensitivity	Skyline Sensitivity
Elevation difference	< 50 m	> 100 m
DTM	< 1300 m	> 1300 m
Distance from roads	< 100 m	> 200 m
CHM	< 6 m	> 6 m
Slope	< 20°	20° - 40°
Roughness	-	-

Table 8 Class sensitivity for the input layers using RF

The KKN has a K score of 87.07, and it is faster than RF. The inputs relative importance for the KNN is reported in Figure 11. The most important input is the elevation difference between the DTM and

(In preparation)

the roads. Then, the distance between roads and CHM. The slope, the roughness and the DTM are fewer important for the classification process. The specific VEC plots are reported in Figure 12, and the values are summarized in Table 9. The sensitivity of the elevation difference is similar to the RF. The forwarder label is assigned for values lower than 50 metres, whereas the skyline is assigned for values greater than 50 metres. The distance from the roads shows a saw shape curve. The forwarder sensitivity ranges between 0.2 and 1, and the skyline sensitivity ranges between 0.1 and 0.7. Still, the peak of one class corresponds to the minimum of the other class. Consequently, in this range, there is a high sensitivity for all the classes, but the forwarder has slight higher values. However, the skyline sensitivity reaches the top when the distance is greater than 300 metres. The CHM trend highlight the value of 6 metres is significant to define the two classes. Below 6 metres of the tree height, the forwarder has the maximum sensitivity. Above 6 metres, the skyline is defined. The slope has a clear peak at 40 degrees. The sensitivity for the forwarder reaches the maximum below the threshold of 40 degrees. In addition, above 60 degrees, forwarder gets a high score, but the result is not is not significant. Indeed, the limit operation of the forestry machine is 40 degrees. Instead, the skyline has a high value between 20 degrees and 60 degrees, where the maximum is 40 degrees. The roughness shows a saw shape trend, where the minimum and the maximum are alternated. The sensitivity is high, but the roughness values do not match with the real operation limits. Finally, the DTM has high sensitivity without variation for both classes, which implicates a low relative importance.
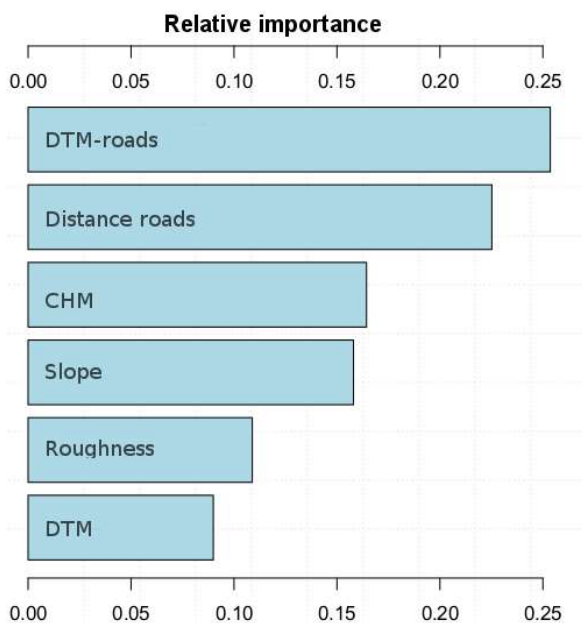

Figure 11 KNN relative importance of the input variables. The x-axis reports the AAD metric
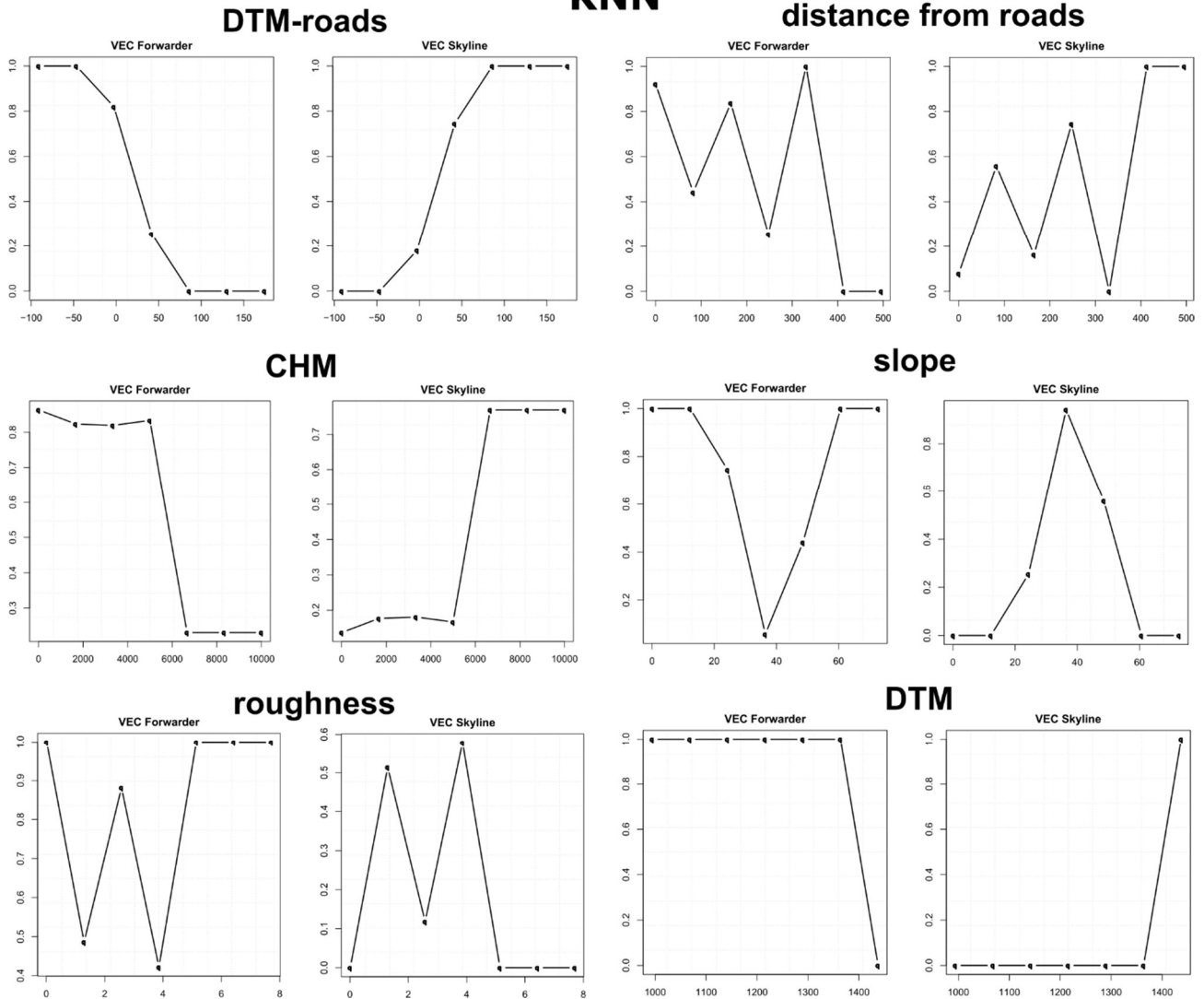
(In preparation)

Figure 12 Inputs sensitivity analysis for the two classes of the KNN classification. The X-axis reports the input level, and the Y-axis reports the sensitivity value. High input sensitivity occurred when the trend is varying, whereas a flat trend suggests low sensitivity.

Input	Forwarder Sensitivity	Skyline Sensitivity
Elevation difference	< 50 m	> 50 m
Distance from roads	< 300 m	> 300 m
CHM	< 6 m	> 6 m
Slope	< 40°	> 40°
Roughness	< 1	> 1
DTM	-	-

Table 9 Class sensitivity for the input layers using KNN

The Cree classifier has a K score of 77.93, and it is the fastest algorithms used in the test. The AAD metric and the relative importance are reported in Figure 13. The VEC plots for the two classes, forwarder and skyline, are reported in the Figure 14, and the values are summarized in Table 10 . A high sensitivity has been found for the distance from roads. Both classes range between 0.2 and 1.

(In preparation)

Thus, the threshold can be set at 300 metres distance. The forwarder is defined below the 300 metres and the skyline above the 300 metres distance.

Regarding the elevation difference input, the forwarder has high sensitivity when the elevation difference ranges between -100 metres and 50 metres. In contrast, the skyline gets a high score only when the elevation difference is greater than 50 metres. Analysing the DTM, forwarder has high sensitivity when the elevation is lower than 1300 metres, whereas the skyline above the 1300 metres of elevation. The slope threshold for the two classes is defined at 20 degrees. Indeed, below 20 degrees forwarder has a score of 1, whereas above 20 degrees the skyline sensitivity increases. The sensitivity of tree height is high until 2 metres, where forwarder sensitivity is high at 0 metres and forwarder at 2 metres. Two metres is a low height for a for a coppice, and it suggests that CHM can be omitted from the dataset. Finally, roughness does not produce relative important output.
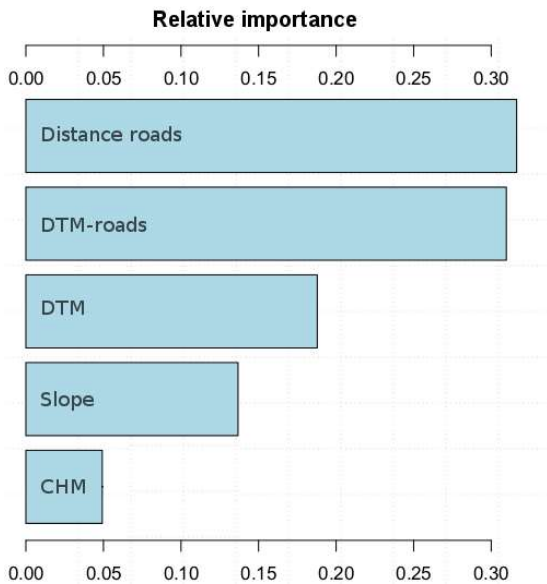

Figure 13 Relative Importance of the input variables using Ctree. The x-axis reports the AAD metric

Input	Forwarder Sensitivity	Skyline Sensitivity
Distance from roads	< 300 m	> 300 m
Elevation difference	< 50 m	> 50 m
DTM	< 1300 m	> 1300 m
Slope	< 10° m	10° - 40°
CHM	-	°-
Roughness	-	-

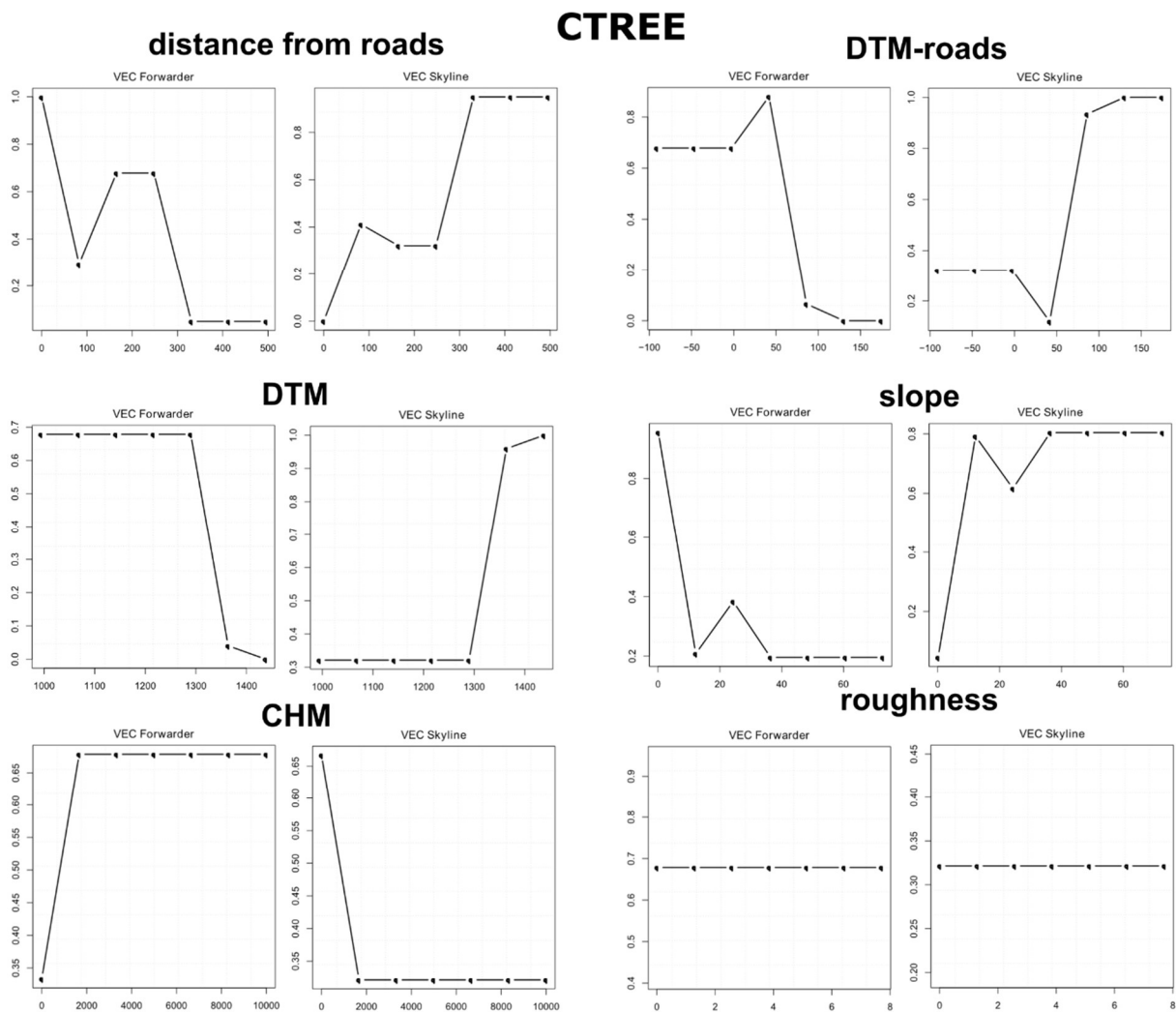Table 10 Class sensitivity for the input layers using Ctree

Figure 14 Inputs sensitivity analysis for the two classes of the Ctree classification. The X-axis reports the input level, and the Y-axis reports the sensitivity value. High input sensitivity occurred when the trend is varying, whereas a flat trend suggests low sensitivity

4. Conclusions

In this paper, we propose to use spatial and morphological information, such as the DTM, the CHM, the slope, the roughness, the elevation difference and the distance from roads using machine learning for testing several algorithms and classifying a suitability map for two forestry machine types: forwarder and skyline. Forestry machine operates in a defined range of technical specifications and parameters, and the parameters are considered by the decision maker for defining the harvesting area. The novel approach consists to integrate the information on the accessibility of the area for simulating the worker choices. The benchmark shows the RF has the best performance in terms of K, but it is the slower in comparison to the KNN and the Ctree. However, the KNN process has a high accuracy, and the processing is very fast. Finally, Ctree is

(In preparation)

fastest, but it has the lower accuracy. To support a decision-maker, understanding and interpretability of the data model is a key issue. For this purpose, the SA analysis has been conducted. The SA evidences the inputs relative importance for the RF, the KNN and the Ctree, where the accessibility have higher relative importance rather than the morphological aspect. The accessibility is described through of the harvesting site describes through the distance from the roads, and the elevation difference between the roads. Consequently, the slope and the roughness are less important for the classification. The forestry machine has some operation limits, specified in terms of maximum slope or roughness of the harvesting site. However, the choice of the route based on the accessibility of the area is a human decision. In addition, the VEC plots report the sensitivity of each input. Then, the RF uses the elevation and the distance from the roads network for making the prediction, and all inputs can give a contribution to the classification. The KNN is similar to the RF, and it considers the CHM as an important input. On the other hand, the roughness and the DTM do not add significant information.

Finally, the Ctree takes into consideration the accessibility of the harvesting site, but the CHM provides an information that has no evidence in the real domain. Moreover, the roughness does not influence the classification. Considering the low relative importance of some inputs, more studies can be conducted using only the important inputs as a strategy to improve the performance and reducing the computing time.

Reference

Anthony, D., Basha, E., Ostdiek, J., Ore, J., Detweiler, C., 2015. Surface classification for sensor deployment from UAV landings, in: *2015 IEEE International Conference on Robotics and Automation (ICRA)*. IEEE, Seattle, pp. 3464–3470. doi:10.1109/ICRA.2015.7139678

Arbib, M.A., 1987. Brains, Machines, and Mathematics (2Nd Ed.). Springer-Verlag, Berlin, Heidelberg.

Atkinson, P.M., Tatnall, A.R.L., 1997. Introduction Neural networks in remote sensing. *International Journal of Remote Sensing*, 18, 699–709. doi:10.1080/014311697218700

Baskent, E.Z., Keles, S., 2005. Spatial forest planning: A review. *Ecological Modelling*,. doi:10.1016/j.ecolmodel.2005.01.059

Benz, U.C., Hofmann, P., Willhauck, G., Lingenfelder, I., Heynen, M., 2004. Multi-resolution, object-oriented fuzzy analysis of remote sensing data for GIS-ready information. *ISPRS Journal of Photogrammetry and Remote Sensing*, 58, 239–258. doi:https://doi.org/10.1016/j.isprsjprs.2003.10.002

Bont, L.G., Heinimann, H.R., Church, R.L., 2012. Concurrent optimization of harvesting and road network layouts under steep terrain. *Annals of Operations Research*, 232, 41–64. doi:10.1007/s10479-012-1273-4

Breiman, L., 2001. Random forests. *Machine Learning*, 45, 5–32. doi:10.1023/A:1010933404324

Cavalli, R., Grigolato, S., 2010. Influence of characteristics and extension of a forest road network on the supply cost of forest woodchips. *Journal of Forest Research*, 15, 202–209. doi:DOI 10.1007/s10310-009-0170-4

Cheng, Q., Varshney, P.K., Arora, M.K., 2006. Logistic Regression for Feature Selection and Soft Classi cation of Remote Sensing Data. *IEEE Geoscience and Remote Sensing Letters*, 3, 491–494. doi:10.1109/LGRS.2006.877949

Cortez, P., Cerdeira, A., Almeida, F., Matos, T., Reis, J., 2009. Modeling wine preferences by data mining from physicochemical properties. *Decision Support Systems*, 47, 547–553. doi:10.1016/j.dss.2009.05.016

Cortez, P., Embrechts, M.J., 2013. Using sensitivity analysis and visualization techniques to open black box data mining models. *Information Sciences*, 225, 1–17. doi:10.1016/j.ins.2012.10.039

Cracknell, M.J., Reading, A.M., 2014. Geological mapping using remote sensing data: A comparison of five machine learning algorithms, their response to variations in the spatial distribution of training data and the use of explicit spatial information. *Computers and Geosciences*, 63, 22–33. doi:10.1016/j.cageo.2013.10.008

Croux, C., Dehon, C., 2010. Influence functions of the Spearman and Kendall correlation measures. *Statistical Methods and Applications*, 19, 497–515. doi:10.1007/s10260-010-0142-z

Duda, R.O., Hart, P.E., 1973. Pattern classification and scene analysis / Richard O. Duda, Peter E. Hart. Wiley New York.

Duka, A., Grigolato, S., Papa, I., Pentek, T., Poršinsky, T., 2017. Assessment of timber extraction distance and skid road network in steep karst terrain. *iForest - Biogeosciences and Forestry*, 10, 886–894. doi:10.3832/ifor2471-010

Gleason, C.J., Im, J., 2012. Forest biomass estimation from airborne LiDAR data using machine learning approaches. *Remote Sensing of Environment*, 125, 80–91. doi:10.1016/j.rse.2012.07.006

Grigolato, S., Mologni, O., Cavalli, R., 2017. GIS Applications in Forest Operations and Road Network Planning: an Overview over the Last Two Decades. *Croatian Journal of Forest Engineering*, 38, 175–

(In preparation)

186.

Hand, D.. J., 1985. Discrimination and Classification. *Biometrical Journal*, 27, 148. doi:10.1002/bimj.4710270204

Hertz, J., Krogh, A., Palmer, R.G., 1991. Introduction to the Theory of Neural Computation. Addison-Wesley Longman Publishing Co., Inc., Boston, MA, USA.

Holzleitner, F., Kastner, M., Stampfer, K., Höller, N., Kanzian, C., 2018. Monitoring Cable Tensile Forces of Winch-Assist Harvester and Forwarder Operations in Steep Terrain. *Forests*, 9, 53. doi:10.3390/f9020053

Hothorn, T., Hornik, K., Zeileis, A., 2015. ctree: Conditional Inference Trees [WWW Document]. *The Comprehensive R Archive Network*,. URL https://cran.r-project.org/web/packages/partykit/vignettes/ctree.pdf

Kewley, R.H., Embrechts, M.J., Breneman, C., 2000. Data strip mining for the virtual design of pharmaceuticals with neural networks. *IEEE Transactions on Neural Networks*, 11, 668–679. doi:10.1109/72.846738

Kuhmaier, M., Stampfer, K., 2010. Development of a Multi-Attribute Spatial Decision Support System in Selecting Timber Harvesting Systems. *Croatian Journal of Forest Engineering*, 31, 75–88.

Li, R., Bettinger, P., Danskin, S., Hayashi, R., 2007. A Historical Perspective on the Use of GIS and Remote Sensing in Natural Resource Management, as Viewed through Papers Published in North American Forestry Journals from 1976 to 2005. *Cartographica: The International Journal for Geographic Information and Geovisualization*, 42, 165–178. doi:10.3138/carto.42.2.165

Marjanović, M., Kovačević, M., Bajat, B., Voženílek, V., 2011. Landslide susceptibility assessment using SVM machine learning algorithm. *Engineering Geology*, 123, 225–234. doi:10.1016/j.enggeo.2011.09.006

Matwin, S., Charlebois, D., Goodenough, D.G., Bhogal, P., 1995. Machine learning and planning for data management in forestry. *IEEE Expert*, 10, 35–41. doi:10.1109/64.483115

Minsky, M.L., Papert, S.A., 1988. Perceptrons: Expanded Edition. MIT Press, Cambridge, MA, USA.

Mologni, O., Dyson, P., Amishev, D., Proto, A.R., Zimbalatti, G., Cavalli, R., Grigolato, S., 2018. Tension monitoring on large winch-assist forwarders operating in British Columbia. *Croatian Journal of Forest Engineering*, 39, 95–105.

Mologni, O., Grigolato, S., Cavalli, R., 2016. Harvesting systems for steep terrain in the Italian Alps: state of the art and future prospects. *Contemporary Engineering Sciences*, 9, 1229–1242.

(In preparation)

doi:10.12988/ces.2016.68137

Murphy, P.N.C., Ogilvie, J., Castonguay, M., Meng, F.R., Arp, P.A., 2007. Verifying calculated flow accumulation patterns of mapped and unmapped forest streams by culvert location. *Forestry Chronicle*, 83, 198–206. doi:10.5558/tfc83198-2

Najafi, A., Richards, E.W., 2013. Designing a Forest Road Network Using Mixed Integer Programming. *Croatian Journal of Forest Engineering*, 34, 17–30.

Owende, P.M.O., 2004. Wood Delivery, in: Burley, J., Evans, J., Youngquist, J.A. (Eds.), *Encyclopedia of Forest Sciences*. Elsevier, Oxford, pp. 269–279. doi:10.1016/B0-12-145160-7/00007-7

Papageorgiou, E.I., Markinos, A.T., Gemtos, T.A., 2011. Fuzzy cognitive map based approach for predicting yield in cotton crop production as a basis for decision support system in precision agriculture application. *Applied Soft Computing Journal*, 11, 3643–3657. doi:10.1016/j.asoc.2011.01.036

Pentek, T., Poršinsky, T., Sušnjar, M., Stankić, I., Nevećerel, H., Sporcić, M., 2008. Environmentally Sound Harvesting Technologies in Commercial Forests in the Area of Northern Velebit. Functional Terrain Classification. *Periodicum Biologorum*, 110, 8.

Piragnolo, M., Masiero, A., Pirotti, F., 2017. Comparison of Random Forest and Support Vector Machine classifiers using UAV remote sensing imagery. *Geophysical Research Abstracts EGU General Assembly*, 19, EGU2017-15692–1.

Pirotti, F., Sunar, F., Piragnolo, M., 2016. Benchmark of machine learning methods for classification of a Sentinel-2 image. *ISPRS - International Archives of the Photogrammetry, Remote Sensing and Spatial Information Sciences*, XLI-B7, 335–340. doi:10.5194/isprsarchives-XLI-B7-335-2016

Pradhan, B., 2013. A comparative study on the predictive ability of the decision tree, support vector machine and neuro-fuzzy models in landslide susceptibility mapping using GIS. *Computers and Geosciences*, 51, 350–365. doi:10.1016/j.cageo.2012.08.023

Proto, A.R., Skoupy, A., Macri, G., Zimbalatti, G., 2016. Time consumption and productivity of a medium size mobile tower yarder in downhill and uphill configurations : a case study in Czech Republic. *Journal of Agriculture Engineering*, 67, 216–221. doi:10.4081/jae.2016.551

Raschka, S., 2014. Naive Bayes and Text Classification I - Introduction and Theory 1–20. doi:10.13140/2.1.2018.3049

Raschka, S., 2015. Python Machine Learning, Fist editi. ed, Igarss 2014. Birmingham.

Stojanova, D., Panov, P., Gjorgjioski, V., Kobler, A., Džeroski, S., 2010. Estimating vegetation height and

(In preparation)

canopy cover from remotely sensed data with machine learning. *Ecological Informatics*, 5, 256–266. doi:10.1016/j.ecoinf.2010.03.004

Strandgard, M., Mitchell, R., 2015. Automated time study of forwarders using GPS and a vibration sensor. *Croatian Journal of Forest Engineering*, 36, 175–184.

Van Der Malsburg, C., 1986. Frank Rosenblatt: Principles of Neurodynamics: Perceptrons and the Theory of Brain Mechanisms, in: Palm, G., Aertsen, A. (Eds.), *Brain Theory*. Springer Berlin Heidelberg, Berlin, Heidelberg, pp. 245–248.

Venables, W.N., Ripley, B.D., 2002. MASS: modern applied statistics with S. doi:10.1198/tech.2003.s33

Visser, R., Stampfer, K., 2015. Expanding ground-based harvesting onto steep terrain: A review. *Croatian Journal of Forest Engineering*, 36, 321–331.

Zhao, K., Popescu, S., Meng, X., Pang, Y., Agca, M., 2011. Characterizing forest canopy structure with lidar composite metrics and machine learning. *Remote Sensing of Environment*, 115, 1978–1996. doi:10.1016/j.rse.2011.04.001

Zheng, Y.J., Song, Q., Chen, S.Y., 2013. Multiobjective fireworks optimization for variable-rate fertilization in oil crop production. *Applied Soft Computing Journal*, 13, 4253–4263. doi:10.1016/j.asoc.2013.07.004

(In preparation)

7. Discussion

The paper I (Piragnolo et. Al. 2014) describe a procedure for classifying and integrate multi-source information based on smulti-level framework for LULC purposes. The framework integrates information extracted using remote sensing techniques and time series. The advantage of multi-level is to move from small scale to high scale, where small scale is represented by satellites and high scale is represented by UAVs. Consequently, the information obtained form the first classification at low scale can be integrated using the high resolution imagery. For example, a classification obtained from Sensintel-2 imagery has been integrated using high resolution imagery, which was acquired using a 7 band multispectral camera with GSD of 18 cm/pixel. Then, classification has been done using popular supervised pixel-based algorithms: the minimum distance and the maximum likelihood. The result indicates the maximum likelihood has higher accuracy in comparison to the minimum distance, but some errors occurred as mixing the crops and the vegetation spectral signature. Thus, maximum likelihood can be used for a fast integration of the satellite and UAVs dataset, but the complex spectral signature can produce a misclassification.

However, the integration of the information between satellite and UAVs can be done in an efficient way in using the time series and the VI. In particular, the integration of temporal series collected from Sentinel-2 satellite and UAVs imagery for monitoring the permanent pastures and been done in the Paper II. A set of vegetation indices, which are NDVI, SAVI, NDWI, and NDBI, has been calculated between May and October to detect permanent pastures and mowed permanent pastures. The first issue studied is the radiometric similarities between the satellite and the sensor of the UAVs. The band 7 and the band 8 of Sentinel-2 have 10 and 20 metres of GSD. In contrast, band 8 radiometric response is very close to UVAs NIR sensor. The comparison between satellite NDVI and UAVs NDVI shows the band 8 is more suitable than 7 because the spatial resolution is higher. However, the identification of the medium size object as e.g. a building is affected by noise due to neighbour areas and obtaining a difference of 0.15. In contrast, the permanent pastures, which are big and homogeneous areas, do not suffer from neighbour noises. Consequently, discarding the marginal pixels, the mean of the DN using UAVs and satellite imagery is similar. Thus, when a mowing occurs it is possible to recognize a negative peak in the NDVI trend. Specifically, when the UAVs campaign overlaps the satellite observation, the NDVI negative peak has a difference of 0.7 between the two sensors. In accordance, the SAVI, NDWI, and NDBI confirm this trend. Therefore, the sensors can be temporally integrated, and UAVs can give useful information on the revisit time.

The results obtained using the classic remote sensing techniques can be applied to UAVs and can be improved using the advanced classification techniques such as machine learning. The Machine learning is a field of data analysis where an algorithm iterates and learns from the dataset, and using a rich dataset the of result the classification can improve. Consequently, a benchmark implemented in R has been integrated into the framework previously described (Paper II) to test multiple algorithms as shown in Figure 15.
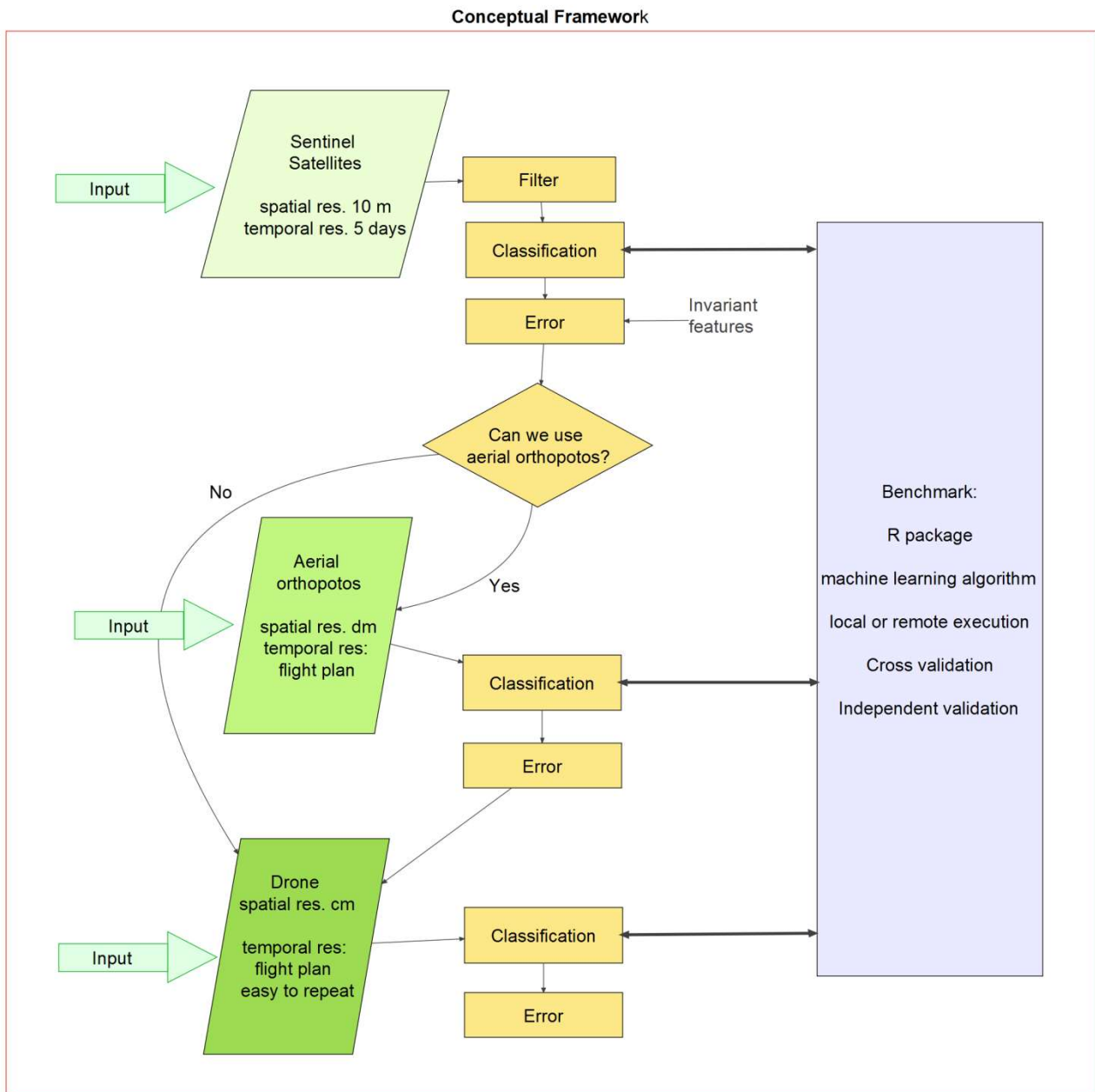

Figure 15 The framework for integrating satellite and UAVs imagery (Paper I) has been integrated with the benchmark for the machine learning studied in the Paper III, Paper IV and Paper V

The benchmark has been applied to satellite imagery, and an increasing number of the pixel from 1% to 20% of the total has been extracted. Varying the dataset, the comparison of different

algorithms evidences that the performance can be expressed both in terms of accuracy and timing. The accuracy is correlated to the size of the training, and the time consumption is influenced both the training size and the complexity of algorithms. On one hand, the subset of the 2% of the total pixel overestimates the accuracy, whereas using the 20% require more time. On the other hand, the complex model such as RF and SVM, require longer processing times for both classification and training. The simpler models are faster in the training phase or in the classification phase. In contrast, the accuracy can not be good. Next, the code of the benchmark has been optimized to increment the number of the test to have a robust result.

Based on previous results, the UAVs imagery has been tested using the RF and the SVM algorithm (paper III). One point of discussion is the dimension of the training area using the high resolution imagery. In fact, if we consider the same training area for satellite and UAVs imagery, the dimension of the dataset is correlated to the resolution. As result, to study the behaviour of the algorithms an increasing number of the pixel from 2% to 20% has been extracted. As expected, the accuracy was higher using a large training dataset, but this trend is not linear, in particular, the trend became stable using a training size larger than 8%.

Finally, the integration of spatial and morphological information has been tested in the paper V (chapter). The dataset consists of six input layers, which have been obtained from a DEM of 1 metre of resolution on an area of 34.32 km2 of size. Using the morphological information, the framework can support the forest technicians classifying a suitability map for two types of forestry machine: forwarder and skyline. An innovative approach is to simulate the worker behaviour in the site. The hypothesis is the worker focus his attention on the accessibility of the site rather than other technical parameters. Thus, the technical parameter such as the slope, the roughness, the height of the trees has been integrated with the accessibility parameter such as the distance and the elevation difference from roads. Considering the issue of big data, and in accordance with the results described in the Paper IV, a subset of 10% of the total pixel has been tested in the benchmark. The three best algorithms are RF, KNN, and Ctree. Likewise, the result presented in Paper III, the RF has the best score, with a result of 91.85, but is very slow. In contrast, Ctree is the faster algorithm, but it is less accurate, and KNN is in an intermediate position. Moreover, a sensitivity analysis shows the accessibility has high relative importance rather than slope, and roughness. The CHM and elevation have medium importance. Finally, some layers do not add significant information, and they can be eliminated in the future implementation if a decision support system.

8. Conclusion

The main objective of this thesis was to investigate the role of the open source GIS software for integrating the information obtained through the UAVs imagery, the satellite imagery, the radiometric analysis, and the spatial information to create LULC maps. The main findings of this thesis relating to the major research question (1) can be summarized as follows: the classic remote sensing techniques can be applied to UAVs high resolution imagery to obtaining fast image classification. The maximum likelihood algorithm has a better result than the minimum distance algorithm in terms of accuracy, but there are some limits for detecting and managing of a spectral signature using multi band information, as e.g. the crops and the vegetation. The issue is related to high variability inside not homogeneous training areas.

The main conclusions of these studies to answer the main research question (2) can be summarized as follows: the information obtained from UAVs can be effectively integrated with the information obtained from the satellite considering two aspects: the spatial scale and the time series. The scale affects the size of the training areas. Thus, to integrate the satellite and UAV information, the size of the analysis object shall be larger than the GSD satellite to avoid noise from nearby areas. Furthermore, the high resolution images shall do not contain many details, because the presence of small details could influence the spectral signature. In accordance, when the areas are homogeneous in terms of DN, the mean value of VI calculated using the spatial statistics is similar between UAVs and satellite. Therefore, the information extracted from high resolution images can be integrated with satellite platforms. Finally, using VI is possible to extract information from UAVs imagery for confirming the satellite analysis or integrating during the satellite review period.

The main conclusions of this study to answer the main research question (3) can be summarized as follows: the pixel-based and object-based classification approaches are common in remote sensing studies, whereas the machine learning is a new approach useful for classifying LULC map. Thus, a benchmark for testing several machine learning implementation has been implemented using R open-source libraries. The result shows the machine learning can be applied to both satellite and UAVs imagery. The dataset derived from high resolution imagery can be considered as a big data paradigm, in terms of data size and the processing time. Therefore, to manage and process a multi-layer dataset the definition of the size of the trained dataset is a critical issue. The analysis has evidenced a limited percentage of the dataset of ten percent is sufficient to train the model and

obtain a good result. Moreover, the comparison of the performances of the algorithms during the training phase, allows identifying the suitable algorithms in terms of accuracy and processing time. In addition, the method can be applied to spatial and morphological information derived from DTM. The machine learning black box produces accurate results, but the interpretation of a trained model is a complex issue. However, the contribution of the inputs in the multi-layer framework can be studied using the sensitivity analysis and visualization techniques.

Future implementations can lead to create a tool to download and clip automatically the satellite imagery, such as Sentinel-2 over a specific area. This implementation allows monitoring the testing area on the time. Moreover, more studies can define an automatic procedure for the data fusion of UAVs and satellite considering the spatial scale. Regarding the spatial information, in this study the morphological information has been studied alone in the benchmark. Consequently, a new investigation can be done to understand which benefit can be achieved form the integration of spectral and the spatial information. Finally, in this study cross validation and confusion matrix has been used. Therefore, other validation methodology, such as the quantity disagreement and the allocation disagreement, can improve accuracy assessment.

9. References

Ambrosia, V.G., Wegener, S., Zajkowski, T., Sullivan, D. V., Buechel, S., Enomoto, F., Lobitz, B., Johan, S., Brass, J., Hinkley, E., 2011. The Ikhana unmanned airborne system (UAS) western states fire imaging missions: from concept to reality (2006–2010). *Geocarto International*, 26, 85–101. doi:10.1080/10106049.2010.539302

Anthony, D., Basha, E., Ostdiek, J., Ore, J.P., Detweiler, C., 2015. Surface classification for sensor deployment from UAV landings, in: *2015 IEEE International Conference on Robotics and Automation (ICRA)*. pp. 3464–3470. doi:10.1109/ICRA.2015.7139678

Arbib, M.A., 1987. Brains, Machines, and Mathematics (2Nd Ed.). Springer-Verlag, Berlin, Heidelberg.

Baluja, J., Diago, M.P., Balda, P., Zorer, R., Meggio, F., Morales, F., Tardaguila, J., 2012. Assessment of vineyard water status variability by thermal and multispectral imagery using an unmanned aerial vehicle (UAV). *Irrigation Science*, 30, 511–522. doi:10.1007/s00271-012-0382-9

Baumann, P., Furtado, P., Ritsch, R., Widmann, N., 1997. Geo/Environmental and Medical Data Management in the RasDaMan System. *In Proceedings of the 23th VLDB Conference*, 548--552. doi:10.1.1.45.2240

Bendig, J., Bolten, a., Bareth, G., 2012. Introducing a Low-Cost Mini-Uav for Thermal- and Multispectral-Imaging. *ISPRS - International Archives of the Photogrammetry, Remote Sensing and Spatial Information Sciences*, XXXIX-B1, 345–349. doi:10.5194/isprsarchives-XXXIX-B1-345-2012

Bendig, J., Yu, K., Aasen, H., Bolten, A., Bennertz, S., Broscheit, J., Gnyp, M.L., Bareth, G., 2015. Combining UAV-based plant height from crop surface models, visible, and near infrared vegetation indices for biomass monitoring in barley. *International Journal of Applied Earth Observation and Geoinformation*, 39, 79–87. doi:10.1016/j.jag.2015.02.012

Berni, J.A.J., Zarco-Tejada, P.J., Sepulcre-Cantó, G., Fereres, E., Villalobos, F., 2009a. Mapping canopy conductance and CWSI in olive orchards using high resolution thermal remote sensing imagery. *Remote Sensing of Environment*, 113, 2380–2388. doi:10.1016/j.rse.2009.06.018

Berni, J.A.J., Zarco-Tejada, P.J., Suárez, L., Fereres, E., Suarez, L., Fereres, E., 2009b. Thermal and narrowband multispectral remote sensing for vegetation monitoring from an unmanned aerial vehicle, in: *IEEE Transactions on Geoscience and Remote Sensing*. pp. 722–738. doi:10.1109/TGRS.2008.2010457

Bishop, C.M., 1995. Neural Networks for Pattern Recognition. Oxford University Press, Inc., New York, NY, USA.

Bishop, M.C., 2006. Pattern recognition and machine learning, 1st ed. Springer-Verlag New York, New York.

Burges, C.J.C., 1998. A Tutorial on Support Vector Machines for Pattern Recognition. *Data Mining and Knowledge Discovery*, 2, 121–167. doi:10.1023/A:1009715923555

Calderón Madrid, R., Navas Cortés, J.A., Lucena León, C., Zarco-Tejada, P.J., 2014. High-resolution hyperspectral and thermal imagery acquired from UAV platforms for early detection of Verticillium wilt using fluorescence, temperature and narrow-band índices. *Workshop on UAV-based Remote Sensing Mehtods for Monitoring Vegetation*, 7–14. doi:10.5880/TR32DB.KGA94.3

Daughtry, C., 2000. Estimating Corn Leaf Chlorophyll Concentration from Leaf and Canopy Reflectance. *Remote Sensing of Environment*, 74, 229–239. doi:10.1016/S0034-4257(00)00113-9

Diaz-Varela, R.A., Zarco-Tejada, P.J., Angileri, V., Loudjani, P., 2014. Automatic identification of agricultural terraces through object-oriented analysis of very high resolution DSMs and multispectral imagery obtained from an unmanned aerial vehicle. *Journal of Environmental Management*, 134, 117–126. doi:10.1016/j.jenvman.2014.01.006

Duda, R.O., Hart, P.E., 1973. Pattern classification and scene analysis / Richard O. Duda, Peter E. Hart. Wiley New York.

Dunford, R., Michel, K., Gagnage, M., Piégay, H., Trémelo, M.-L., 2009. Potential and constraints of Unmanned Aerial Vehicle technology for the characterization of Mediterranean riparian forest. *International Journal of Remote Sensing*, 30, 4915–4935. doi:10.1080/01431160903023025

Frankenberger, J.R., Huang, C., Nouwakpo, K., 2008. Low-Altitude Digital Photogrammetry Technique to Assess Ephemeral Gully Erosion 4, IV-117-IV-120.

Fuentes, D.A., Gamon, J.A., Qiu, H., Sims, D.A., Roberts, D.A., 2001. Mapping vegetation cover types in the Canadian boreal forest using pigment and water absorption features derived from AVIRIS. *Journal of Geophysical Research*, 106, 565–577.

Gademer, A., Petitpas, B., Mobaied, S., Beaudoin, L., Riera, B., Roux, M., Rudant, J.P., 2010. Developing a low cost vertical take off and landing unmanned aerial system for centimetric monitoring of biodiversity the fontainebleau forest case. *International Geoscience and Remote Sensing Symposium (IGARSS)*, 600–603. doi:10.1109/IGARSS.2010.5649994

Gamon, J.A., Surfus, J.S., 1999. Assessing leaf pigment content and activity with a reflectometer. *New Phytologist*, 143, 105–117. doi:10.1046/j.1469-8137.1999.00424.x

Gonçalves, J., Henriques, R., Alves, P., Sousa-Silva, R., Monteiro, A.T., Lomba, Â., Marcos, B., Honrado, J., 2016. Evaluating an unmanned aerial vehicle-based approach for assessing habitat extent and condition in fine-scale early successional mountain mosaics. *Applied Vegetation Science*, 19, 132–146. doi:10.1111/avsc.12204

Grenzdörffer, G., Engel, a, Teichert, B., 2008. The photogrammetric potential of low-cost UAVs in forestry and agriculture. *International Archives of Photogrammetry Remote Sensing and Spatial Information Sciences*, 1, 1207–1213.

Guo, X., Denman, S., Fookes, C., Mejias, L., Sridharan, S., 2014. Automatic UAV forced landing site detection using machine learning, in: *2014 International Conference on Digital Image Computing: Techniques*

and Applications, DICTA 2014. doi:10.1109/DICTA.2014.7008097

Haboudane, D., Miller, J.R., Tremblay, N., Zarco-Tejada, P.J., Dextraze, L., 2002. Integrated narrow-band vegetation indices for prediction of crop chlorophyll content for application to precision agriculture. *Remote Sensing of Environment*, 81, 416–426. doi:10.1016/S0034-4257(02)00018-4

Haghighattalab, A., González Pérez, L., Mondal, S., Singh, D., Schinstock, D., Rutkoski, J., Ortiz-Monasterio, I., Singh, R.P., Goodin, D., Poland, J., 2016. Application of unmanned aerial systems for high throughput phenotyping of large wheat breeding nurseries. *Plant Methods*, 12, 35. doi:10.1186/s13007-016-0134-6

Hand, D.. J., 1985. Discrimination and Classification. *Biometrical Journal*, 27, 148. doi:10.1002/bimj.4710270204

Hertz, J., Krogh, A., Palmer, R.G., 1991. Introduction to the Theory of Neural Computation. Addison-Wesley Longman Publishing Co., Inc., Boston, MA, USA.

Herwitz, S.R., Johnson, L.F., Dunagan, S.E., Higgins, R.G., Sullivan, D. V., Zheng, J., Lobitz, B.M., Leung, J.G., Gallmeyer, B. a., Aoyagi, M., Slye, R.E., Brass, J. a., 2004. Imaging from an unmanned aerial vehicle: Agricultural surveillance and decision support. *Computers and Electronics in Agriculture*, 44, 49–61. doi:10.1016/j.compag.2004.02.006

Honkavaara, E., Kaivosoja, J., Mäkynen, J., Pellikka, I., Pesonen, L., Saari, H., Salo, H., Hakala, T., Marklelin, L., Rosnell, T., 2012. Hyperspectral Reflectance Signatures and Point Clouds for Precision Agriculture By Light Weight Uav Imaging System. *ISPRS Annals of Photogrammetry, Remote Sensing and Spatial Information Sciences*, I-7, 353–358. doi:10.5194/isprsannals-I-7-353-2012

Hothorn, T., Hornik, K., Zeileis, A., 2015. ctree: Conditional Inference Trees [WWW Document]. *The Comprehensive R Archive Network*,. URL https://cran.r-project.org/web/packages/partykit/vignettes/ctree.pdf

Howard, S.M., Ohlen, D.O., Mckinley, R.A., Itss, R., Falls, S., Dakota, S., Kitchen, J., 2002. HISTORICAL FIRE SEVERITY MAPPING FROM LANDSAT DATA, in: *HISTORICAL FIRE SEVERITY MAPPING FROM LANDSAT DATA*. p. 1.

Huete, A.R., 1988. A soil-adjusted vegetation index (SAVI). *Remote Sensing of Environment*, 25, 295–309. doi:10.1016/0034-4257(88)90106-X

Hung, C., Bryson, M., Sukkarieh, S., 2012. Multi-class predictive template for tree crown detection. *ISPRS Journal of Photogrammetry and Remote Sensing*, 68, 170–183. doi:10.1016/j.isprsjprs.2012.01.009

Hung, C., Xu, Z., Sukkarieh, S., 2014. Feature learning based approach for weed classification using high resolution aerial images from a digital camera mounted on a UAV. *Remote Sensing*, 6, 12037–12054. doi:10.3390/rs61212037

Hunt, E.R., Dean Hively, W., Fujikawa, S.J., Linden, D.S., Daughtry, C.S.T., McCarty, G.W., 2010. Acquisition of NIR-green-blue digital photographs from unmanned aircraft for crop monitoring. *Remote Sensing*,

2, 290–305. doi:10.3390/rs2010290

Idso, S.B., Jackson, R.D., Pinter, P.J., Reginato, R.J., Hatfield, J.L., 1981. Normalizing the stress-degree-day parameter for environmental variability. *Agricultural Meteorology*, 24, 45–55. doi:10.1016/0002-1571(81)90032-7

Jackson, R.D., Idso, S.B., Reginato, R.J., Pinter, P.J., 1981. Canopy temperature as a crop water stress indicator. *Water Resources Research*, 17, 1133–1138. doi:10.1029/WR017i004p01133

Jensen, A.M., Chen, Y., McKee, M., Hardy, T., Barfuss, S.L., 2009. AggieAir — a low-cost autonomous multispectral remote sensing platform: New developments and applications. *2009 IEEE International Geoscience and Remote Sensing Symposium*, 4, IV-995-IV-998. doi:10.1109/IGARSS.2009.5417547

Johnson, L.F., Herwitz, S., Dunagan, S., Lobitz, B., Sullivan, D., Slye, R., 2003. Collection of ultra high spatial and spectral resolution image data over California vineyards with a small UAV. *Proceedings of the 30th International Symposium on Remote Sensing of Environment (ISRSE)*, 3–5.

Korhonen, L., Korpela, I., Heiskanen, J., Maltamo, M., 2011. Airborne discrete-return LIDAR data in the estimation of vertical canopy cover, angular canopy closure and leaf area index. *Remote Sensing of Environment*, 115, 1065–1080. doi:10.1016/j.rse.2010.12.011

Laliberte, A.S., Rango, A., 2009. Texture and scale in object-based analysis of subdecimeter resolution unmanned aerial vehicle (UAV) imagery. *IEEE Transactions on Geoscience and Remote Sensing*, 47, 1–10. doi:10.1109/TGRS.2008.2009355

Laliberte, A.S., Rango, A., 2011. Image Processing and Classification Procedures for Analysis of Sub-decimeter Imagery Acquired with an Unmanned Aircraft over Arid Rangelands. *GIScience & Remote Sensing*, 48, 4–23. doi:10.2747/1548-1603.48.1.4

Lee, S., Choi, Y., 2016. Reviews of unmanned aerial vehicle (drone) technology trends and its applications in the mining industry. *Geosystem Engineering*, 9328, 1–8. doi:10.1080/12269328.2016.1162115

Lei, S., Ren, D., Huang, Z., Xiao, T., Zhang, L., 2014. Comparison of feature point extraction methods based on UAV remote sensing image 1044–1049.

Lelong, C.C.D., Burger, P., Jubelin, G., Roux, B., Labbé, S., Baret, F., 2008. Assessment of unmanned aerial vehicles imagery for quantitative monitoring of wheat crop in small plots. *Sensors*, 8, 3557–3585. doi:10.3390/s8053557

Lin, F.-C., Chung, L.-K., Ku, W.-Y., Chu, L.-R., Chou, T.-Y., 2013. The Framework of Cloud Computing Platform for Massive Remote Sensing Images. *Advanced Information Networking and Applications (AINA), 2013 IEEE 27th International Conference on*, 621–628. doi:10.1109/AINA.2013.94

Lucieer, A., Robinson, S. a, Turner, D., 2010. Using an unmanned aerial vehicle (UAV) for ultra-high resolution mapping of Antarctic moss beds. *15th Australasian Remote Sensing & Photogrammetry Conference*,.

M. Woebbecke, D., E. Meyer, G., Von Bargen, K., A. Mortensen, D., 1995. Color Indices for Weed

Identification Under Various Soil, Residue, and Lighting Conditions. *Transactions of the ASAE*, 38, 259. doi:https://doi.org/10.13031/2013.27838

Ma, L., Cheng, L., Li, M., Liu, Y., Ma, X., 2015. Training set size, scale, and features in Geographic Object-Based Image Analysis of very high resolution unmanned aerial vehicle imagery. *ISPRS Journal of Photogrammetry and Remote Sensing*, 102, 14–27. doi:10.1016/j.isprsjprs.2014.12.026

Merino, L., Caballero, F., Martínez-De-Dios, J.R., Maza, I., Ollero, A., 2012. An unmanned aircraft system for automatic forest fire monitoring and measurement. *Journal of Intelligent and Robotic Systems: Theory and Applications*, 65, 533–548. doi:10.1007/s10846-011-9560-x

Meuel, H., Reso, M., Jachalsky, J., Ostermann, J., 2013. Superpixel-based segmentation of moving objects for low bitrate ROI coding systems. *2013 10th IEEE International Conference on Advanced Video and Signal Based Surveillance, AVSS 2013*, 395–400. doi:10.1109/AVSS.2013.6636672

Minsky, M.L., Papert, S.A., 1988. Perceptrons: Expanded Edition. MIT Press, Cambridge, MA, USA.

Papageorgiou, E.I., Markinos, A.T., Gemtos, T.A., 2011. Fuzzy cognitive map based approach for predicting yield in cotton crop production as a basis for decision support system in precision agriculture application. *Applied Soft Computing Journal*, 11, 3643–3657. doi:10.1016/j.asoc.2011.01.036

Peña, J.M., Torres-Sánchez, J., de Castro, A.I., Kelly, M., López-Granados, F., 2013. Weed Mapping in Early-Season Maize Fields Using Object-Based Analysis of Unmanned Aerial Vehicle (UAV) Images. *PLoS ONE*, 8, 1–11. doi:10.1371/journal.pone.0077151

Pérez-Ortiz, M., Peña, J.M., Gutiérrez, P.A., Torres-Sánchez, J., Hervás-Martínez, C., López-Granados, F., 2015. A semi-supervised system for weed mapping in sunflower crops using unmanned aerial vehicles and a crop row detection method. *Applied Soft Computing Journal*, 37, 533–544. doi:10.1016/j.asoc.2015.08.027

Pérez-Ortiz, M., Peña, J.M., Gutiérrez, P.A., Torres-Sánchez, J., Hervás-Martínez, C., López-Granados, F., 2016. Selecting patterns and features for between- and within- crop-row weed mapping using UAV-imagery. *Expert Systems with Applications*, 47, 85–94. doi:10.1016/j.eswa.2015.10.043

R.B Haarbrink, E.K., 2006. Helicopter UAV For Photogrammetry And Rapid Response. *The International Achives Photogrammetry, Remote Sensing and Spatial Information Sciences,Antwerp Belgium. Vol XXXVI-I/W44*, XXXVI, 2–5.

Rango, A., Laliberte, A., Herrick, J.E., Winters, C., Havstad, K., Steele, C., Browning, D., 2009. Unmanned aerial vehicle-based remote sensing for rangeland assessment, monitoring, and management. *Journal of Applied Remote Sensing*, 3, 1–15. doi:10.1117/1.3216822

Raschka, S., 2015. Python Machine Learning, Fist editi. ed, Igarss 2014. Birmingham.

Remondino, F., Barazzetti, L., Nex, F., Scaioni, M., Sarazzi, D., 2011. UAV photgrammetry for mapping and 3D modeling – current status and future perspectives, in: *International Archives of the Photogrammetry, Remote Sensing and Spatial Information Sciences*. pp. 14–16.

Remondino, F., Del Pizzo, S., 2012. Low-cost and open-source solutions for automated image orientation–a critical overview. *Progress in Cultural …*, 40–54.

Rondeaux, G., Steven, M., Baret, F., 1996. Optimization of soil-adjusted vegetation indices. *Remote Sensing of Environment*, 55, 95–107. doi:10.1016/0034-4257(95)00186-7

Rouse, J.W., Haas, R.H., Schell, J.A., Deering, D.W., 1973. Monitoring the vernal advancement and retrogradation (green wave effect) of natural vegetation. *Progress Report RSC 1978-1*, 112.

Samuel, A.L., 1959. Some Studies in Machine Learning Using the Game of Checkers. *IBM J. Res. Dev.*, 3, 210–229. doi:10.1147/rd.33.0210

Singh, S., Singh, N., 2012. Big Data analytics. *2012 International Conference on Communication, Information & Computing Technology (ICCICT)*, 1–4. doi:10.1109/ICCICT.2012.6398180

Smith, G.M., Milton, E.J., 1999. The use of the empirical line method to calibrate remotely sensed data to reflectance. *International Journal of Remote Sensing*, 20, 2653–2662. doi:10.1080/014311699211994

Solberg, S., Brunner, A., Hanssen, K.H., Lange, H., Næsset, E., Rautiainen, M., Stenberg, P., 2009. Mapping LAI in a Norway spruce forest using airborne laser scanning. *Remote Sensing of Environment*, 113, 2317–2327. doi:10.1016/j.rse.2009.06.010

Sona, G., Pinto, L., Pagliari, D., Passoni, D., Gini, R., 2014. Experimental analysis of different software packages for orientation and digital surface modelling from UAV images. *Earth Science Informatics*, 7, 97–107. doi:10.1007/s12145-013-0142-2

Sugiura, R., Noguchi, N., Ishii, K., 2005. Remote-sensing technology for vegetation monitoring using an unmanned helicopter. *Biosystems Engineering*, 90, 369–379. doi:10.1016/j.biosystemseng.2004.12.011

Techy, L., Woolsey, C.A., Schmale, D.G., 2008. Path planning for efficient UAV coordination in aerobiological sampling missions. *Proceedings of the IEEE Conference on Decision and Control*, 2814–2819. doi:10.1109/CDC.2008.4739456

Tokekar, P., Hook, J. Vander, Mulla, D., Isler, V., 2013. Sensor planning for a symbiotic UAV and UGV system for precision agriculture. *IEEE International Conference on Intelligent Robots and Systems*, 5321–5326. doi:10.1109/IROS.2013.6697126

Torres-Sánchez, J., López-Granados, F., Peña, J.M., 2015. An automatic object-based method for optimal thresholding in UAV images: Application for vegetation detection in herbaceous crops. *Computers and Electronics in Agriculture*, 114, 43–52. doi:10.1016/j.compag.2015.03.019

Torres-Sánchez, J., Peña, J.M., de Castro, a. I., López-Granados, F., 2014. Multi-temporal mapping of the vegetation fraction in early-season wheat fields using images from UAV. *Computers and Electronics in Agriculture*, 103, 104–113. doi:10.1016/j.compag.2014.02.009

Tucker, C.J., 1979. Red and photographic infrared linear combinations for monitoring vegetation. *Remote Sensing of Environment*, 8, 127–150. doi:10.1016/0034-4257(79)90013-0

Turner, D., Lucieer, A., Watson, C., 2010. Development of an Unmanned Aerial Vehicle (UAV) for hyper resolution vineyard mapping based on visible, multispectral, and thermal imagery. *Proceedings of 34th International Symposium on Remote Sensing of Environment*, 4.

Turner, D., Lucieer, A., Watson, C., 2012. An automated technique for generating georectified mosaics from ultra-high resolution Unmanned Aerial Vehicle (UAV) imagery, based on Structure from Motion (SFM) point clouds. *Remote Sensing*, 4, 1392–1410. doi:10.3390/rs4051392

Van Asselen, S., Verburg, P.H., 2013. Land cover change or land-use intensification: Simulating land system change with a global-scale land change model. *Global Change Biology*, 19, 3648–3667. doi:10.1111/gcb.12331

Van Der Malsburg, C., 1986. Frank Rosenblatt: Principles of Neurodynamics: Perceptrons and the Theory of Brain Mechanisms, in: Palm, G., Aertsen, A. (Eds.), *Brain Theory*. Springer Berlin Heidelberg, Berlin, Heidelberg, pp. 245–248.

Wallace, L., 2013. Assessing the stability of canopy maps produced from UAV-LiDAR data. *International Geoscience and Remote Sensing Symposium (IGARSS)*, 3879–3882. doi:10.1109/IGARSS.2013.6723679

Walter, V., 2004. Object-based classification of remote sensing data for change detection. *ISPRS Journal of Photogrammetry and Remote Sensing*, 58, 225–238. doi:10.1016/j.isprsjprs.2003.09.007

Weih, R.C., Riggan, N.D., 2010. Object-based classification vs. pixel-based classification: Comparitive importance of multi-resolution imagery. *The International Archives of the Photogrammetry, Remote Sensing and Spatial Information Sciences*, XXXVIII, 1–6.

Zarco-Tejada, P.J., Berni, J.A.J., Suárez, L., Sepulcre-Cantó, G., Morales, F., Miller, J.R., 2009. Imaging chlorophyll fluorescence with an airborne narrow-band multispectral camera for vegetation stress detection. *Remote Sensing of Environment*, 113, 1262–1275. doi:10.1016/j.rse.2009.02.016

Zarco-Tejada, P.J., González-Dugo, V., Berni, J.A.J., 2012. Fluorescence, temperature and narrow-band indices acquired from a UAV platform for water stress detection using a micro-hyperspectral imager and a thermal camera. *Remote Sensing of Environment*, 117, 322–337. doi:10.1016/j.rse.2011.10.007

Zarco-Tejada, P.J., González-Dugo, V., Williams, L.E., Suárez, L., Berni, J.A.J., Goldhamer, D., Fereres, E., 2013a. A PRI-based water stress index combining structural and chlorophyll effects: Assessment using diurnal narrow-band airborne imagery and the CWSI thermal index. *Remote Sensing of Environment*, 138, 38–50. doi:10.1016/j.rse.2013.07.024

Zarco-Tejada, P.J., Guillén-Climent, M.L., Hernández-Clemente, R., Catalina, A., González, M.R., Martín, P., 2013b. Estimating leaf carotenoid content in vineyards using high resolution hyperspectral imagery acquired from an unmanned aerial vehicle (UAV). *Agricultural and Forest Meteorology*, 171–172, 281–294. doi:10.1016/j.agrformet.2012.12.013

Zaslavsky, A., Perera, C., Georgakopoulos, D., 2013. Sensing as a Service and Big Data, in: *ArXiv Preprint ArXiv:1301.0159*. Bangalore.

Zhao, W., Ma, H., He, Q., 2009. Parallel K-Means Clustering Based on Map Reduce. *Cloud Computing*, 5931, 674–679.

Zheng, Y.J., Song, Q., Chen, S.Y., 2013. Multiobjective fireworks optimization for variable-rate fertilization in oil crop production. *Applied Soft Computing Journal*, 13, 4253–4263. doi:10.1016/j.asoc.2013.07.004

10. Annex I. Band ratio and vegetation index (VI)

The band ratio and indices are common techniques for the spectral enhancement. They are calculated as combinations of bands applying mathematical operations such as sum and division to a raster image. The popular indices reported in the literature review are described in the next section.

10.1.   NDVI

The Normalized Difference Vegetation Index NDVI (Tucker, 1979), is a common widely used for vegetation monitoring (Baluja et al., 2012; Bendig et al., 2015, 2012; Berni et al., 2009a; Diaz-Varela et al., 2014; Herwitz et al., 2004; Pérez-Ortiz et al., 2015; Sugiura et al., 2005; Tokekar et al., 2013; Torres-Sánchez et al., 2015; Turner et al., 2010). Indeed, the leaf structure adsorbs the red wavelength, and it reflects NIR bands to avoid overheating. It is calculated as the ratio of red band (R) and near-infrared (NIR) (Rouse et al., 1973). The formula is (5):

$$NDVI = \frac{NIR - R}{NIR + R} \qquad (5)$$

NDVI ranges between -1 to 1 and is used to monitor vegetation. The value of -1 indicates no vegetated area and the value of 1 indicates full-vegetated area. NDVI was widely used in the literature coupled with other indices for study crop vigour and biomass and water stress (Herwitz et al., 2004). A relation between NDVI and TCARI/OSAVI has been found in grapevine (Baluja et al., 2012), and a good correlation between NDVI, Photochemical Reflectance Index (PRI) and canopy temperature ($r2 = 0.69$) have been found on corn and olive trees (Berni et al., 2009a). The NDVI can be used combined with topographic indices or to model real data in UAV simulation sampling (Tokekar et al., 2013) or for threshold images in object-based classification (Torres-Sánchez et al., 2015). Some indices were developed from NDVI such as Modified GRVI (MGRVI) and red green blue vegetation index (RGBVI). Both GRVI and RGBVI were introduced by (Bendig et al., 2015). In addition, MGRVI has been defined as the normalised difference of the squared green reflectance and the squared red reflectance. The RGBVI has been defined as the normalised difference of the squared green. These indices have a better ability to model biomass in early growth stages in comparison to late growth stages.

10.2.   SAVI

The Soil-adjusted Vegetation Index (SAVI) (Huete, 1988) and the Optimized Soil-adjusted Vegetation Index (OSAVI) (Rondeaux et al., 1996) are based on the NDVI index. Thus, to discriminate better the soil contribution, the SAVI adds a soil brightness correction factor L to NDVI (6). L is related to soil and vegetation coverage, and it ranges from 0 to 1. The value of 0 indicates the high vegetated area, and a value of 1 indicates a very low vegetated area. Intermediate vegetation cover is 0.5.

$$SAVI = \frac{NIR - R}{NIR + R + L} * (1 + L) \tag{6}$$

The OSAVI has the same formula of SAVI, but the correction factor L is equal to 0.16 in order to minimize the soil effect.

10.3.   MCARI

The Modified Chlorophyll Absorption Ratio Index (MCARI) (7) indicates a relative abundance of the chlorophyll (Daughtry, 2000). The chlorophyll has the maximum absorption peak at 680 nm, and it reaches minimum pick at 550 nm. Indeed, MCARI was centred in the region of maximum absorption between 550 and 700 nm. Consequently, the ratio R700/R670 was introduced to minimize the combined effects of the underlying soil reflectance and the canopy non-photosynthetic materials.

$$MCARI = \ (R700 - R670) - 0.2 * (R700 - R550) * (\frac{R700}{R670}) \tag{7}$$

where:

R700 = reflectance at 700 nm

R550 = reflectance at 550 nm

R670 = reflectance at 670 nm

10.4.   TCARI

The leaf area indices (LAI), the chlorophyll and the soil reflectance influence MCARI (8). Therefore, MCARI is affected by low chlorophyll level. Hence, to reduce this effect MCARI was modified as Transformed Chlorophyll Absorption in Reflectance (TCARI).

$$TCARI = \ 3*[(R700 - R670) - 0.2*(R700 - R550*(\frac{R700}{R670}) \qquad (8)$$

The TCARI is influenced to soil reflectance in particular in poor leaf coverage. Hence, the ratio TCARI/OSAVI overcomes this problem. The advantage is high sensibility to chlorophyll variation and low sensibility to LAI, solar zenith angle and soil reflectance (Haboudane et al., 2002).

10.5.   TCARI/OSAVI

The TCARI/OSAVI was used to calculate the concentration of chlorophyll at the crown. A strong positive correlation was found on corn, olive, and peach trees between chlorophyll estimated from the multispectral camera and chlorophyll measured in the field ($R2 = 0.89$) (Berni et al., 2009a). An airborne campaign over the vineyard found a positive correlation between spectral indices derived from aerial images with stem water potential, and stomatal conductance for NDVI has ($R2 =0.68$) ($R2=0.75$) and for TCARI/OSAVI ($R2 =0.58$), ($R2=0.84$) (Baluja et al., 2012). Likewise, TCARI/OSAVI has been applied to study the chlorophyll content and physiological condition in grapevine. The index has been calculated from thermal and multispectral imagery (Zarco-Tejada et al., 2013a). A study on olive trees using TCARI and TCARI/OSAVI highlights a decrease in chlorophyll content. TCARI and TCARI/OSAVI showed an upward trend at early stages of the disease, reaching a maximum at the low disease severity level (Calderón Madrid et al., 2014).

10.6.   PRI

The Photochemical Reflectance Index (PRI) (Fuentes et al., 2001; Gamon and Surfus, 1999) has been used in studies of vegetation health and productivity for monitoring the stress responses. The PRI ranges from –1 to 1 and it is calculated as follows (9):

$$PRI = \frac{R531 - R570}{R531 + R570} \qquad (9)$$

where:

R531 = reflectance at 531 nm

R570 = reflectance at 570 nm

The PRI has been used successfully as an indicator of water stress at the leaf level in the orange and mandarin orchard (Turner et al., 2010). Indeed, the result has demonstrated a correlation between seasonal PRI and crown temperature, where NDVI had a low sensibility to water potential and stomatal conductance (Zarco-Tejada et al., 2012). Then, a new formulation of the normalised PRI (PRInorm), was proposed, because it was more stable against change background of altered pigments and structure (Zarco-Tejada et al., 2013a)(Zarco-Tejada et al., 2013a). In addition, PRI was also used as an indicator of possible diseases and moderate to severe damage in olive crops (Calderón Madrid et al., 2014).

10.7. CWSI

The Crop Water Stress Index (CWSI) estimates crop water status using thermal data (Idso et al., 1981; Jackson et al., 1981). The CWSI equation is (10):

$$CSWI = (T°canopy - T°wet) - (T°dry - T°wet) \qquad (10)$$

where:

T° canopy = was the canopy temperature obtained from the thermal images

T° dry = lower boundary temperatures corresponding to a fully transpiring leaf with open stomata

T° wet = upper boundary temperatures, corresponding to not- transpiring leaf with closed stomata

The CWSI derived from UAVs thermal has been used to study the water stress in an olive orchard, where a strong correlation between CWSI and leaf water potential (R2=0.82), and CWSI and canopy conductance (R2=0.91) has been found. Consequently, the result suggests that CWSI can be used as

a good indicator to map water stress in open tree canopies (Berni et al., 2009b, 2009a) and disease (Calderón Madrid et al., 2014).

10.8.   ExG

The Excess green index (ExG) (M. Woebbecke et al., 1995) can be used for set imagery threshold to discriminate if a pixel corresponds to vegetation or soil (Pérez-Ortiz et al., 2016, 2015; Torres-Sánchez et al., 2015). It is computed as (11):

$$ExG = \ 2G*-R*+B \tag{11}$$

where:

R= R/(R + G + B)

G= G/(R + G + B)

B= B/(R + G + B)

The R, G and B are the matrices associated with the green, red and blue spectral channels.

10.9.   DEM/DSM derived indices

Some indices can be computed from DEM and DSM. For this reason, the digital model accuracy is very important, especially in height, where there are more errors. Consequently, the model accuracy affects the index value. Examples of these indices are the minimum value (DifMin), the position index (TopIndex), the Terrain Shape Index (Diaz-Varela et al., 2014), and the Topographic Wetness index (WI) (Lucieer et al., 2010). They have been used to identify terraces and anomalies in the landscape or spatial distribution of potential surface wetness caused by snow melt.

10.10.   NBR

The post-fire normalised burn ratio (NBR) algorithm was designed originally for Landsat TM analysis. Next, it has been tested to highlight the burned area using UAVs imagery (Ambrosia et al., 2011; Howard et al., 2002). The formula (12) is similar to the NDVI, but it uses near-infrared (NIR) and shortwave-infrared (SWIR). Before the fire event, vegetation has high reflectance in NIR, but low reflectance in SWIR. After a fire event, vegetation has a low reflectance in NIR, and high reflectance in SWIR, so burned areas can be highlighted.

$$\text{NBR} = \frac{\text{NIR} - \text{SWIR}}{\text{NIR} + \text{SWIR}} \tag{12}$$

11. Annex II. Machine learning techniques

11.1. Machine learning introduction

This section illustrates the machine learning algorithm applied in this PhD.

The machine learning is a field of study that gives computers the ability to learn from experience without being explicitly programmed (Samuel, 1959), and this ability can be applied for image classification. Considering a binary classification, two classes exist, (1) and (-1). The membership to a specific class is determined using an algorithm called an activation function ø (z) stated as (13):

$$\emptyset(x) = \begin{cases} 1 \text{ if } z \geq 0 \\ -1 \text{ otherwise} \end{cases} \tag{13}$$

The activation function combines the input values x and the weight w, and when the function is greater than a threshold, the classification is positive. The weights and the prediction error are calculated during the learning process, whereas a quantizer function can be used to predict the class label, as in Figure 16.
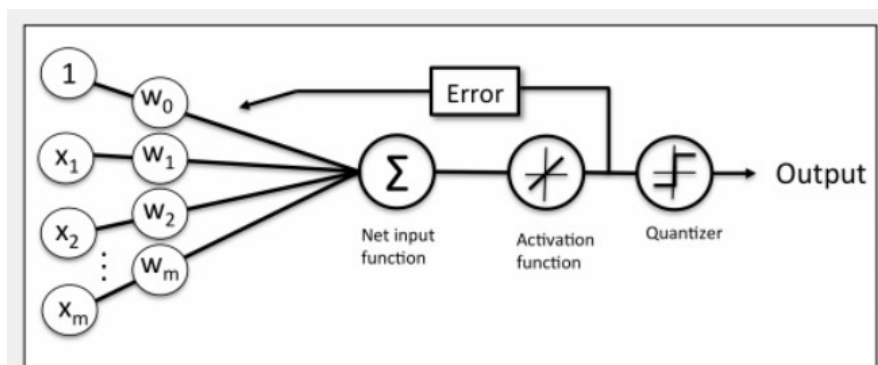
Figure 16 Description of the activation function, which combines input and weights, and the quantizer, which is used for class prediction (Raschka, 2015)*.*

The squared error between the prediction and true class label is described with the cost function. During the iterations of the learning process, the important point is to minimize the cost function, e.g., using a gradient algorithm to reach the minimum, as shown in Figure 17.
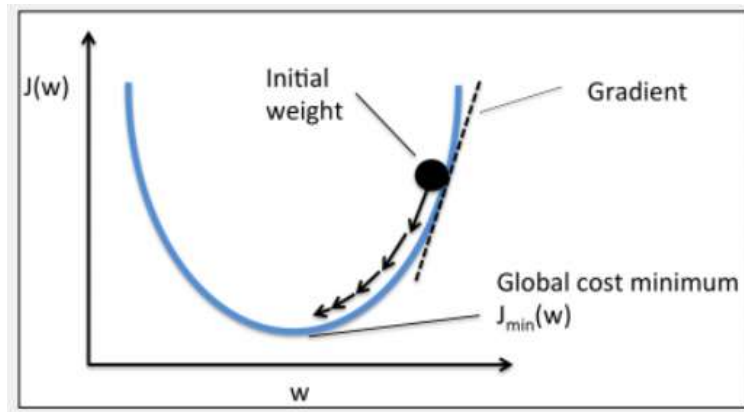
Figure 17 The minimum of cost function J (w) and weights (w) is defined as the slope of the gradient (Raschka, 2015).

The machine learning techniques applied to image classification can be grouped into supervised and unsupervised methods. The supervised learning uses an example set or ROIs for algorithm training, whereas the unsupervised learning finds patterns and relationships among the data without training. Furthermore, the dataset is split between a subset training set, a validation set, and a test set. The training set is a subset of the dataset used for the machine learning training. In applying a predictive model, a class label that was in the test set can be assigned to an unlabelled instance. For assessing the fit performance of the classifier to the training set without using the test data, the validation subset is used, and the best predictive algorithm is chosen. Likewise, the test set is a subset of the dataset used to assess the performance of the trained model. The machine learning algorithms can be grouped into parametric and nonparametric. Parametric models estimate the learning function and a fixed number of parameters from the training set without requiring the original dataset. In contrast, the parameters number of the nonparametric methods is not fixed, but it grows during the training. Nevertheless, the training process can suffer from the overfitting and the underfitting problems. The overfitting means the model has high variance. On one hand, the performance of the model is good with the training set; on the other hand, the model and the performance are not good with test data. The reason is the model complexity due to too many parameters. In contrast, the underfitting means the model has a low performance with the test set, and the simplicity of the model is not adequate to recognize the training data. To limit this problem,

the regularization technique and validation on an independent data set of the set shall be used. Regularization helps to reduce extreme values of weight parameters by applying a bias (14). Consequently, the regularization parameter maintains low weights, and it controls how the model fits the training data.

$$\frac{\lambda}{2}\|w\|^2 = \frac{\lambda}{2}\sum_{j=1}^{m} w_j^2 \qquad (14)$$

where:

λ is the regularization parameter.

Finally, the validation shall be done on the independent dataset using different metrics and techniques such as the Kappa index (K), classification error (CE), accuracy index (ACC). The independence means to split the dataset into two subsets, the training set, and the validation set. This holdout method is fast, but it can suffer from high variance. Consequently, the output depends on how the division between the two set is made. A more sophisticated technique is the K-fold cross-validation. The K-fold cross-validation is an improvement of the holdout method, because It splits the data K (10) into sets (folds) of equal size. K − 1 subsamples are used as the training test set, and a single subsample is used for validation. The procedure is repeated K times, but each subset is used only once for the validation.

The machine learning algorithms tested in this research, and described in the following paragraph, are:

- Logistic Regression (LR)
- Support Vector Machines (SVM)
- Random Forests (RF)
- K-nearest Neighbour (KNN)
- Linear Discriminant Analysis (LDA)
- Multi Layered Perceptron (MLP)
- Multi Layered Perceptron Ensemble (MLPE)
- Boosting (B)

- Conditional inference trees (Ctree)

- Naive Bayes (NB)

11.2. Logistic regression (LR)

The Logistic regression (LR) is an algorithm for linear and binary classification based on a neural network, where the classes are linearly separable. Accordingly, the binary classification is extended to multiclass classification using the One-vs-Rest (OvR) method. Indeed, the OvR trains one classifier for a class. Then, it assigns a positive value to the class membership, and all the other classes are considered as negative values. Consequently, the logistic regression approach tries to maximize the likelihoods of the training data. Indeed, iterating n times, where n is the number of classes, the specific sample is assigned to a class considering the highest probability of membership. The activation function for logistic regression is the sigmoid function Figure 18. The sigmoid function is the logarithm of the odds ratio, and it transforms real numbers into values in the range of [0,1]. Indeed, the threshold is set to 0.5.
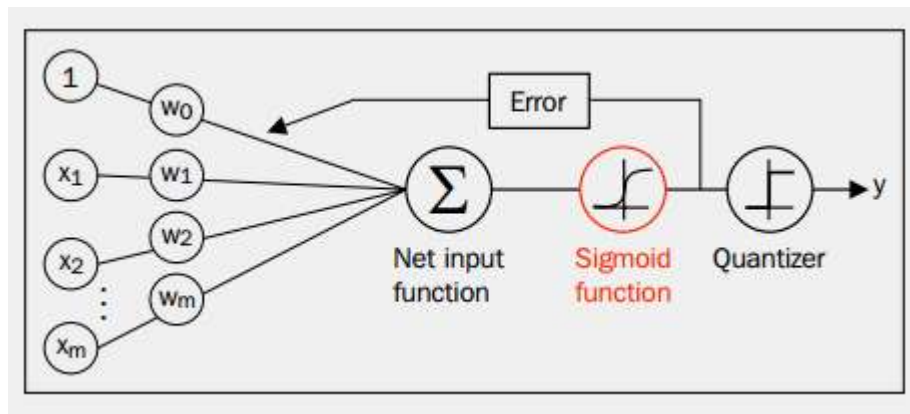
Figure 18. Net function combine inputs x and weights w. Sigmoid function transform real numbers into the 0-1 interval. The Quantizer is used to predict a class (Raschka, 2015.)

The regularization is performed through the λ parameter, where increasing λ means increasing the strength of regularization (15). In contrast, the C parameter is the inverse of the regularization parameter λ, and it is applied to the logistic regression algorithm.

$$C = \frac{1}{\lambda} \tag{15}$$

11.3.   Support Vector Machine (SVM)

The support vector machine (SVM) is a well-known and widely used algorithm. The SVM is based on a hyperplane that divides the training set into two classes. The positive and negative hyperplanes, which are parallel to the hyperplane, are stated as in (16) and (17):

$$w_{0+}w^T x_{pos} = 1 \qquad (16)$$

$$w_{0+}w^T x_{pos} = -1 \qquad (17)$$

Subtracting (16) and (17)

$$w^T(x_{pos} - x_{neg}) = 2 \qquad (18)$$

The margin is the normalized by the vector w (19)

$$\|w\| = \sqrt{\sum_{j=1}^{m} w_j^2} \qquad (19)$$

Thus, the margin is defined as the distance between the positive and negative classes that are defined by a hyperplane, and it is stated as follows (20):

$$\frac{w^T(xpos - xneg)}{\|w\|} = \frac{2}{\|w\|} \qquad (20)$$

The samples closest to the hyperplane are called support vectors, as seen in Figure 19. Taking into consideration the support vectors, the goal of the algorithm is to maximize the margin in order to reduce the distance between support vectors. Maximize the margin is equal to minimizing the reciprocal term stated as $\frac{1}{2}\|w^2\|$ (Burges, 1998).
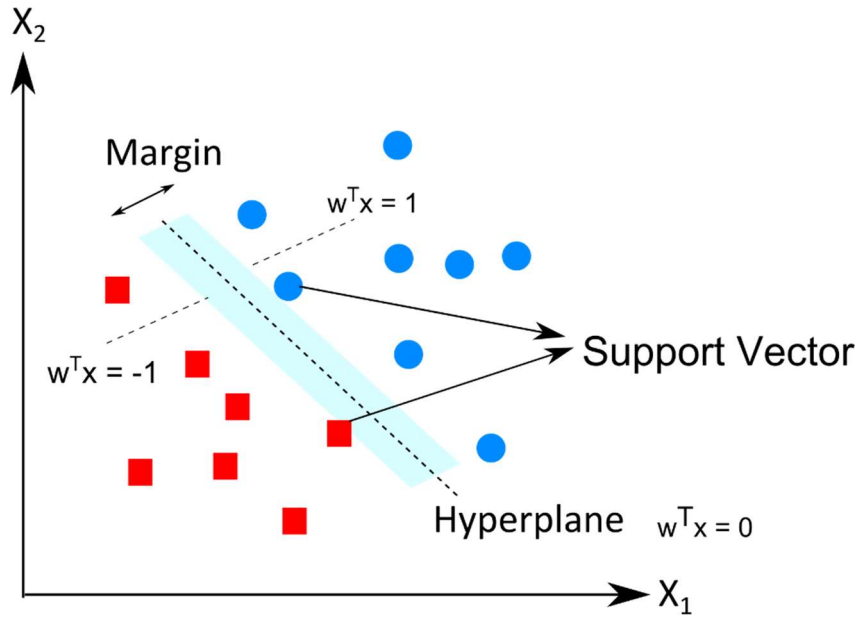
Figure 19 Illustration of the decision boundary of the SVM algorithm and the margin

The regularization in SVM is done using two parameters, the C parameter and slack variable ξ (21).

$$\frac{1}{2}\|w^2\|+C\left(\sum_i \xi^{(i)}\right)$$

(21)

In case of non-linearly separable data, the penalization is applied as a cost function. The C parameter is the inverse of the regularization parameter λ, so large C values introduce large errors. Consequently, large errors decrease the variance of the model and increase misclassification error.

11.4. Random Forest (RF)

Decision tree classifiers treat the analysis as a binary decision splitting the dataset at child nodes (Dleft and Dright). Therefore, iterating the process, a complete decision tree grows from branches to leaves, but it can easily introduce the overfitting problem. The objective of the algorithm is to maximize the information gain (IG) at each node through a function (22):

$$IG(D_p, f) = I(D_p) - \frac{Nleft}{Np}I(D_{left}) - \frac{Nright}{Np}I(D_{right})$$

(22)

where:

I is the impurity measure

Np is the total number of samples at the parent node

Dp is the dataset at the parent node

Nleft and Nright are the number of samples at the child node

Dp is the dataset at the parent node

Dleft and Dright are the datasets at the child node

The Random forest is decision tree derived a by method that overcomes the overfitting problem. It is based on a bootstrap technique that creates a large number of training sets to compute the statistic. Hence, it draws randomly a sample of size n with no replacement, and the value of n controls the bias and variance. Replacement means an element can appear multiple times in the sample. On one hand, large values of n reduce the randomness and increase the overfitting risk. On the other hand, small values of n reduce the risk and the model performance. Then, a decision tree grows, selecting d features without replacement, so an element can appear only once in the sample. The nodes are split using the function (22). The D parameter should be smaller than the number of features (m) in the training set as follows (23):

$$d = \sqrt{m} \qquad\qquad (23)$$

The procedure is repeated k times. Finally, the class label is assigned by majority vote to the aggregated prediction (Figure 20).
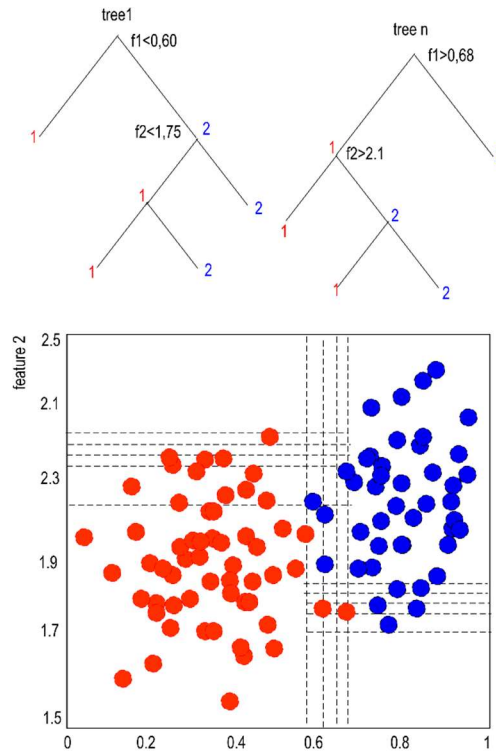
Figure 20 Example of random forest classification

11.5.   K-nearest neighbors (KNN)

The K-nearest neighbors (KNN) classifier is based on a distance metric. Indeed, it finds the k nearest neighbors of the sample, and it assigns the sample with a majority vote. This method has the advantage of adapting to a new training data set but the computational requirement and storage space is significant. Moreover, the key to avoiding the overfitting and the underfitting problem is the right choice of k, for example, using the standardized Euclidean distance (24).

$$d\left(x^{(i)}, x^{(j)}\right) = \sqrt[p]{\sum_k \left| x_k^{(i)} - x_k^{(j)} \right|^p} \tag{24}$$

The steps of the methods are:

Choose the number of k nearest neighbors and a distance metric.

Determine the k nearest neighbors

Count the majority vote and assign the class label

11.6.   Multi Layered Perceptron (MLP)

The multi layered perceptron (MLP) is a neural network composed of two perceptron layers. The perceptron algorithm was developed in the 50s, and it is a single neural network layer with a threshold activation function g($\cdot$), where the inputs $\emptyset_j$ are connected directly to the output using adaptive weights w_j, as stated in (25) and Figure 21.
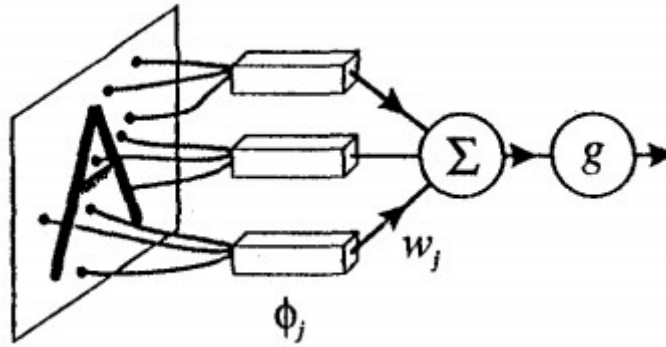

Figure 21 Schema of the perceptron algorithm (Bishop, 1995).

$$y = g\left(\sum_{j=0}^{M} w_j \emptyset_j(x)\right) = g(w^T \emptyset) \tag{25}$$

where:

$\emptyset$ is the feature vector composed of the activations $\emptyset_0,\dots, \emptyset_m$
w is the weight vector composed of the activations $w_0,\dots, w_m$

The output is chosen in accordance with (26):

$$g(a) = \begin{cases} -1 \text{ when } a < 0 \\ +1 \text{ when } a > 0 \end{cases} \tag{26}$$

Considering misclassified elements on the training set the error function, also called the perceptron criterion, can be stated as (27):

$$E^{perc}(w) = - \sum_{\emptyset^n \in M} w^T(\emptyset^n t^n) \qquad (27)$$

where:

M is the set of vector misclassified by $\emptyset^n$

t^n is the desired output -1 or +1

The error function is the sum of positive terms, so when all points are classified correctly the error function is equal to 0. Therefore, the error function is proportional to the misclassified input and to the sum of distances from the decision boundary. Hence, during the training, the decision boundary moves. When the pattern is correctly classified, nothing happens. In case the pattern is misclassified, the boundary is adjusted by adding or subtracting the feature vector to the weight vector. Thus, a new decision boundary is created. Cycling through the pattern of the training set, the sequence of weight vectors can be expressed as a gradient (28):

$$w_j^{(r+1)} = w_j^r + \eta \theta_j^n t^n \qquad (28)$$

where:

w^r is the sequence of weight vectors

η is the learning rate parameter, and a small value the error reduction is slow. Large values can produce divergent output.

The advantage of the perceptron applied to the linear dataset is to find a solution in a finite number of steps, as studied by several authors (Arbib, 1987; Duda and Hart, 1973; Hand, 1985; Hertz et al., 1991; Minsky and Papert, 1988; Van Der Malsburg, 1986). However, when the dataset is not linearly separable, the learning algorithm cycles infinitely and never terminates.

Derived from the perceptron, the multi layer perceptron is a network composed of layers of adaptive weights. Thus, the input units of the first layer are connected to the output layer through intermediate layers. Intermediate layers are composed of units called hidden units. The output a is the combination of input weight d and adding a bias (29):

$$a_j = \sum_{i=1}^{d} w_{ji}{}^{(1)}x_i + w_{j0}{}^{(1)} \tag{29}$$

where:

$w_{ji}{}^{(1)}$ is the weight of the first layer, going from input i to hidden unit j

$w_{j0}{}^{(1)}$ is the bias of the hidden unit j

Using the second layer of units and transforming the input layer in agreement with a non-linear function $\tilde{g}(\cdot)$, the output is obtained. The function is (30):

$$y_k = \tilde{g}\left(\sum_{j=0}^{M} w_{ji}{}^{(2)}g\left(\sum_{i=0}^{d} w_{ji}{}^{(1)}x_i\right)\right) \tag{30}$$

The value of the weight parameter is adaptive, so it changes during the training process. The non-linear activation function can be a threshold or sigmoidal. Considering an input of 0 and 1, the threshold units have a binary value, so the hidden unit responds to values of one specific pattern. In the case of a continuous variable, the hidden units divide the space using and hyperplane. Consequently, the output of 1 is created through the logical operator AND, which means all hidden units shall have a value of 1. The sigmoidal units use the logistic sigmoid activation or the tanh function, as seen in Figure 22. The logistic sigmoid activation function is (31):

$$g(a) \equiv \frac{1}{1 + \exp(-a)} \tag{31}$$

The tanh activation function is (32):

$$g(a) \equiv \tanh(a) \equiv \frac{e^a - e^{-a}}{e^a + e^{-a}} \tag{32}$$

Applying a linear transformation to the input $\tilde{a} = a/2$ and the output $\tilde{g} = 2g - 1$, the tanh function is equivalent to the logistic function, but the advantage is the faster convergence in the training process.
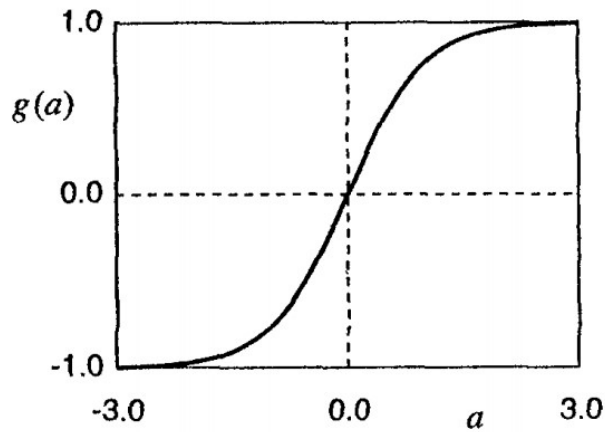

Figure 22 The tanh activation function (Bishop, 1995)

11.7. Linear Discriminant Analysis (LDA)

The linear discriminant analysis (LDA) is an algorithm based on multiple predictors and multivariate normal distribution. LDA assumptions are the dataset normality and the feature independence. Thus, each individual predictor follows a one-dimension normal distribution, so there is a correlation between each pair of predictors, as shown in Figure 23.
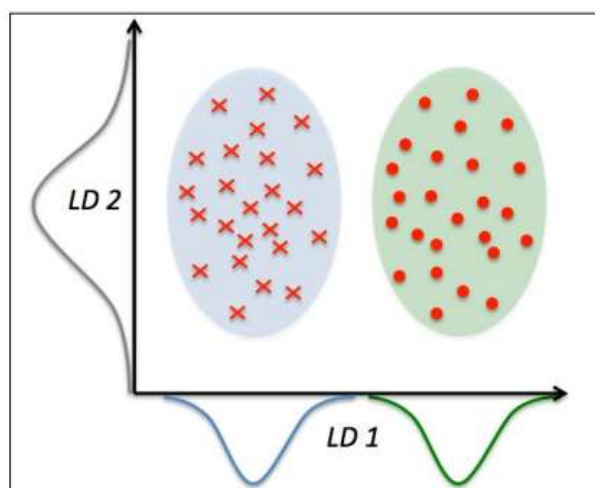
Figure 23 Example of two normal distributed on the x-axis. The y-axis recognizes high variance, but it does not discriminate between the two classes (Raschka, 2015).

The normal distribution is (33):

$$N(\mu_k, \Sigma) \tag{33}$$

where:

μ_k is the kth class mean vector

Σ is the covariance matrix common to all classes

μ_k can be written as (34):

$$\mu_{k=}\frac{1}{n_k}\sum_{k=1}^{K}\sum_{i:y_i=k}(x_i-\mu_k)^2 \tag{34}$$

where:

n is the total number of observations

n_k is the number of training observation in the kth class

μ_k is the mean of all training observations from the kth class

Then, the discriminant function δ_k is (35):

$$\delta_k(x) = x^T\Sigma^{-1}\mu_k - \frac{1}{2}\mu_k^T\Sigma^{-1}\mu_k + \log\pi_k \tag{35}$$

where:

π_k is the class membership probability, and it is calculated as (36):

$$\pi_k = \frac{n_k}{n} \tag{36}$$

where:

n is the number of training observation

The LDA has better performance than logistic regression when it identifies more than two classes because it is more stable, reduces the risk of overfitting and the dimension of the dataset. The steps are:

- To standardize of the d-dimensional dataset, where d is the number of features.
- To compute the mean vector for the d-dimensional dataset. The mean vector is the mean of each variable.
- To compute the class scatter matrix Sb between classes
- To compute the scatter matrix Sw within the classes
- To compute the eigenvectors and corresponding eigenvalues of the matrix Sw-1 and Sb
- The W matrix is d x k –dimensional transformation matrix computed from the k largest eigenvalues.
- To project the samples using matrix W

11.8. Boosting (B)

The boosting (B) technique uses weak learners to randomly subdivide the training set without replacement. Without replacement means no element can be selected more than once in the first training. Then, a second training sample is aggregated mixing random training samples and misclassified training samples. Consequently, a new training set that differs from the previous two is created. Finally, the algorithm counts majority votes among the tree dataset. The boosting technique has the tendency to overfit, and some implementations, e.g., AdaBoost, use the re-weighted sample in each iteration to overcome the overfitting. The AdaBoost steps are the following:

- Set the weight vector of two uniform weights.

Then, for j in m boosting cycle, do the following:

- Train a weighted weak learner
- Predict class labels
- Compute weighted error rate
- Compute coefficient
- Update weights
- Normalize weights to sum to 1
- Compute final prediction

11.9.   Conditional inference trees (Ctree)

The Ctree uses a tree to partition recursively the covariate M that influence the variable Y. M is an m-dimensional covariate vector X=(X1…., Xm) as stated in (37). The algorithm fits a learning sample, where the learning sample is a random sample composed of an n observations vector. Consequently, the algorithm works recursively on the vector. The steps of binary partitioning are: testing the null hypothesis between the m covariate and Y and selecting the covariate Xi with the strongest association with Y. Measuring the associated P-values. Running the algorithm until the hypothesis is accepted. Splitting the variable into two subgroups, and repeating the previous steps. In case the covariate Xi is missing, a new split can be calculated leading to the same division of the original split. When the null hypothesis is accepted, the algorithm stops (Hothorn et al., 2015). The variable is split into two subgroups, repeating the two steps. In case of the covariate Xi is missing, a new split can be calculated leading to the same division of the original split, as shown in Figure 24.

$$D(Y|X) = D(Y|X_{(1,)}...,X\_m) = D(Y|f(X_{(1,)}...,X\_m)) \qquad (37)$$
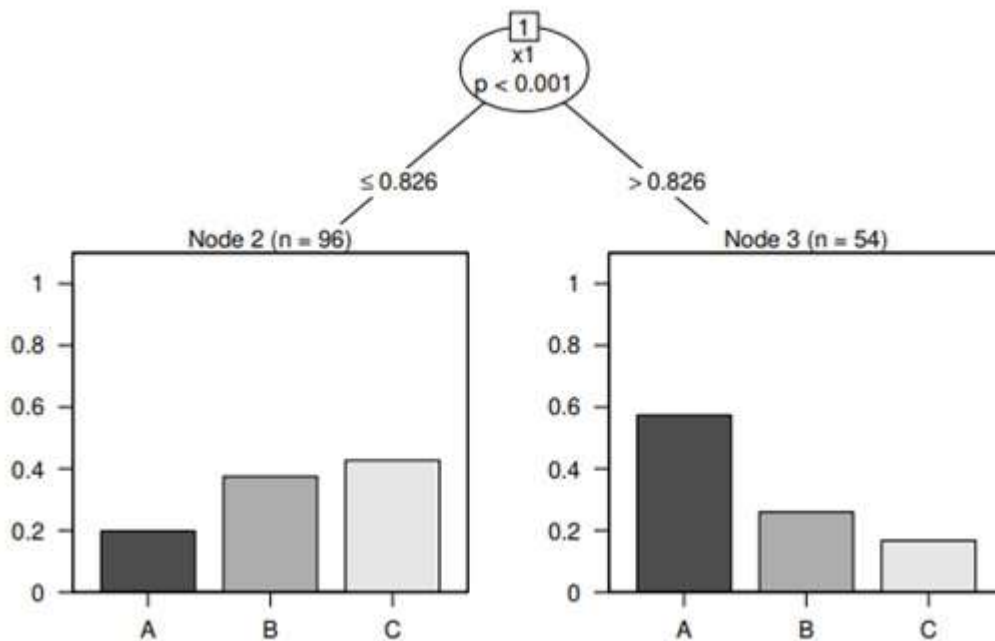

Figure 24 Binary partitioning using Ctree with the p-value (Hothorn et al., 2015).

11.10.   Naive

The Naive algorithm tries to solve the classification problem using a simple and direct way. It could be described as a query that searches from the beginning to the end of the dataset. Derived from Naive, the Naive Bayes (NB) uses the probability theorem to classify a dataset. The assumptions are the independence of the feature classes and the normality of the dataset distribution. The probability model was formulated by Thomas. The probability model formulated by Thomas Bayes (1701-1761) is (38):

$$\text{poster probability} = (\text{conditional probability} \cdot \text{prior probability}) / \text{evidence} \qquad (38)$$

The posterior probability is the likelihood that an object fit the class j given its observed feature x (predictor). Therefore, posterior probability depends on conditional probability and prior probability divided by model evidence. Conditional probability is the likelihood that an event occurs given another event has occurred. Prior probability is the original probability of an outcome of the class j stated as (39):

$$P(C_j | x_i) = (P(C_i | C_j) = P(C)) / (P(C_i)) \qquad (39)$$

where:

$P(C_j | x_i)$ is the posterior probability of class j given the observed feature x_i (predictor).

$P(C_j)$ is the prior probability for the class C_j.

$P((x_i | C_j)$ is the likelihood of observed sample x_i fit in the class C_j.

$P(C_i)$ is the prior probability of feature.

Assuming to have only two classes, $\omega 1$ and $\omega 2$, a decision rule is necessary to assign x_i the correct class ω_j. Therefore, the decision rule divides the space into two regions. The boundaries between the regions are called decision boundaries. Considering two classes and two regions R, an error occurs when an input for the class C_1 is assigned to class C_2 (40):

$$p(\text{mistake}) = p(x \in R\_2\, C\_1) + p(x \in R\_1\, C\_2) \qquad\qquad (40)$$

$$= \int_{R_1} p(x, C_1)\, dx + \int_{R_2} p(x, C_2)\, dx$$

To minimize the error, the decision rule has to assign the classes minimizing the integrals in the previous equation. Therefore, the class ω has the highest $P((x\_ | ω\_)$ as reported in Figure 25.
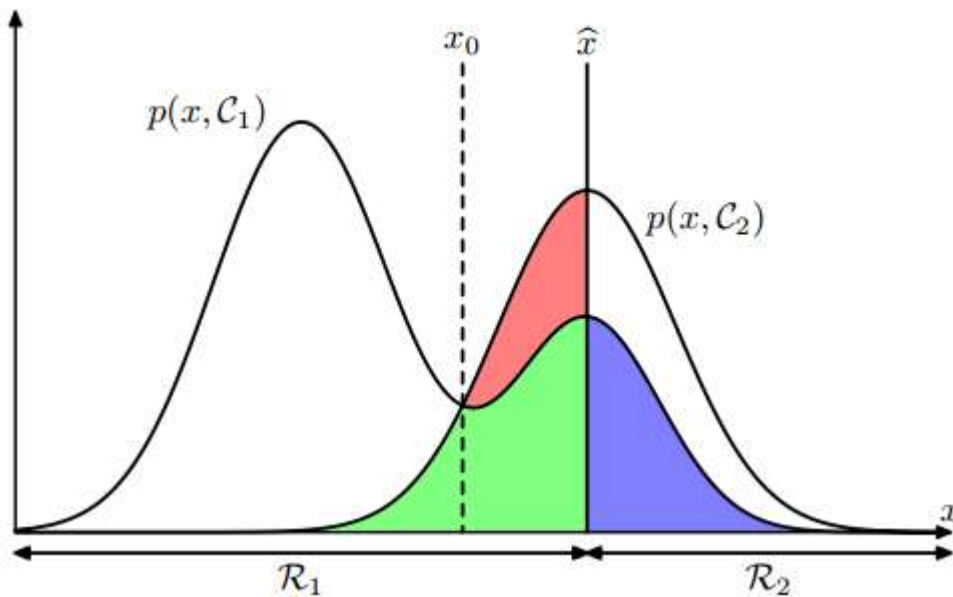

Figure 25 The decion boundary is set $\hat{x}$, the classification error are the sum of green and red areas. When the decision boundary moves from x to x_0 the mistake probability is minimized, and the red area disappears (Bishop, 2006).

Given a training data and assuming that the data are independent of the model, to minimize the wrong class assignment of x the naive Bayes build a decision rule maximizing posterior probability. For each class of the model, labelled data are obtained by fitting model. The naive Bayes is useful in the case of the high dimensionality of input, and the density estimation is difficult. When the assumptions are violated, naive Bayes can give a good performance because the decision boundaries does not influenced by class (Bishop, 2006).

12. Acknowledgements